POLITECNICO
DI MILANO

Civil, Environmental and Land Management Engineering School

SEISMIC RISK ASSESSMENT FOR HIGH-RISE BUILDINGS IN BEIJING BASED ON 3D PHYSICS-BASED NUMERICAL SIMULATIONS

Supervisor: Dr. Chiara Smerzini

Co-supervisor: Dr. Marco Stupazzini

WANG XIANJIE

849997

Academic year 2016/2017

Abstract

The main objective of this work is to carry out seismic risk assessment studies for the urban area of Beijing, China, using an advanced representation of seismic hazard based on deterministic 3D physics-based numerical simulations of ground shaking from the source to the site. For seismic risk assessment for a specific class of buildings, i.e. high-rise buildings, has been considered, as it is an important component of building stock in China.

In general, the seismic risk assessment uses seismic hazard information combined with the suitable vulnerability models of structures and/or facilities in order to estimate the probabilities of damages and to measure expectancies of losses.

Regarding the hazard assessment, innovative simulation-based tools for characterization of earthquake ground motion prediction have been used, as opposed to standard tool based on Ground Motion Prediction Equations (GMPEs). This approach makes use of 3D physics-based numerical simulations of earthquakes (3DPBNS), including a detailed model of the seismic source, the propagation path and local geology (e.g. alluvial basin). Such tools are particularly appealing for earthquake ground motion prediction in those cases where earthquake records are scarce, such as in the near-source region of large earthquakes. The 3D earthquake scenarios have been generated with a high-performance spectral element code called SPEED (http://speed.mox.polimi.it/).

Regarding vulnerability assessment, existing fragility curves for high-rise buildings in China were used. Combining the ground motion scenarios produced by the 3DPBNS with the selected fragility curves, the probability of exceedance of each damage state and mean damage ratios have been obtained. Consideration of a rather wide set of earthquake scenarios with magnitude ranging from 6.5 to 7.3 has allowed to evaluate also the variability of the seismic damage scenarios. Comparisons of results obtained from GMPEs and 3DPBNS have been carried out in order to verify the differences of two approaches. Finally, sensitivity of results to the fragility curves was addressed to check the variability of the seismic risk assessment with respect to the vulnerability model.

Results of the study demonstrate that compared to the standard empirical

methods, 3D physics-based numerical simulation could provide a more accurate and detailed characterization of ground motion, especially in the near source region and in complex geologic conditions, and this can be effectively used to improve the seismic risk studies at urban scale.

Keywords: seismic risk assessment; 3D physics-based numerical simulation; fragility curves; high-rise buildings, Beijing

L'Abstratto

L'obiettivo principale di questo lavoro di tesi è quello di svolgere studi di valutazione del rischio sismico per l'area urbana di Pechino, in Cina, utilizzando una rappresentazione avanzata della pericolosità sismica basata su simulazioni in grado di determinare lo scuotimento del terreno dall'origine al sito impiegando la fisica 3D. La valutazione del rischio sismico è stata effettuata considerando una specifica classe di edifici, ovvero i grattacieli, che costituiscono una componente importante del costruito in Cina.

In generale, la valutazione del rischio sismico utilizza informazioni di pericolosità sismica combinati con i modelli di vulnerabilità di strutture e/o servizi, al fine di stimare le probabilità dei danni e valutare le perdite attese.

Per quanto riguarda la valutazione dei rischi, sono stati utilizzati strumenti innovativi basati su simulazioni per la caratterizzazione dello spostamento delle terre previsto durante i terremoti. Questo approccio, che si discosta da quello standard basato su equazioni di previsione dello spostamento delle terre (GMPEs), fa uso di simulazioni numeriche dei terremoti basate sulla fisica 3D (3DPBNS), comprendenti un modello dettagliato della sorgente sismica, del percorso di propagazione e della geologia locale (ad esempio conca alluvionale). Tali strumenti sono particolarmente idonei per la previsione dello spostamento della terra durante il terremoto nei casi in cui le registrazioni di terremoti siano scarse, come nelle regioni prossime alle fonti di forti terremoti. Gli scenari di terremoto in 3D sono stati generati con un codice di elementi spettrali altamente performante denominato SPEED (http://speed.mox.polimi.it/).

Per quanto riguarda la valutazione delle vulnerabilità, sono state impiegate curve di fragilità esistenti per grattacieli in Cina. Combinando gli scenari del movimento della terra prodotti da 3DPBNS con le curve di fragilità selezionate, sono state calcolate la probabilità del superamento di ogni stato di danno e i rapporti dei danni medi. Poichè è stata considerata una serie piuttosto ampia di scenari di terremoto con magnitudo variabile da 6.5 a 7.3, è stato possibile valutare anche la variabilità degli scenari di danneggiamento sismico. Il confronto dei risultati ottenuti da GMPEs e 3DPBNS è stato effettuato al fine di verificare le differenze dei due approcci. Infine è stata valutata la sensibilità dei risultati al variare delle curve di fragilità, il che ha permesso di verificare la variabilità della valutazione del rischio sismico rispetto al modello di vulnerabilità.

I risultati dello studio dimostrano che, rispetto ai metodi empirici standard, la simulazione numerica basata sulla fisica 3D è in grado di fornire una più accurata e dettagliata caratterizzazione del moto del suolo, soprattutto nelle regioni prossime alla fonte ed in complesse condizioni geologiche: ovvero in definitiva costituisce una soluzione efficace per migliorare gli studi di rischio sismico a scala urbana.

Parole chiave: valutazione del rischio sismico; Simulazione numerica basata sulla fisica 3D; curve di fragilità; grattacieli, Beijing

Table of Contents

1. Introduction

1.1 Background

The impressive chain of catastrophic earthquakes from 2010 to 2016, starting from the Haiti earthquake in January 2010, followed by the Canterbury seismic sequence in New Zealand in 2010-2011, the huge Tohoku earthquake in Japan in March 2011, up to the Po Plain and Amatrice-Norcia, Italy, earthquakes of May 2012 and August-October 2016 and to the Kumamoto, Japan, earthquake in April 2016, revealed the extreme fragility of modern society. All these events have shown a dramatic increase of loss potential of seismic disasters, producing overall losses of the order of tens up to hundreds of billion dollars (Munich RE: https://www.munichre.com), see Table 1.1 annd Figure 1.1.

Date	Event	Affected Area	Overall losses (US$m, original values)	Fatalities
12 Jan. 2010	Earthquake	Haiti: Port-au-Prince, Petionville, Jacmel, Carrefour, Leogane, Petit Goave, Gressier	8,000	159,000
4 Sep. 2010	Earthquake	New Zealand: Canterbury, Christchurch, Avonside, Omihi, Timaru, Kaiapoi, Lyttelton	10,000	
11 Mar. 2011	Earthquake, Tsunami	Japan: Honshu, Miyagi, Sendai, Aomori, Tohoku, Fukushima, Mito, Ibaraki, Tochigi, Utsunomiya, Iwate, Morioka, Yamagata, Chiba, Tokyo	210,000	15,880
20/29 May 2012	Earthquake	Italy: Emilia-Romagna, San Felice del Panaro, Ferrara, Cavezzo, Rovereto di Novi, Carpi, Concordia, Bologna, Mailand, Aosta Valley, Venice, Mirandola	16,000	18
24 Aug. 2016	Earthquake	Italy: Lazio, Accumoli, Amatrice, Posta, Saletta, Marche, Arquata del Tronto, Pescara del Tronto, Umbria, Norcia	5,000	299
26/30 Oct. 2016	Earthquake	Italy: Umbria, Norcia, Marche, Ussita, Caldarola, Camerino, Castelsantangelo sul Nera, Muccia, Pieve Torina, San Ginesio, Visso, Latio, Rieti, Amatrice, Rome	6,500	2
14/16 Apr. 2016	Earthquake	Japan: Kumamoto, Aso, Chuo Ward, Mashiki, Minamiaso, Oita, Miyazaki, Fukuoka, Yamaguchi	32,000	205

Table 1.1 The impressive catastrophic earthquake events and their losses from 2010-2016 (Munich RE: https://www.munichre.com).

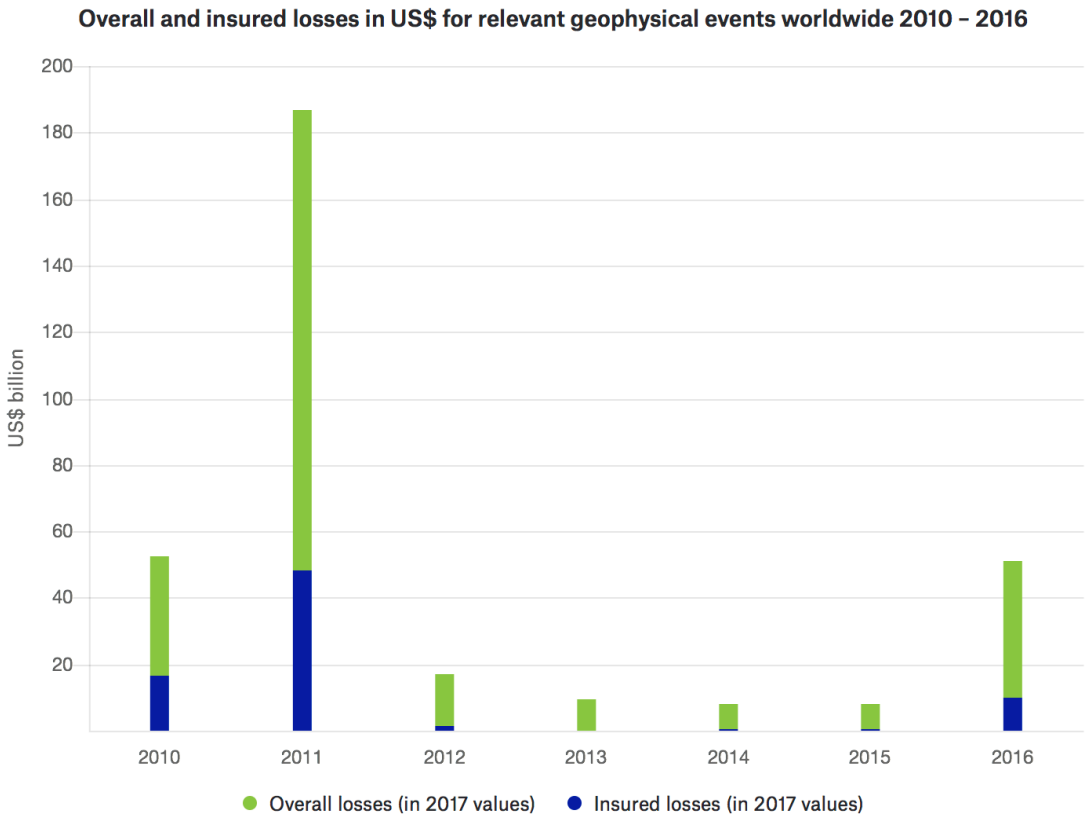

Figure 1.1 Overall and insured losses in US$ for relevant geophysical events worldwide 2010 – 2016

Seismic risk studies at urban scale are crucial: (i) to assess quantitatively the socio-economic impact of an earthquake in a densely populated area, of potential interest also for insurance and reinsurance industries; (ii) to plan effective actions for seismic risk mitigation and preparedness; (iii) to improve decision making in support to emergency response and disaster management; and eventually (iv) to optimize retrofitting strategies. The goal of such studies is to provide the spatial distribution of expected damage and loss to structures and people due to an earthquake of any intensity. Key ingredients are, on one hand, the evaluation of seismic hazard and of its spatial variability, and, on the other one, the vulnerability model, which establishes a correlation between hazard and structural damage.

Standard tools for hazard assessment, both in a probabilistic and deterministic framework, are based on the use of Ground Motion Prediction Equations (GMPEs), which are empirical regression laws for peak ground motion parameters calibrated on instrumental observations from past earthquakes. However, in spite of their simplicity, they have the following major limitations:

(i) They are poorly constrained in the range of large magnitude and small source-to-site distances, i.e. in the near-source region of large, destructive earthquakes;

(ii) They cannot account for complex site conditions, such as in the case of large sedimentary basins;

(iii) They cannot provide an accurate description of the spatial variability of ground motion at regional scale.

Driven by the increasing computational resources, 3D physics-based numerical simulations have emerged as a powerful tool for prediction of earthquake ground motion, as an alternative to GMPEs. Such tools have the merit of incorporating all physical factors that affect ground shaking, from the seismic fault rupture, the propagation path in Earth media to near-surface geology.

In this context, a research project between Politecnico di Milano and the reinsurance company Munich RE has been established with the objective of constructing ground shaking scenarios from hypothetical earthquakes in large urban areas worldwide and incorporating them in risk assessment studies. This work makes use of the 3D seismic scenarios produced in the framework of this project for the urban area of Beijing, China.

With its more than 20 million inhabitants, Beijing is one of the many megacities around the world situated in a high seismicity region. As a matter of fact, Beijing area was struck by many destructive earthquakes in the past, with the magnitude varying from Mw 6 to Mw 6.5. such as the Great Tangshan earthquake on July 28, 1976, which hit Tangshan, Hebei that caused 655 thousand deaths officially, 164 thousand severe injuries, and US$10 billion in 1976 (Grossi et al. 2006). Therefore, analysis of the seismic risk in this city is very relevant for risk reduction purposes.

One the other hand, Beijing is a modern city undergoing rapid growth and is full of high-rise buildings, which could relieve the problem of accommodation due to the extremely increasing of population and flourishing of the development. Therefore, high-rise buildings represent an important component of building stock exposed to seismic risk in Beijing and the assessment of damage to high-rise buildings in case of strong earthquakes could be of great significance for seismic risk mitigation and civil protection mechanisms.

1.2 Scope of the work

The goal of this work is to perform seismic risk assessment studies in the urban area of Beijing area for the class of high-rise buildings, making use of 3D physics-based numerical simulations of ground shaking. To achieve this goal, a set of different earthquake scenarios with magnitude ranging from Mw6.5 to 7.3 were considered and combined with suitable vulnerability models for high-rise building.

Referring to the vulnerability assessment, fragility curves were chosen from the ones available in the literature, namely Wu et al. 2013 (hereinafter WU13), which produced fragility curves for high-rise buildings in China. .

Damage assessments for high-rise buildings in Beijing will be produced by combining the 3D seismic scenarios with the fragility curves and their variability with respect to the considered earthquakes scenarios will be considered. Damage scenarios obtained considering 3D physics-based simulations will be then compared with the ones obtained using standard empirical tools (GMPEs) for ground motion prediction to demonstrate the superiority of the numerical approach.

1.3 Organization of the thesis

This research contains seven sections which focus on the estimation of seismic hazard analysis in Beijing area.

Chapter 1 discusses the general background of this research and the objectives. Moreover, the scope of the work has been laid out in this chapter.

Chapter 2 shows the overview on seismic risk assessment. Here the definition of risk and essential components of risk are defined in this chapter. Also, GMPE (Ground Motion Prediction Equations) method for hazard estimation, vulnerability evaluation methods were introduced here.

Chapter 3 describes the overview of the literature study for the high-rise buildings nowadays, then the two different fragility curves for high-rise buildings in different locations were introduced in this chapter.

Chapter 4 shows the case study in Beijing area, China. Initially 3D physics-based numerical simulations for ground motion prediction was described in a very detailed way. And then available scenarios about the case study were introduced in this chapter. At last some mains results and ground shaking

maps are summarized here.

Chapter 5 summarized the damage scenarios to high rise buildings for specific magnitude earthquakes (Mw6.5, Mw, 6.9, and Mw 7.3) for the fragility curve obtained from WU13. besides, comparison among different fragility curves for specific scenario and in terms of mean values for all the scenarios of the given magnitude are shown and results are discussed in this chapter, such as fragility curves from the reference WU13, Taipei and Istanbul. Finally, a comparison between GMPEs method and 3D physics based simulated method were carried out in this chapter.

Chapter 6 provides a conclusion for this research. We also conclude the observations and outcomes from this research and provides future recommendation.

2. Overview of seismic risk assessment

2.1 Definition of Seismic Risk

In a wide sense, risk denotes the social and/or economic expected degree of losses within a given area, during a specific time frame, due to a particular hazardous phenomenon such as an earthquake or a flood.

Risk is general quantified in terms of two kinds of losses, social losses and economic losses. The social losses comprise expected number of lives lost, persons injured, permanently displaced people. While, the economic losses mainly refer to the damage to the structures and contents, the public infrastructures, impact on environment and business interruption.

Losses can be also classified into two categories, direct(primary) losses and indirect(secondary) losses. Direct losses refer to the immediate physical or structural damage to life, property, infrastructure and natural resources by the particular hazardous phenomenon. Indirect losses refer to subsequent and secondary damages, including losses due to loss of function and disruption of economic activity.

Risk also can be defined as a combination or a convolution of three main factors; hazard, vulnerability, exposure (UNESCO, 1972; UNDRO, 1979), see Figure 2.1. Further explanation about seismic risk framework is shown Figure 2.2 (Nnovelli, V., I. 2017). The definition of hazard, vulnerability, and exposure will be discussed in detail consequently.

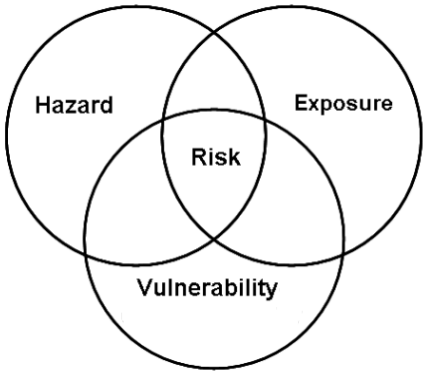

Figure 2.1 Risk Composition (Reese & Schmidt 2008)

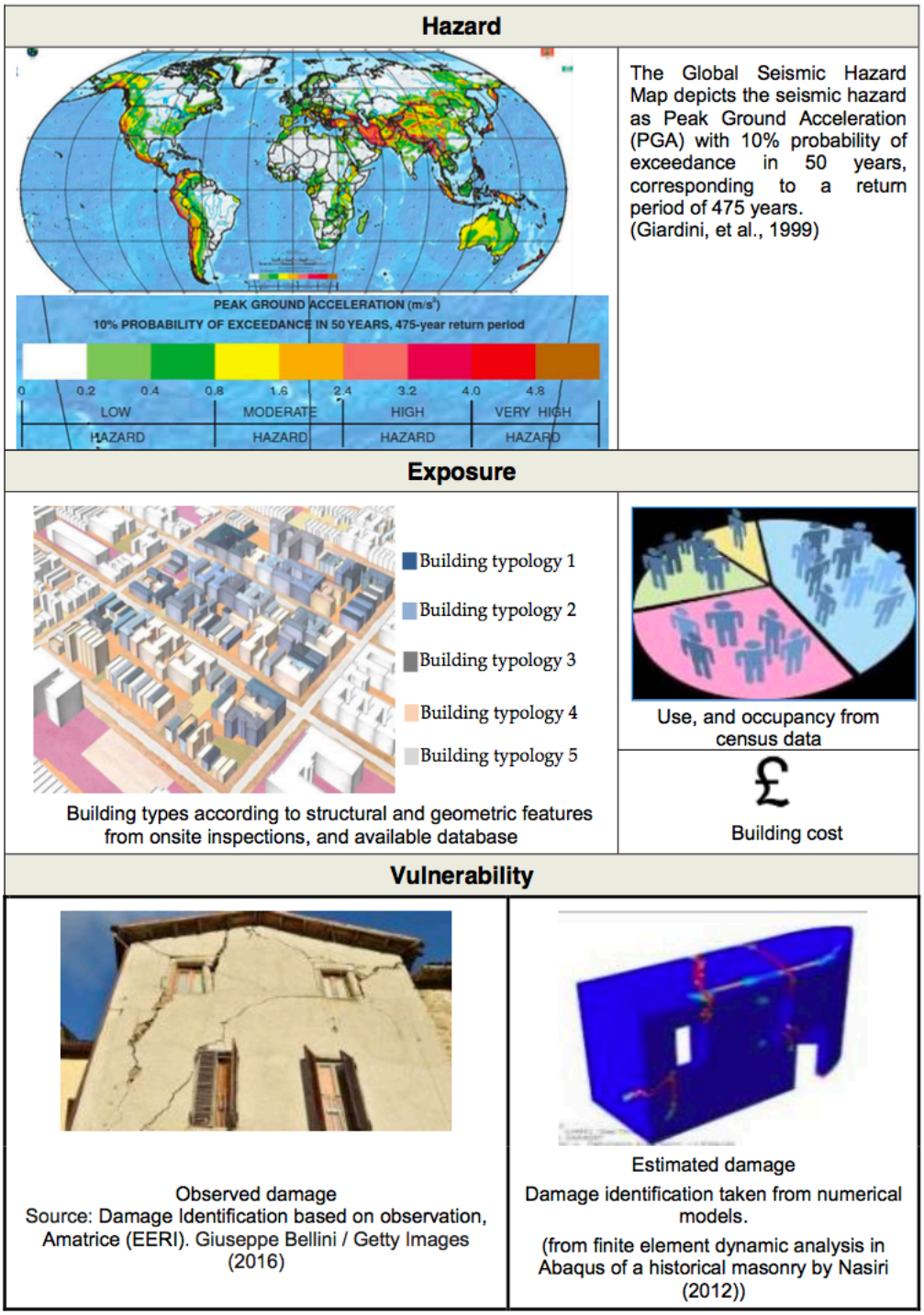

Figure 2.2 Seismic risk framework (Nnovelli, V., I. 2017)

Seismic Hazard, is defined as the probability that an earthquake will occur in a given geographic area, within a given window of time, and with ground motion intensity exceeding a given threshold. It is therefore quantitatively

defined by three parameters: severity level (physical measurement), spatial measurement (where), and temporal measurement (when and how often), as well as associated uncertainties. The evaluation of seismic hazard can be carried out by two different approaches, a probabilistic approach involving the use of probabilistic concepts to quantify and combine the uncertainties in the size, location, rate of occurrence of earthquakes and in the ground motion attenuation (peak ground acceleration, spectral acceleration, spectral displacement vs return period), a deterministic approach where ground motion scenarios are produced for postulated earthquakes events (seismic scenarios for given events). Nevertheless, both these two approaches are based on geological and seismological data. In this work, a deterministic approach has been adopted.

Seismic Vulnerability, is defined as the degree of fragility of a natural or socioeconomic community or a natural or socio-economical system towards seismic hazard. Here seismic vulnerability was quantified as the expected amount of damage of a given structure as a function of given intensity measure of earthquake ground motion. The functions are fragility functions which define the probability of exceedance of some limit damage states (i.e. severe damage state, collapse state).

Seismic Exposure, focuses on the socially valued elements that may potentially be damaged by a seismic hazard. Exposure could be measured through the use of monetary values even though this could be problematic for values elements that are not simply equated to a monetary measure.

However, we have to pay attention that even though seismic hazard and seismic risk are very common used terms in engineering design and analysis, and also generally used interchangeably, they are basically different concepts. Seismic hazard is a property of an earthquake that can cause damage and loss'' (Mcguire, 2004), while, seismic risk is defined as ''the probability of occurrence of these adverse consequences caused by a seismic hazard, such as the destruction of buildings or the loss of life that could result from seismic hazards'' (Reiter, 1990).

To carry out the risk assessment, first of all seismic hazard assessment should be evaluated through surveying the past earthquake history, seismic sources, and also the local soil characteristics. From the seismic scenarios and fragility curves, vulnerability assessments could be obtained to evaluate the exceedance probability of a given damage limit level for a particular class of structures. Finally, the risk assessment of a single building or of a specific area

has been carried out to provide the expected losses.

Since the earthquakes could lead a huge economic losses and property damage, human life, seismic risk assessment is very significant to create awareness on the seismic hazard and risk, take mitigation measures (structural measures and non-structural measurements) as well as the emergency plans.

2.2 Methods for seismic hazard assessment

Seismic Hazard Analysis involves the quantitative estimation of earthquake ground shaking hazard at a particular site. (Kramer. 1996). Seismic hazards analysis could be separated into two categories, Deterministic Seismic Hazard Analysis(DSHA) and Probabilistic Seismic Hazard Analysis (PSHA). For DSHA, empirical and numerical methods are employed to estimate ground shaking due to the occurrence of a specific earthquake. And the output is the estimation of a given set of ground motion parameters such as Peak Ground Acceleration (PGA), Peak Ground Velocity(PGV) and of its spatial variability during the postulated earthquake scenario. However, for PHSA, probabilistic analysis has been used to get the probability that a give ground motion parameter such as PGA will be exceeded at a given site and in a given time interval. The main output is the hazard map. Some further discussion about these two methods will be introduced in the following content. The main output is the hazard curve.

2.2.1 Probabilistic Seismic Hazard Analysis

Probabilistic Seismic Hazard Analysis(PSHA) involves the use of probabilistic concepts to quantify and combine the uncertainties in the size, location, rate of occurrence of earthquakes and in the ground motion attenuation, to provide a more complete picture of the seismic hazard. PSHA could also be described by four steps procedure shown in Figure 2.3.

Step 1. Seismotectonic model. Identification and characterization of all earthquake sources capable of producing significant ground motion at the site. Here it should be noted that the probability distribution of potential rupture distance within the source has to be characterized also. The distributions are then combined with the source geometry to find the corresponding probability distribution source-to-site distance.

Step 2. Characterization of source seismicity or temporal distribution of earthquake recurrence. The recurrence relationship is used to characterize the

seismicity of each source zone by specifying the average rate at which an earthquake of a given size will be exceeded. It might accommodate the maximum size earthquake.

Step 3. Ground Motion Prediction Equations (GMPEs). The ground motion produced at the target size by earthquakes of any possible size occurring at any possible point of the source zone is estimated using empirical predictive equations. The uncertainty associated with these predictive relationships is also accounted for (standard deviation of empirical law). GMPEs will be described in detail in the following section.

Step 4. The uncertainties in earthquake location, earthquake size and prediction of ground motion parameter are combined using the total probability theorem to obtain the probability that the ground motion parameter will be exceeded during a particular time period.

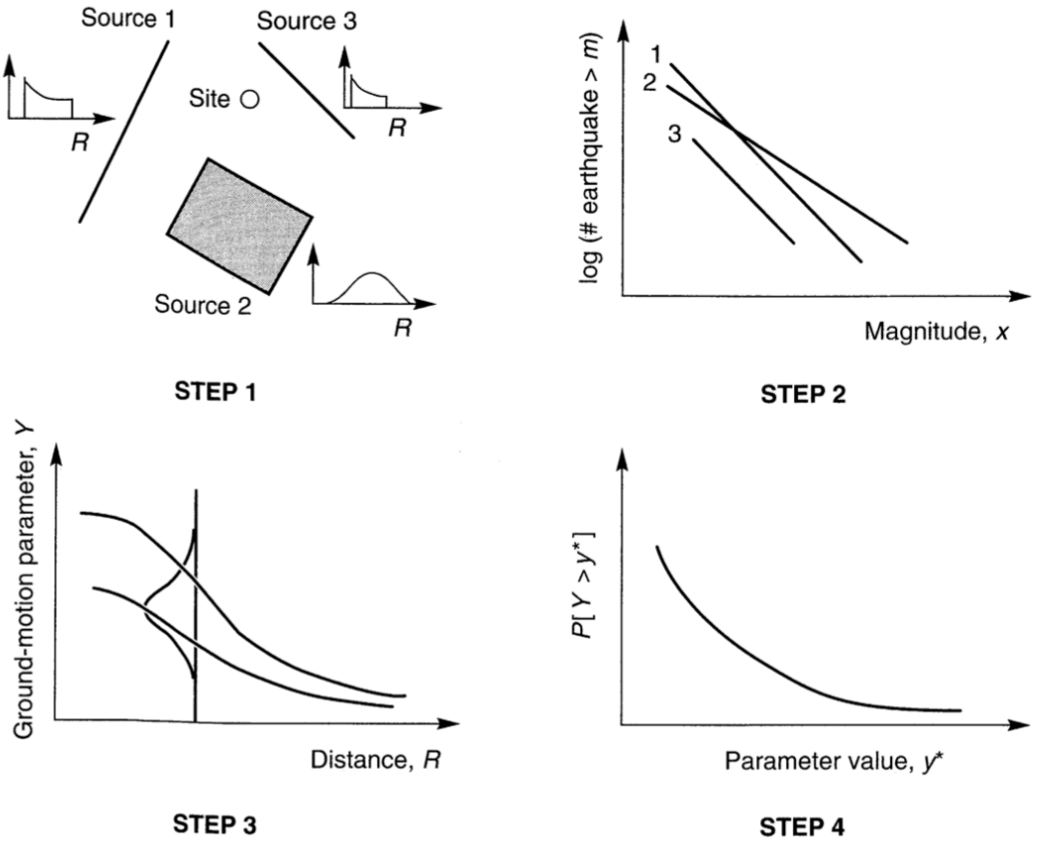

Figure 2.3 Four steps procedure of a probabilistic seismic hazard analysis (Kramer. 1996).

The appropriate performance of a PSHA needs carefully pay attention to the

problems of source characterization, the probability computations and ground motion parameter prediction.

2.2.2 Deterministic seismic hazard analysis

Deterministic seismic hazard analysis might be employed when a particular earthquake is assumed. DSHA involves the development a particular seismic scenario consisting of the postulated occurrence of an earthquake of a specified size occurring at a specified location. Generally, DHSA provides the basic for seismic risk assessment for critical strategic structures and for emergency plans, post-earthquake damage evaluations. DSHA could be expressed in a very simple procedure called four –step process (Reiter, 1990) as follows.

Step 1. Identification and characterization of all earthquake sources capable of producing significant ground motion at the site. Definition of each source's geometry and earthquake potential belong to the source characterization.

Step 2. Selection of a source-to-site distance parameter for each source zone. Hypocentral distance is usually selected since it is the shortest distance between the source and the site. However, it depends on the measure of distance of the predictive relationship.

Step 3. Selection of the controlling earthquake, which is generally expressed in terms of some ground motion parameters at the site. Earthquake magnitude and distance from the site usually describe the controlling earthquake.

Step 4. Definition of the hazard at the site in terms of the ground motions produced at the site by the controlling earthquake, whose characteristics are usually described by one or more ground motion parameters such as peak ground acceleration, peak ground velocity and response spectral acceleration or spectral displacement.

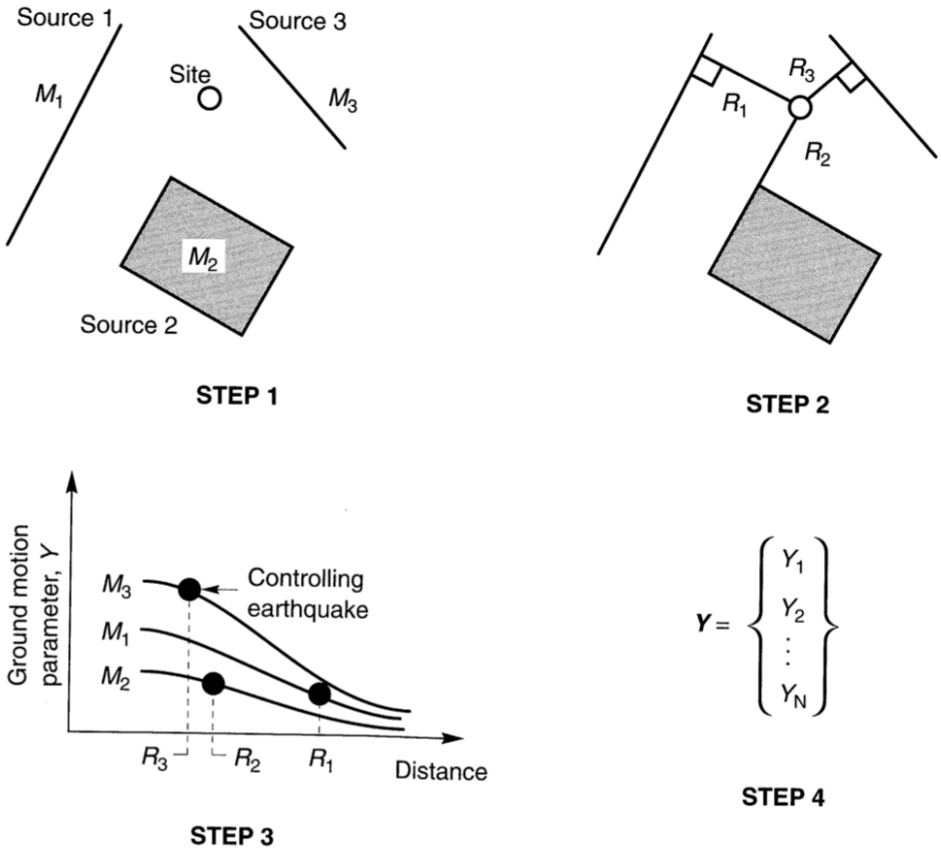

Figure 2.4 Four steps procedure of a deterministic seismic hazard analysis (Kramer. 1996).

DSHA provides a straightforward framework for evaluation of worst-case design ground motions, when applied to structures whose failure could have catastrophic consequences, such as nuclear power plants and large dams. Nevertheless, it is not an easy task to choose the controlling earthquake which is generally based on the analysis of historical seismicity and geological evidences of active seismic faults.

DSHA can be carried out using two main approaches: ground motion prediction equations (GMPEs), which are empirical regression laws providing peak values of ground motion as a function of magnitude, distance, site conditions, etc.., and numerical approaches, such as 3D physics-based numerical simulations (3PBNS), which account for details of both rupture process and propagation from the source to the site. GMPEs will be described in detail in the following section, while 3PBNS will be addressed in Chapter 3.

2.2.3 Ground Motion Prediction Equations

Ground Motion Prediction Equations (GMPEs), usually describes the distribution of expected ground motion intensity measures (such as PGA and Sa) as a function of independent parameters, such as magnitude, site classification and source-to-site distance. The relationship could show in Figure 2.5

Figure 2.5 Ground Motion Prediction Equations (Kramer. 1996).

One of the prediction function form is shown as follows,

$$Y=f(M,R,P_i)$$

Where;

Y is the ground motion parameter, such as peak ground motion (PGA)， peak ground velocity (PGV), spectral displacement (Sd) for a given vibration period;
M is the earthquake magnitude according to the given scale;
R is a measure of the distance between the source and the site being considered;
Pi are other parameters which may be used to characterize the earthquake source, wave propagation path, and/or local site conditions, which could be rock or rigid soil, or alluvial deposits.

Here different distances could be taken, such as Hypocenteral distance (R_{hy}), epicentral distance(R_e), Joyner-Boore distance(R_{jb}) and rupture distance(R_{rup}). R_{jb} is the closest distance from the surface projection of the fault while R_{rup} is the closest distance from the fault to the site. Figure 2.6 shows the different source-site distances.

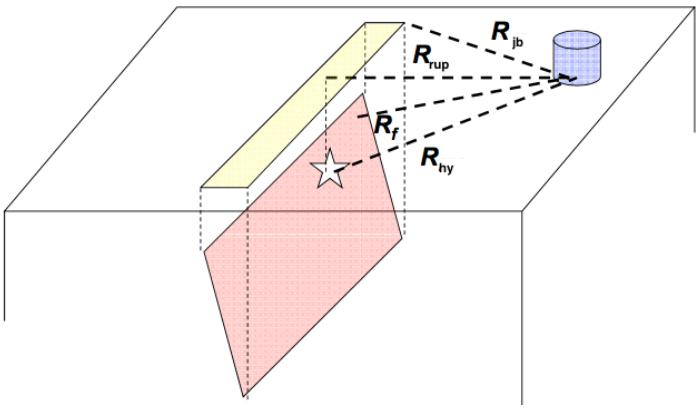

Figure 2.6. Different source-site distance diagram

The peak values of the ground motion parameters are approximately logarithmically distributed. Therefore, the regression is usually performed logarithm of Y and ln*Y* should be approximately proportional to M. Ground motion parameters maybe influenced by source characteristics or site characteristics.

Here we introduce one of the GMPEs selected for this study, Cauzzi et al. 2015 (CAEA15), which aimed at a simple though physically sound interpretation of the available data and used the following predictive model:

$$\log_{10} y = f_M + f_R + f_S + f_{SOF} + \varepsilon$$

where

$$f_M = c_1 + m_1 M_W + m_2 M_W^2,$$
$$f_R = (r_1 + r_2 M_W) \log_{10}(R_{RUP} + r_3),$$
$$f_S = s_B S_B + s_C S_C + s_D S_D, \text{ or alternatively}$$
$$f_S = b_V \log_{10}\left(\frac{V_{S,30}}{V_A}\right), \text{ or alternatively}$$
$$f_S = b_{V800} \log_{10}\left(\frac{V_{S,30}}{800}\right),$$
$$f_{SOF} = f_N F_N + f_R F_R + f_{SS} F_{SS}.$$

y can be either the 5 %-damped displacement response spectrum *DRS* (T; 5 %) in cm or peak ground acceleration *PGA* (cm s^{-2}) or peak ground velocity *PGV* (cm s^{-1}). Prediction of pseudo-spectral acceleration values can be obtained as PSA (T; 5%) = DRS (T; 5 %) × ($4\pi^2/T^2$). *PGA* ~ *PSA* (0.01s;5%). Consistently with many other ground-motion prediction models in Europe and worldwide

(e.g. Douglas et al. 2014), the horizontal seismic action is represented here by the geometric mean (GM) of the DRS ordinates of the two orthogonal horizontal components at a given vibration period T or by the GM of the two orthogonal horizontal PGA and PGV values. c_1, $m_{1,2}$, $r_{1,2,3}$, s_B, C, D, b_V, b_{V800}, V_A, $f_{N,R,SS}$ are numerical coefficients function of period, to be determined through regressions. ε is a random error term assumed as normally distributed with zero mean and standard deviation σ ($\log_{10}$ y), given by the combination of a within-event component ϕ and a between-event component τ resulting from the regression procedure.

$$\sigma = \sqrt{\phi^2 + \tau^2}$$

S_B, S_C, S_D are dummy variables for the main ground categories contemplated in Eurocode 8 (CEN 2004), with the following values: $S_B = S_C = S_D = 0$ for ground type A (rocklike, with $V_{S,30} \geqslant 800\text{ms}^{-1}$);$S_B = 1$ and $S_C = S_D = 0$ for ground type B (stiff, with $360\text{ms}^{-1} \leqslant V_{S,30} < 800\text{ms}^{-1}$); $S_B = S_D = 0$, $S_C = 1$ for ground type C (soft, with $180\text{ms}^{-1} \leqslant V_{S,30} < 360\text{ms}^{-1}$) and $S_B = S_C = 0$, $S_D = 1$ for ground type D (very soft, with $V_{S,30} < 180\ \text{ms}^{-1}$). $V_{S,30}$ is the travel-time averaged shear-wave velocity in the uppermost 30 m of the soil column. F_N, F_R, F_{SS} are dummy variables for the main faulting styles (normal, reverse, strike-slip) attributed based on the plunges of the P-, T -, and B-axes, following Boore and Atkinson (2008).

The GMPEs are derived empirically from strong-motion databases of past earthquakes and easy to use. Nevertheless, the GMPEs might be not an appropriate when a single causative fault and its associated characteristic earthquake are considered as the threat for the site of interest. Therefore, there are some limitations existing to mention for empirical ground motion prediction equations illustrated as below.

(1) They refer to generic site conditions, in the best cases represented in terms of $V_{S,30}$;

(2) Considering the relatively few records available in the near-field of large earthquakes, the available records hardly cover the range of major potential interest for engineering applications.

(3) They are not available to be used for seismic scenario studies when require the realistic representation of spatial variability of ground motion.

(4) They cannot provide the entire time history, but only peak values of ground motions.

(5) There is no correlation of ground motion intensities among multiple sites and among different spectral periods.

Nowadays, may alternative approaches for earthquake ground motion prediction has been proposed, see Figure 2.7:

(i) Stochastic models, based on the statistical properties of the seismic ground motion.

(ii) Empirical models, based on existing records of small events.

(iii) Deterministic Numerical models, based on the numerical simulation of the physics of the seismic wave propagation from the earthquake fault rupture up to the site of interest through arbitrarily complex media (physics-based simulation, PBS). Deterministic Numerical models focus on: (1) computing the exact response of a given local geological model, (2) estimating the effect of potential 3D heterogeneities (interface morphology, basin structure, etc.) and (3) estimating the ground motion variability induced by different source description (fault orientation, directivity) or basin structure.

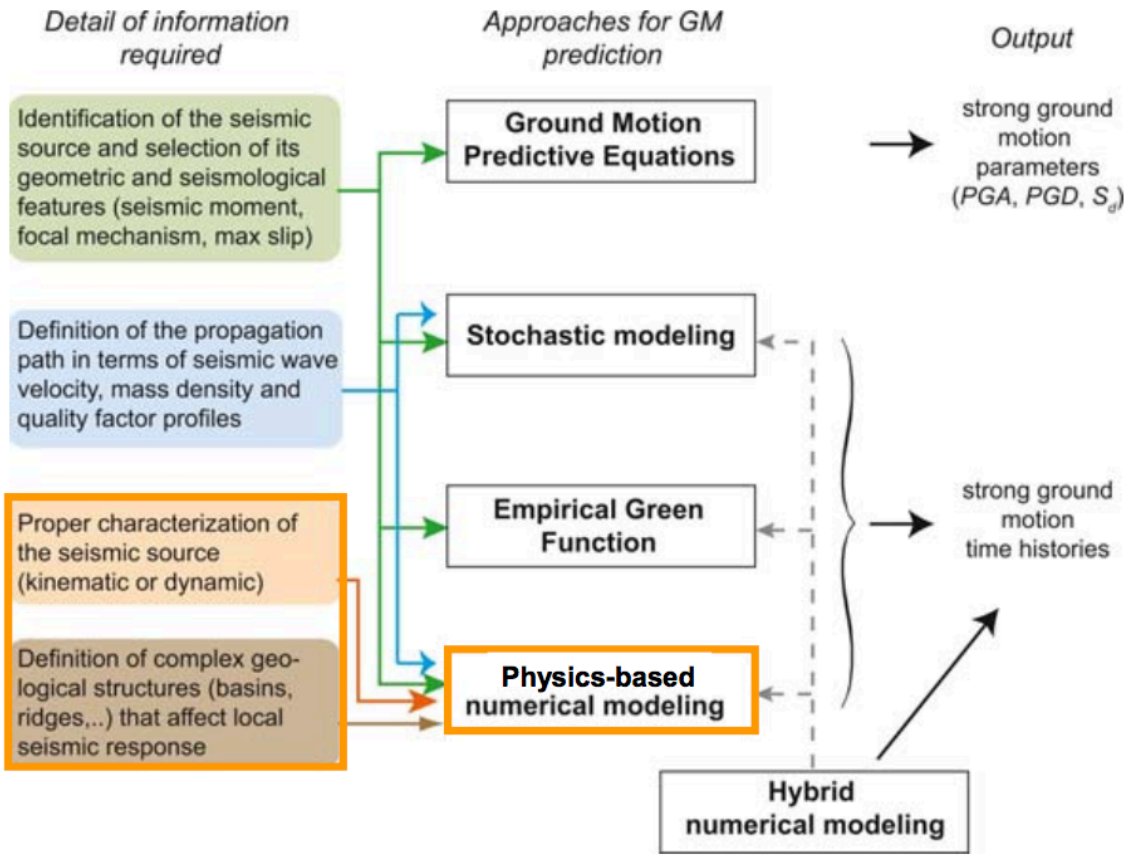

Figure 2.7 Overview of approaches for earthquake ground motion prediction (Paolucci et al., 2014).

All above, deterministic numerical models can be a good tool for earthquake ground motion prediction when the source-to-site distance is small and complex geological conditions are present, which overcome the limitation of GMPEs, see Chapter 3.

2.3 Methods for seismic vulnerability assessment

The seismic vulnerability of a structure could be considered as its susceptibility to damage for a ground motion of a given intensity. It is defined as the expected amount of damage of a given structural type or system as a function of a given intensity measure of earthquake ground motion.

In loss estimation, there are two main possible categories of methods to assess the seismic vulnerability: the empirical, hybrid and analytical.

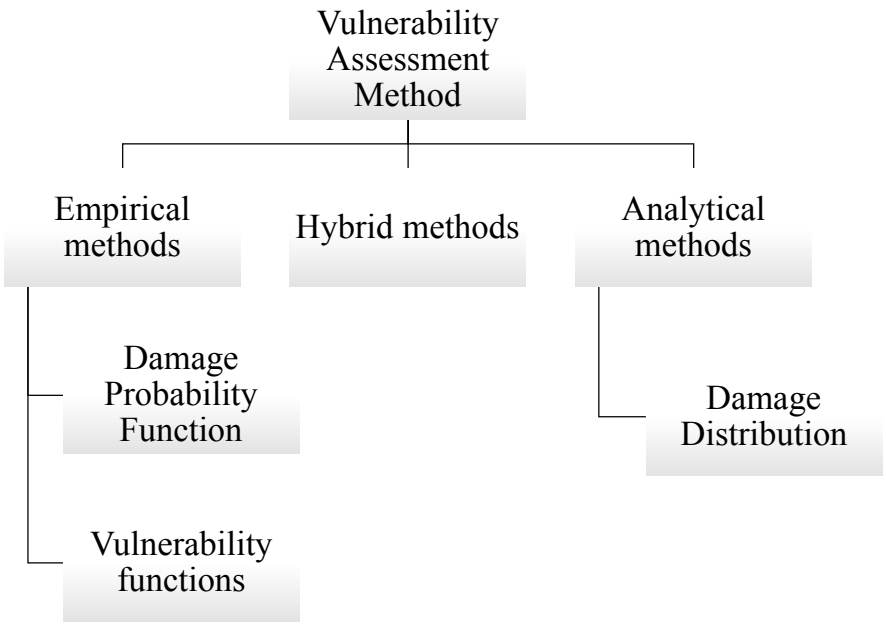

Figure 2.8 The methods for seismic vulnerability assessment

2.3.1 Empirical methods

The empirical approaches depend on awareness of the past building performance in a given seismic event. Afterwards the statistic functions could be obtained, which correlate the probability of the damage and expected intensity. There are two main types of empirical methods for the seismic vulnerability assessment of buildings based on the damage observed after earthquake, damage probability matrix (DPM) and vulnerability functions (Calvi et al. 2006). Whitman et al. (1973) is considered as the first attempt to use the damage probability matrices for the probabilistic prediction of damage to buildings from earthquakes.

Damage probability matrix expresses the conditional probability of a damage level due to a ground motion corresponding to a given macro intensity grade. DPM is based on existing data of damage for a given site exposed to a specific level of ground motion. The damage probability matrices are mainly used for probabilistic prediction of damage levels on buildings. These methods are developed and calibrated for specific regions, therefore, they are valid only for the areas and building types whereby they are defined for.

Vulnerability functions are continuous functions that are used to express the probability of exceedance at a given damage level for given an earthquake with a specific macro seismic intensity. Vulnerability functions are derived by

associating a number of building types characteristics to a corresponding expected level of damage given a shaking intensity. The methods are also developed and calibrated for specific regions.

Continuous Vulnerability Curves are continuous functions, which can express the probability of exceedance a given damage state. These curves are based on observed damage of buildings collected from past earthquakes and derive vulnerability functions by Medvedev–Sponheuer– Karnik (MSK) damage scale through the use of Parameterless Scale of Intensity (PSI).

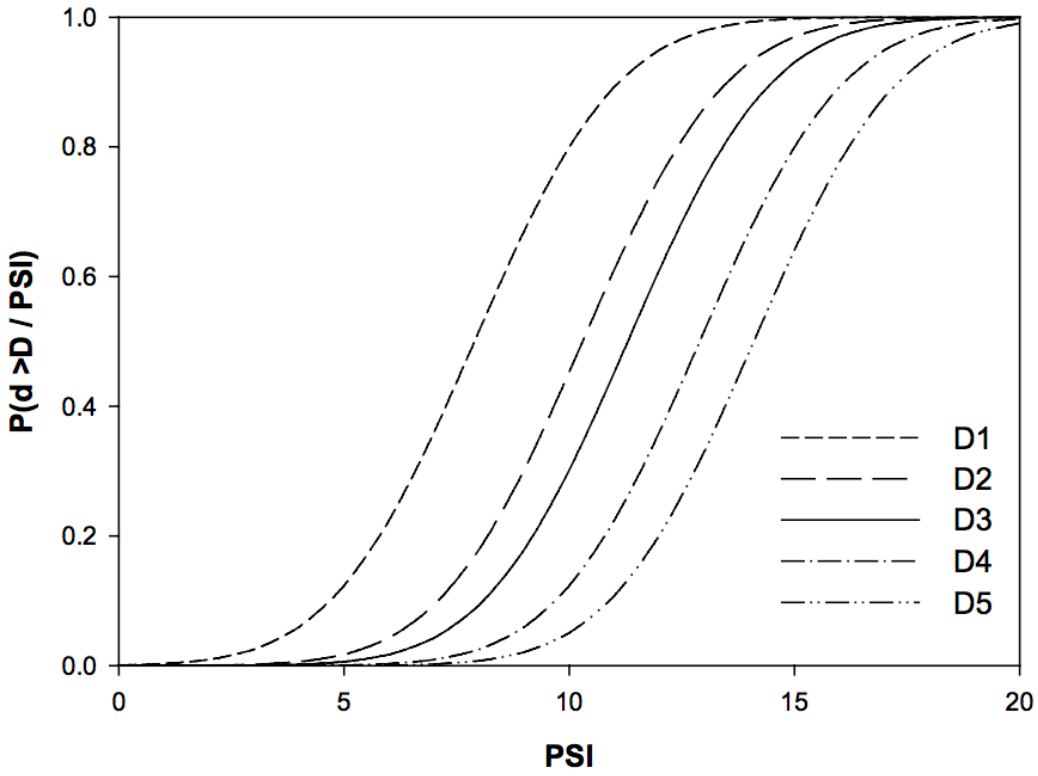

Figure 2.11 Vulnerability curves produced by Spence et al. (1992) for bare moment-resisting frames using the parameterless scale of intensity (PSI); D1 to D5 relate to damage states in the MSK scale

2.3.2 Analytical methods

Analytical approach depends on the possibility of determining the response of a particular building through employing structural analysis techniques and numerical tools. Analytical methods could feature some more detailed and transparent vulnerability assessment algorithms with physical meaning. The reliability is highly depending on the numerical tools available and specific

data available. The calibration is necessary due to various characteristics of building stock and hazard, which could be useful for loss assessment approaches. Analytically-derived vulnerability curves and DPMs with the help of computational analyses could be very good methods for seismic risk assessment, see flowchart illustrated in Figure 2.12.

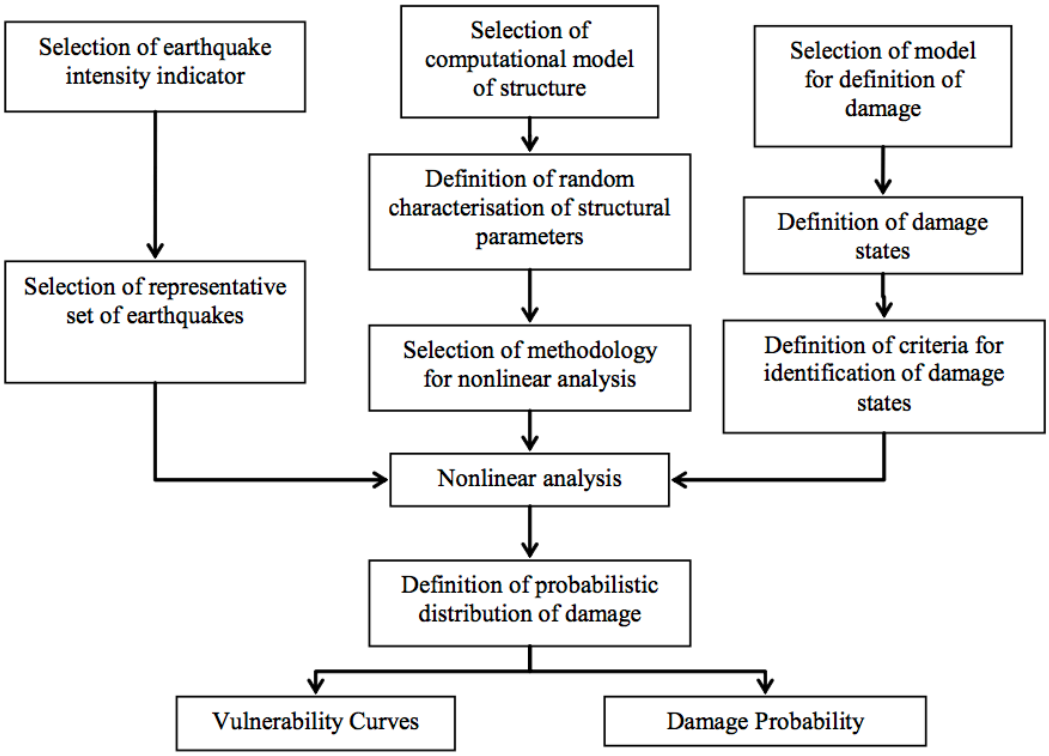

Figure 2.12 Flowchart to describe the components of the calculation of analytical vulnerability curves and damage probability matrices (Dumova-Jovanoska. 2004)

Fragility curves and damage probability matrices for reinforcement concrete frame structures by using Monte Carlo simulations developed by Singhal and Kiremidjian (1996). The evaluation of the probabilities of different damage states requires statistical analysis of damage indices and finally fragility functions and DPMs were evaluated (Figure 2.13 and Table 2.2)

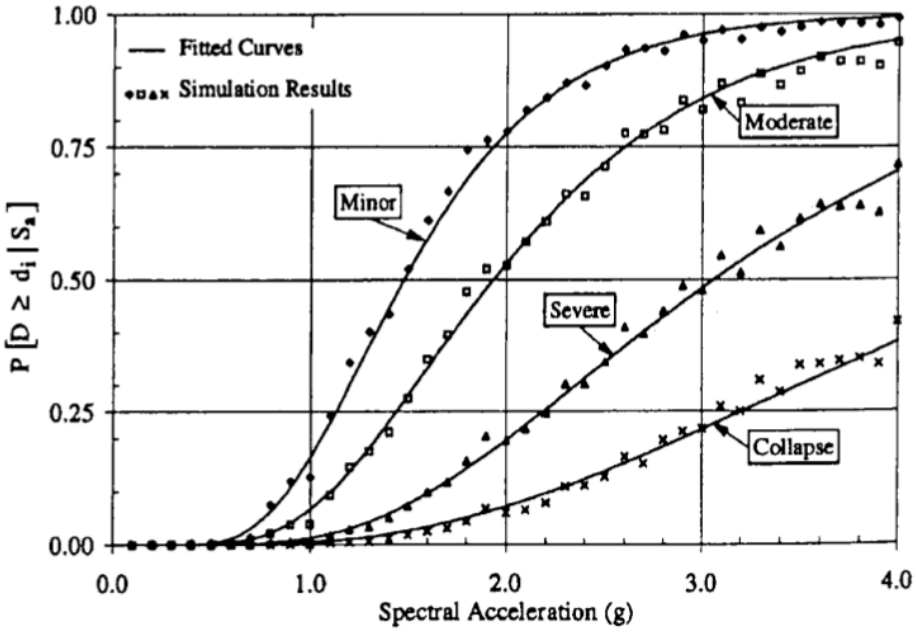

Figure 2.13 Fragility curves for sample low-rise buildings (Singhal & Kiremidjian. 1996)

Damage state (1)	Modified Mercalli Intensity VI (2)	VII (3)	VIII (4)	IX (5)	X (6)	XI (7)	XII (8)
None	99.5	97.0	85.4	52.9	14.1	0.9	—
Minor	0.3	1.6	6.9	16.9	15.5	3.4	0.1
Moderate	0.2	1.1	5.4	18.5	30.5	17.6	2.8
Severe	—	0.2	1.4	7.0	20.7	28.0	14.6
Collapse	—	0.1	0.9	4.7	19.2	50.1	82.5

Table 2.2 Damage probability matrix for sample low-rise buildings (Singhal & Kiremidjian. 1996)

The derivation of analytical vulnerability curves is that the procedure is extremely computationally intensive and time consuming. Therefore, for different areas or countries with diverse construction characteristics the curves couldn't be easily developed.

2.3.3 Hybrid Methods

Hybrid methods are based on estimating the seismic vulnerability by using different methods, from simplified to more sophisticated ones that are characterized by features derived from either empirical or analytical approaches. This implies that the hybrid approaches, based on more than one

method to estimate the seismic vulnerability, are generally very adaptable to heterogeneous data, since they allow choosing. Therefore, if the level of information on a building is detailed, the most advanced method in the hybrid approach is favored; otherwise, a simplified approach is adopted, if the level of information on a building is not accurate.

Hybrid methods refer that hybrid damage probability matrices, vulnerability functions combine the post-earthquake damage statistics with simulated, analytical damage statistics from a mathematical model of the building typology under consideration. When damage data at certain intensity levels for the geographical area under consideration is not available, hybrid models have particularly advantages. Moreover, it would be required to produce a complete set of analytical vulnerability curves of DPMs.

Kappos et al., (1998) was considered as the first one to develop the hybrid approach, who proposed a method involving elements from both empirical and theoretical methods. A model for correlating analytically calculated structural damage indices to loss (in monetary terms) is also proposed and calibrated against available statistical data. Probability damage matrices (Whitman et al., 1973) derived using this methodology are incorporated into a cost-benefit model tailored to the problem of estimating the feasibility of seismic interventions in existing building stocks.

Most recently, hybrid method proposed by Maio et al., 2015 based on the integration of TREMURI software (Lagomarsino et al., 2013) with the VIM by Vicente et al. (2014) and Formisano (2012). This approach was applied on the urban block of San Pio delle Camere in Abruzzo (Italy) damaged by the earthquake in 2009 with epicenter in L'Aquila.

2.4 Probabilistic Seismic Risk Assessment

Seismic risk analysis relates a set of earthquakes, the correlations between the damage or loss and the probabilities of occurrence of the damage during different time periods, as follows.

$$P(\text{damage exceeds } d/\text{earthquake}) = P(D>d|E,S)$$

Where P(D>d) is the probability of exceedance of the damage level d. E is the earthquake source; and S means site parameters.

Pratically, the probability of seismic risk is estimated as a function of a ground motion Intensity Measure (IM)

$$\mathrm{P(D > d)} = \int P(D > d|IM) \times d\lambda(IM > im)$$

Where P($D>d|IM$) is called fragility function and $\lambda(IM > im)$ is total frequency. Seismic hazard at one site is represented as the IM exceeds an intensity measure level *IM*.

A comprehensive framework for Probabilistic Seismic Risk Analysis (PSRA) has been created by the development of Performance-Based Earthquake Engineering (PBEE) (Cornell and Krawinkler, 2000; Krawinkler, 2002), which is based four conditional random variables. Here we have to clarify these four variables as follows.

The ground motion Intensity Measure(IM) is considered as a quantitative measure of ground motion shaking intensity such as PGA, Sa(T_0) and Sd(T_0).

The engineering demand parameter(EDP) is considered as a quantitative measure of maximum demand on the asset such as interstory drift.

The component-specific damage measure(DM) represents a discrete component damage state such as crack width.

The decision variable(DV) refers to the outcome of the earthquake such as the exceedance of damage limit states or economic loss, repair lost.

In PBEE-PSRA, the total probability integral could represent the annual rate of the DV shown in the following equation. And the components are shown in the Figure 2.14.

$$\lambda(\mathrm{DV}) = \int_{DM} \int_{EDP} \int_{IM} G(DV|DM) \times dG(DM|EDP) \times dG(EDP|IM) \times d\lambda(IM)$$

The more detailed explanation is illustrated clearly in Figure 2.14.

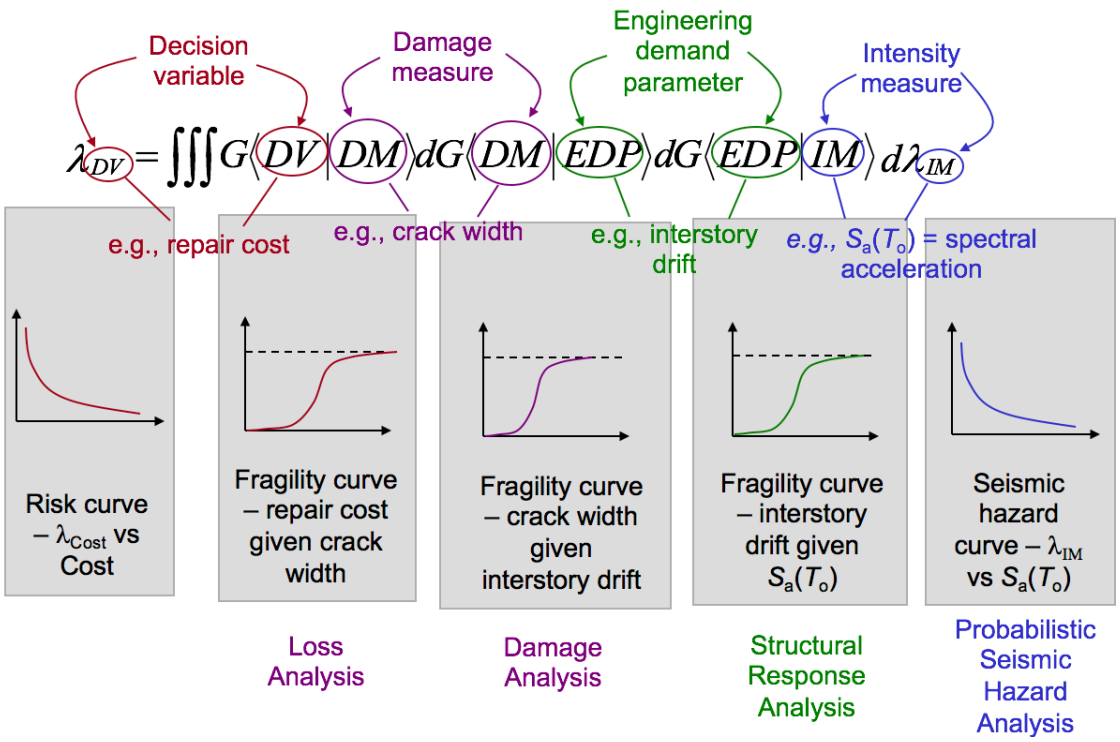

Figure 2.14 Components of seismic risk assessment (Courtesy Prof. S. Kramer 2012)

where $\lambda(DV)$ is the annual rate of the probability of exceedance of the decision variable DV;

G(DV|DM) represents the probability of exceedance of the decision variable given a damage measure (DM); dG(DM|EDP) is the derivative of the probability of exceedance of the damage measure given an EDP (e.g., story drift ratio, peak floor acceleration); dG(EDP|IM) is the derivative of the probability of exceedance of the EDP given an Intensity Measure (IM); and $d\lambda(IM)$ is the derivative of the probability of exceedance of the intensity measure.

The final aim is to obtain the risk curve by several analysis procedures, i.e. loss analysis, damage analysis, structure response analysis and probabilistic seismic hazard analysis.

3. The case study: Beijing, China

3.1 Seismic Risk in Beijing Area

Many catastrophic earthquakes occurred in China from 2000 to 2016, such as the Wenchuan earthquake on 12 May 2008, the Ya'an earthquake on 20 April 2013, which cause huge overall losses, see Table 3.1 and Figure 3.1 (Munich RE: https://www.munichre.com). These facts demonstrate that seismic risk assessment for China is a crucial issue nowadays, especially for the urban area with high concentration population, such as the capital city of China, Beijing.

5 Costliest earthquake / tsunami events in China 2000 – 2016 ordered by nominal overall losses					
Date	**Event**	**Affected Area**	**Overall losses(US$m, original values)**	**Insured losses (US$m, original values)**	**Fatalities**
12 May 2008	Earthquake	Sichuan, Mianyang, Beichuan, Wenchuan, Shifang, Chengdu, Guangyuan, Ngawa, Ya'an, Ziyang, Meishan, Suining, Garzê, Neijiang, Gansu, Shaanxi, Chongqing, Yunnan, Maoxian	85,000	300	87,149
20 Apr. 2013	Earthquake	Sichuan, Ya'an, Baoxing, Baosheng, Lingguang, Taiping, Zignong, Deyang, Meishan, Neijiang	6,800	23	196
3 Aug. 2014	Earthquake	Yunnan, Ludian, Qiaojia, Zhaoyang, Huize	5,000		617
7 Sep. 2012	Earthquake, Landslides	Yunnan, Yiliang, Guizhou	1,000	45	89
21 Jul. 2013	Earthquake	Gansu, Dingxi, Longnan	1,000		95

Table 3.1 5 Costliest earthquake from 2000 to 2016 in China ordered by nominal overall losses (Munich RE: https://www.munichre.com).

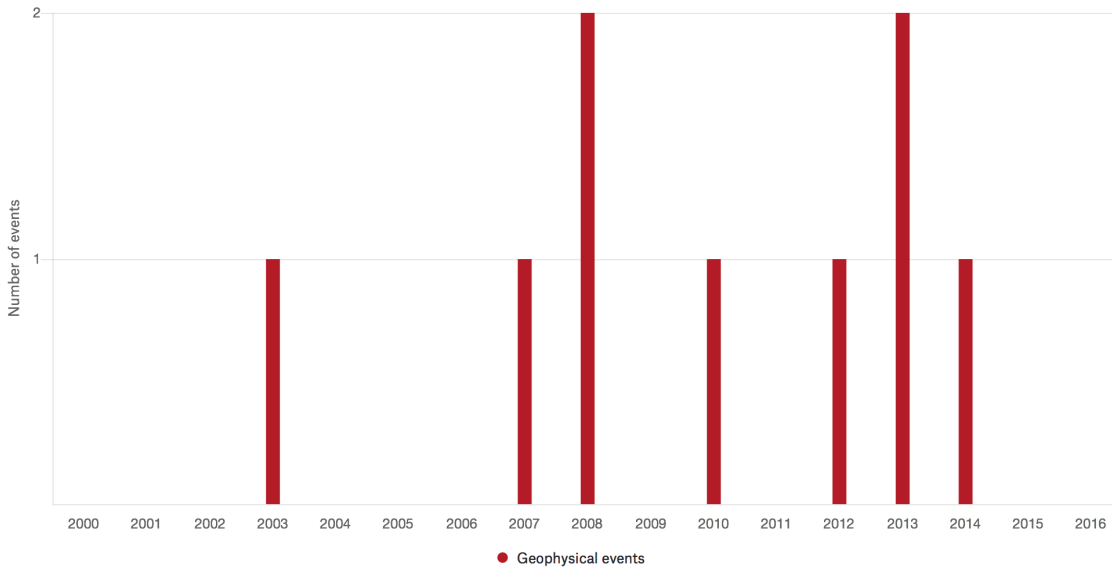

Figure 3.1 Number of catastrophic earthquake events in China from 2000 to 2016(Munich RE: https://www.munichre.com).

Beijing is the capital city in China and one of the megacities in the world with more than 20 million inhabitants within the municipality, which has an area of 16,4411 km^2 for municipality with a high GDP (Gross Domestic Product) of 2.5 trillion RMB (391 billion dollars) in 2016 (National Bureau of Statistics of China).

Beijing is exposed to high seismic threat and in the past many destructive earthquakes have occurred in this area around Beijing, with magnitude varying from Mw 6 to Mw 6.5 (Gu et al. 1983). Therefore, it is very crucial to carry out the assessment of seismic risk in Beijing area, especially for the locations with high-rise buildings.

Beijing city is located in the northwestern of North China Plain, where the Taihangshan Mountain is in the west and the Yanshan Mountain is in the north (Gao et al. 2004). Figure 3.1 shows the contour of depth of the sedimentary base in Beijing area, which shows that the topography of northwestern part is higher and the southeastern part is lower. The deep basin of more than 1000 m depth is very near to Beijing, which will cause very adverse site amplification effects when earthquake occurs.

From the Figure 3.2, we could see the Shunyi-Qianmen fault very clearly, which crosses the urban area in Beijing city. Regarding this, it is necessary to analysis the seismic scenarios for Beijing city.

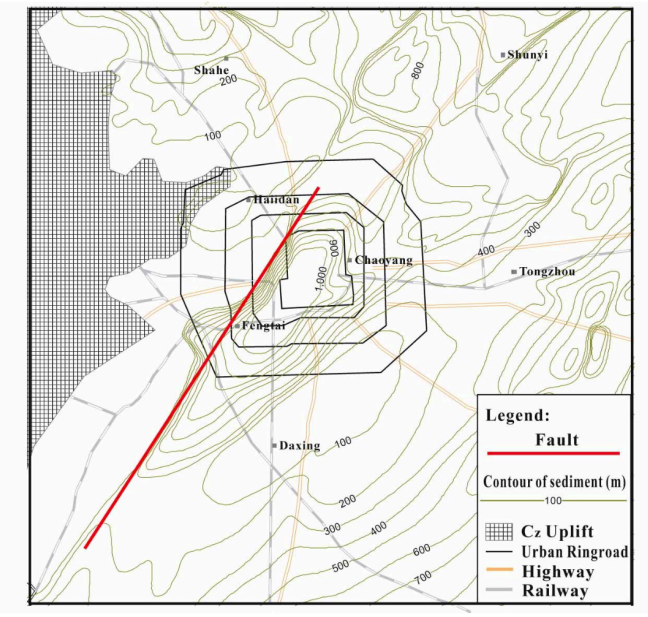

Figure 3.2 Fault in Beijing area (Gao et al. 2004)

Seismic Hazard Map in China, as shown in Figure 3.3, has seven levels: <0.05g, 0.05g, 0.10g, 0.15g, 0.20g, 0.30g and ≥0.40g, according to the seismic peak ground acceleration (PGA) in each region and the 10 % of probability of exceedance in the class (medium hard) site over 50 yr. You could see that in Beijing Area, the PGA is pretty high, which means Beijing area is high seismic hazard zone and Beijing area is vulnerable to seismic hazard.

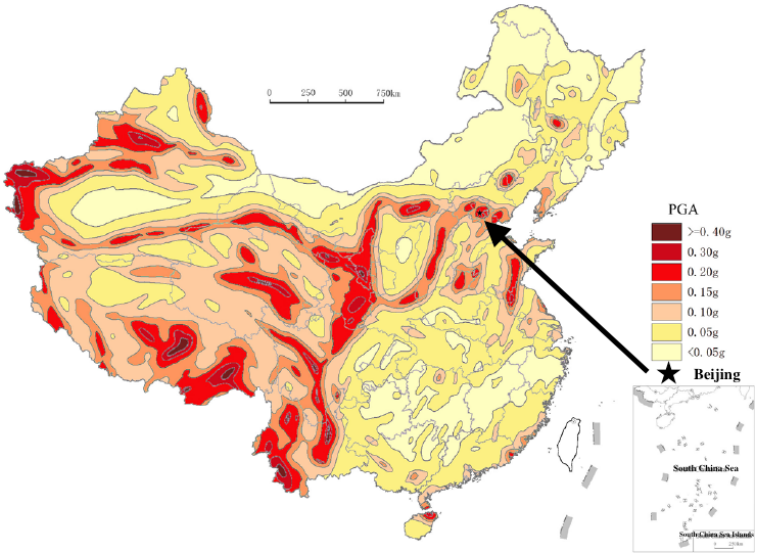

Figure3.3 Seismic Hazard Map of China, 10% probability of exceedance in the class (medium hard) site over 50 years of peak ground acceleration, return period 475 years (Li et al. 2013).

From Figure 3.4 China population density map, it is easy to see that Beijing is a city with extremely high population density, which means large numbers of people are exposed to the seismic hazard. Therefore, seismic hazard analysis for Beijing area is a crucial topic.

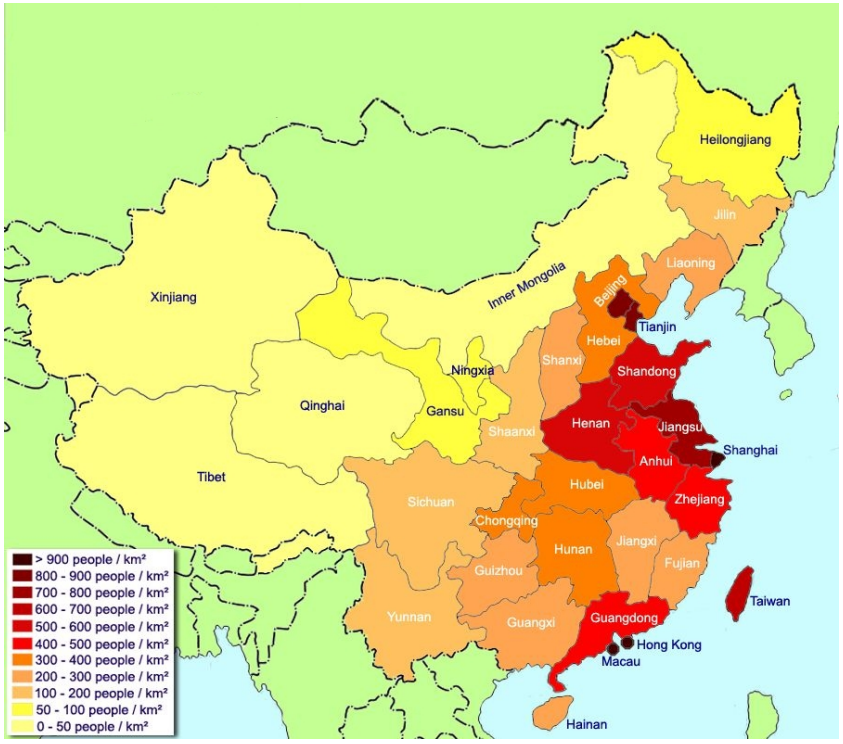

Figure 3.4 China population density map (China Mike: http://www.china-mike.com)

To accommodation the increasing urban population, high-rise buildings could be a good solution, especially for megacities, like Beijing. Nowadays, there are many high-rise buildings built or under construction in Beijing city. The already built tall buildings over 120 m are listed in the Table 3.2, from where you could observe that the height of most of high-rise buildings are less than 200 m.

No.	Name	Height [m/ft]	Floors	Year
1	China World Trade Center Tower 3	330 / 1,083	74	2009
2	Fortune Plaza Office Building 1	260 / 853	63	2008
3	Park Tower	250 / 820	63	2007
4	Beijing TV Centre	239 / 784	41	2006
5	CCTV Headquarters	234 / 768	51	2009
6	Jing Guang Center	208 / 682	53	1989
7	Pangu Plaza Office Building	192 / 629	39	2008
8	Yintai Office Tower	186 / 610	42	2007
9	PICC Office Tower	186 / 610	42	2007
10	Capital Mansion	183 / 602	52	1990
11	China Central Place Tower 1	167 / 548	36	2006
12	TVCC	159 / 522	31	2009
13	Fortune Plaza Office Building II	155 / 509	46	2005
14	China World Trade Center Tower II	155 / 509	39	1999
15	China World Trade Center Tower I	155 / 509	39	1989
16	China Central Place Tower 2	151 / 495	32	2007
17	Zhongguancun Financial Center	150 / 492	37	2006
18	Central International Trade Center - Tower B	150 / 492	36	2005
19	Beijing Silver Tower	145 / 476	32	1997
20	LG Twin Tower 1	141 / 461	30	2005
21	LG Twin Tower 2	141 / 461	30	2005
22	Central International Trade Center - Tower A	139 / 455	34	2005
23	Crown Tower A	138 / 453	38	2004
24	Central International Trade Center - Tower D	136 / 445	33	2005
25	China Central Place Tower 3	135 / 443	28	2007
26	Anzhen Building	131 / 430	30	1999
27	Beijing World Financial Center	131 / 429	32	1998
28	Central International Trade Center - Tower D	127 / 415	32	2005
29	Cyber Tower A	125 / 410	28	2001
30	Kerry Centre North Tower	124 / 405	31	1998
31	Kerry Centre South Tower	124 / 405	31	1998
32	Fortune Plaza Apartments I	123 / 404	40	2005
33	Beijing Tengda Building	123 / 404	33	2000
34	Jinggang City Plaza	121 / 397	34	1995
35	SOHO Tower A	120 / 394	42	2001

Table 3.2 high-rise buildings over 120 meters built in Beijing (Sky Scraper Page: http://skyscraperpage.com)

3.2 3D physics-based numerical simulations

For seismic hazard assessment studies, especially for earthquake ground motion prediction, empirical ground motion prediction equations(GMPEs) and 3D physics-based numerical simulations(3DPBNS) are two main tools. GMPEs have some limitations of these conditions, such as near-source, soft soil sites, complex geological irregularities, large earthquake magnitude, which will decrease the reliability of probabilistic seismic hazard assessment (PSHA) results.

Nevertheless, in recently years, 3D physics-based numerical simulations of seismic wave propagation from source to the site have emerged as a powerful tool for advanced seismic hazard assessment studies (e.g. Graves et al.2010).

3D physics-based earthquake ground motion simulations could be used to create a numerical simulation of earthquake ground shaking scenarios as realistic as possible in terms of all the factors that affect the earthquake ground motion, i.e.: the propagation path in heterogeneous Earth media, directivity of seismic waves, complex site effects due to the localized topographic and geologic irregularities, the features of the seismic fault rupture, variability of soil properties at a regional and local scale and sit or soil structure interaction.

The procedure to generate 3D numerical simulations is illustrated in Figure 3.5 and consists of the following steps.

（i） Collect the input data (identification of the active faults, geological and geotechnical characterization, topography and bathymetry model).

（ii） Setup 3D numerical model with the previous information.

（iii） Produce a set of kinematic slip models along a given fault within a prescribed magnitude by using a pre-processing tool such as a rupture generator.

（iv） Numerical simulation through SPEED code running on parallel computer architectures.

（v） Generate broadband (BB) ground motions starting from the results of SPEED by using a post-processing tool based on an Artificial Neural Network (ANN).

3D physics-based numerical simulations have many advantages. First of all, obviously it could model complex interaction of source effects such as directivity and irregularities of localized soil. Besides, 3D variability of the dynamic properties of soils, could be described, which have an impact on the spatial variability of ground motion. It also could model the full wave field from the extended fault rupture to the site of interest. All above, it is possible to generate realistic scenarios from future earthquake concerning for the seismic hazard at the site.

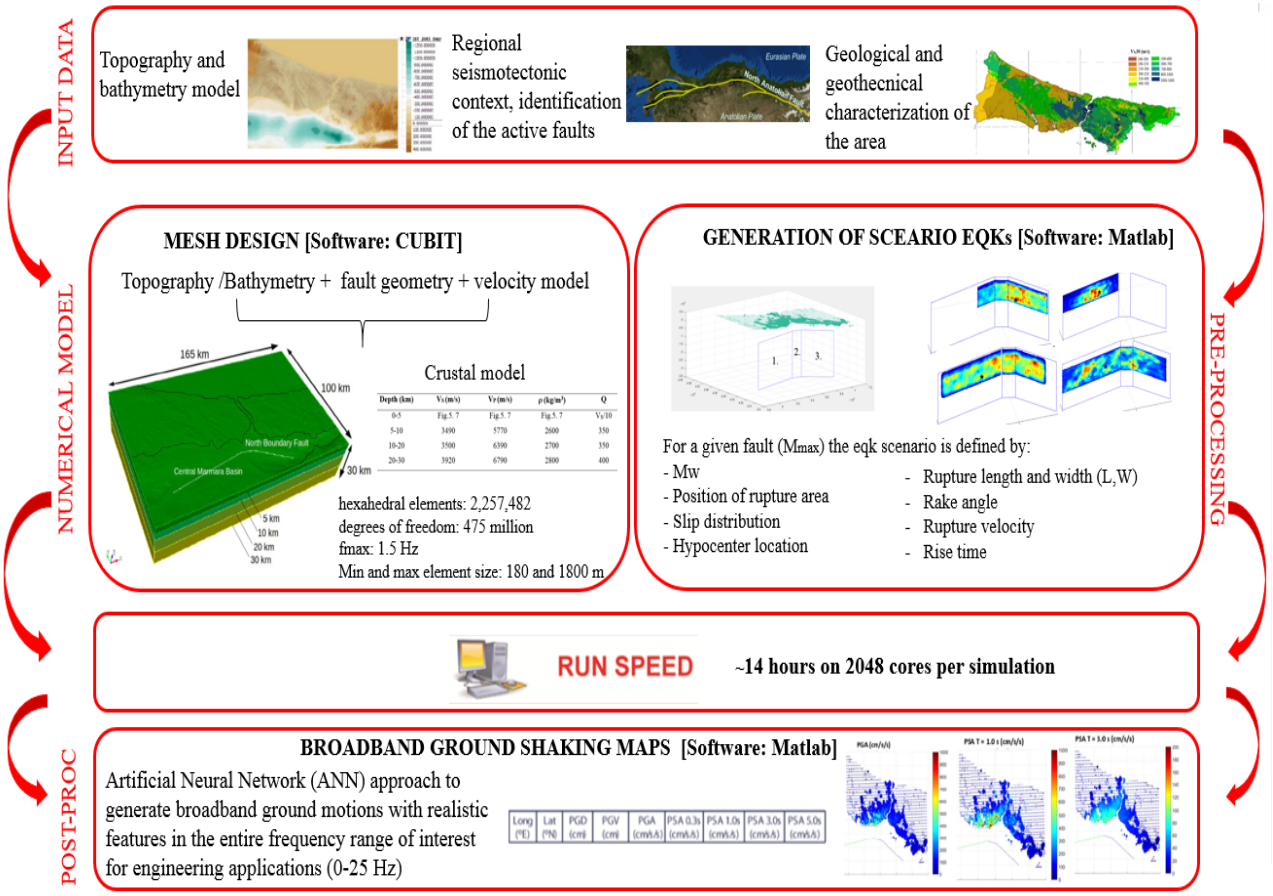

Figure 3.5 Procedure to generate 3D Numerical simulations

Nevertheless, despite the benefits of using the numerical simulations, there are some drawbacks related the use of such an approach, specifically:

(i) Difficulties in construction large-scale 3D meshes including all the features mentioned above, i.e. seismic fault rupture, crustal Earth model, topography, complex geologic irregularities, variability of soil properties, within a single model. It requires the coexistence of extremely different spatial scales to include all these features.

(ii) Too much computational cost due to large size of the model.

(iii) High level of details of input data required (identification of the active faults, geological and geotechnical characterization, etc.)

(iv) Limitation of the frequency range reliable to 1 or 2Hz.

	PROs	CONs
GMPE	- ease-of-use - calibrated on records - adapted to different tectonic environments and site conditions	- lack of records to solve important conditions, such as near-source and complex geological environments - only peak values of motion - recalibration when new data are available - no correlation of ground motion intensities among multiple sites and among different spectral periods
3DPBNS	- flexibility to produce synthetics in arbitrary site and source conditions - parametric analyses allowed - spatial correlation of simulated ground motion - insight into the earthquake physics	- high-frequency computational and modelling limit - high computational costs - need of expert users - hardly available information to construct a reliable 3D model - large epistemic uncertainties - few well documented validation case studies on real earthquakes

Table 3.3 Advantages and limitations of GMPEs and 3DPBNSs (Paolucci et al. 2017)

Table 3.3 summarizes that the advantages and limitations of GMPEs and 3DPBNS. All above, regardless of the limitations, 3D numerical approaches are expected to be the most promising tool to generate ground shaking scenarios from future realistic earthquakes.

3.3 3D model for Beijing area

For Beijing area, the 3D numerical model comprises the following features: the topography model; ii) a kinematic model for the seismic fault rupture; iii) the 3D basin model, defined from the depth of basement of sedimentary deposits and shear wave velocity profiles.

For the elevation model, free-available digital elevation dataset of CGIAR-CSI for the Beijing region has been downloaded from the website http://www.cgiar-csi.org(with a precision of roughly 90x90 m^2, for east-west and north-south directions around Beijing city). The Shunyi-Qianmen-Liangxiang(SQL) fault, lying across the urban area of Beijing (see the superimposed line in Figure 3.6), has been considered as the seismic fault. The total length of the fault is around 90 km. The source is a quasi-vertical segmental fault (with dip angle of about 80°), considering approximately of

three main segments with different strike angles.

In order to define the 3D velocity model, the sediments thickness derived from the digitalization of the map proposed in Gao et al. (2004) and the V_{S30} (shear wave velocity in the top 30 m) map of the area were used (see Figure 1 left and center). For the first layer at depths between 0 and 2 km, the shear wave velocity map (V_S) of Figure 4.2 (right) was used. The properties of the underlying bedrock layers (depth > 2 km) have been selected in agreement with Gao et al. (2004). The quality factor Q_S is estimated directly by the V_S values and is assumed to be proportional to frequency, for the target value $Q_S = V_S/10$ to be obtained at frequency f = 1 Hz.

The computational model was then set up by combining all information above and extends over an area of 70x70 km^2 down to 30 km depth, as illustrated in Figure 3.7. The conforming mesh has a size varying from a minimum of 150 m, on the top surface, up to 600 m at 4 km depth and reaching 1800 m in the underlying layers. The model consists of 859,677 hexahedral elements, resulting in approximately 160 million degrees of freedom, using a fourth order polynomial approximation degree. Considering a rule of thumb of 5 grid points per minimum wavelength for non-dispersive wave propagation in heterogeneous media by the spectral element approach, the model can propagate up to a maximum frequency f_{max} = 1.5 Hz.

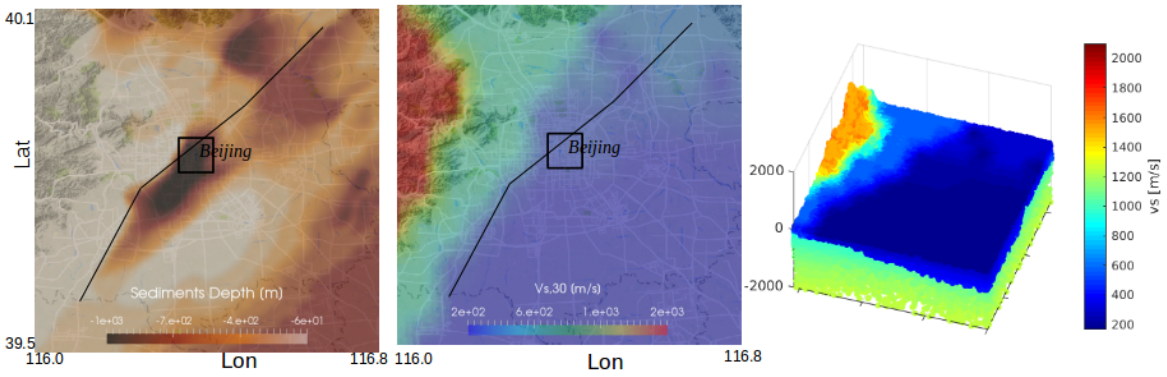

Figure 3.6 Sediment thickness (left), V_{S30} model (center) and $V_S(z)$ model (right) for the first layer 0-2 km.

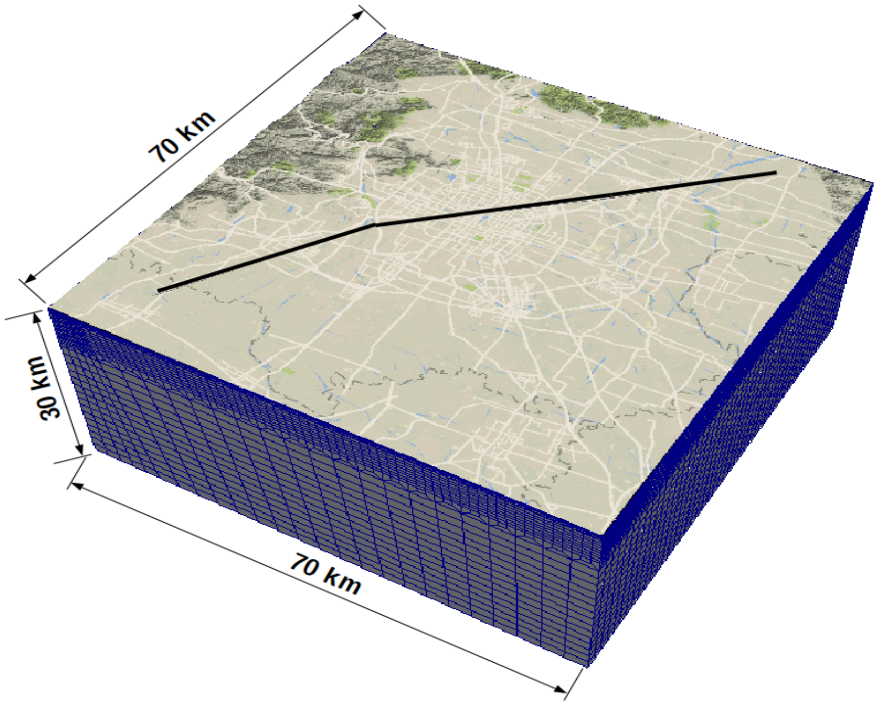

Figure 3.7 3D computational model for the Beijing area. Black segments represent the trace of the considered Shunyi-Qianmen-Liangxiang fault.

3.4 3D scenarios for Beijing cases

In total 30 scenarios have been simulated by different magnitudes (Mw 6.5, Mw 6.9 and Mw 7.3), the kinematic slip distribution, the hypocenter location and location of the rupture area.

The simulations were performed on the Marconi cluster at CINECA, Italy (http://www.cineca.it/en/content/marconi). Each simulation takes around 12 hours on 512 cores. To automatically construct N physically constrained slip distributions for a given fault and a given earthquake magnitude, a pre-processing tool has been devised taking into account joint probability distributions of the main kinematic parameters, which can ensure that the resulting scenario variability will not be affected by systematic bias in the input parameters. In particular, we considered the kinematic source rupture generator proposed by Crempien and Archuleta (2015). Note that for each scenario, the rupture velocity follows the built-in scheme proposed in previously quoted paper, and the source time function is a simplified smoothed Heaviside function. A time step equal to 0:001 s has been chosen and a total observation time T = 60 s has been considered. In order to model the non-linear soil behaviour of the soft soil deposits (VS30 <= 400 m/s) in

the top 300 m, a simple Non-Linear Elastic (NLE) soil model has been considered. Coordinates of the hypocenters, magnitude and source model of the scenarios are summarized, see Table 3.3.

ID Senario	Mw	Lon(degree)	Lat(degree)	Z(m)
S1	6.5	116.34	39.86	-13560.73
S3	6.5	116.46	39.96	-8513.78
S4	6.5	116.37	39.90	-10946.46
S5	6.5	116.42	39.94	-10047.94
S6	6.5	116.41	39.92	-11071.71
S7	6.5	116.42	39.93	-9429.93
S8	6.5	116.34	39.87	-10815.14
S9	6.5	116.39	39.91	-10728.67
S10	6.5	116.42	39.94	-7477.28
S11	6.5	116.46	39.96	-9885.77
S28	6.5	116.48	39.95	-10411.45
S29	6.5	116.28	39.76	-10389.65
S30	6.5	116.28	39.76	-10389.65
S13	6.9	116.28	39.76	-12092.64
S14	6.9	116.43	39.90	-11718.23
S16	6.9	116.36	39.83	-10214.99
S17	6.9	116.50	39.96	-15042.88
S19	6.9	116.31	39.78	-13753.35
S21	6.9	116.35	39.82	-9869.39
S22	7.3	116.43	39.90	-13032.57
S23	7.3	116.50	39.96	-11838.66
S25	7.3	116.48	39.94	-11033.10

Table 3.3 Coordinates of the hypocenters, magnitude and source model of the scenarios.

For each scenario of Beijing, we could see know the location of the hypocenter, the situation of the fault and also the peak ground acceleration (PGA) or other values.

Some snapshots of the peak ground velocity wave field for a target scenario with magnitude Mw 7.3 are reported here, see Figure 3.8. It can be observed that the wave field propagates from south-west to north-east. Another observation is that PGV values are higher when they are closed to the projection of the fault rupture on the surface.

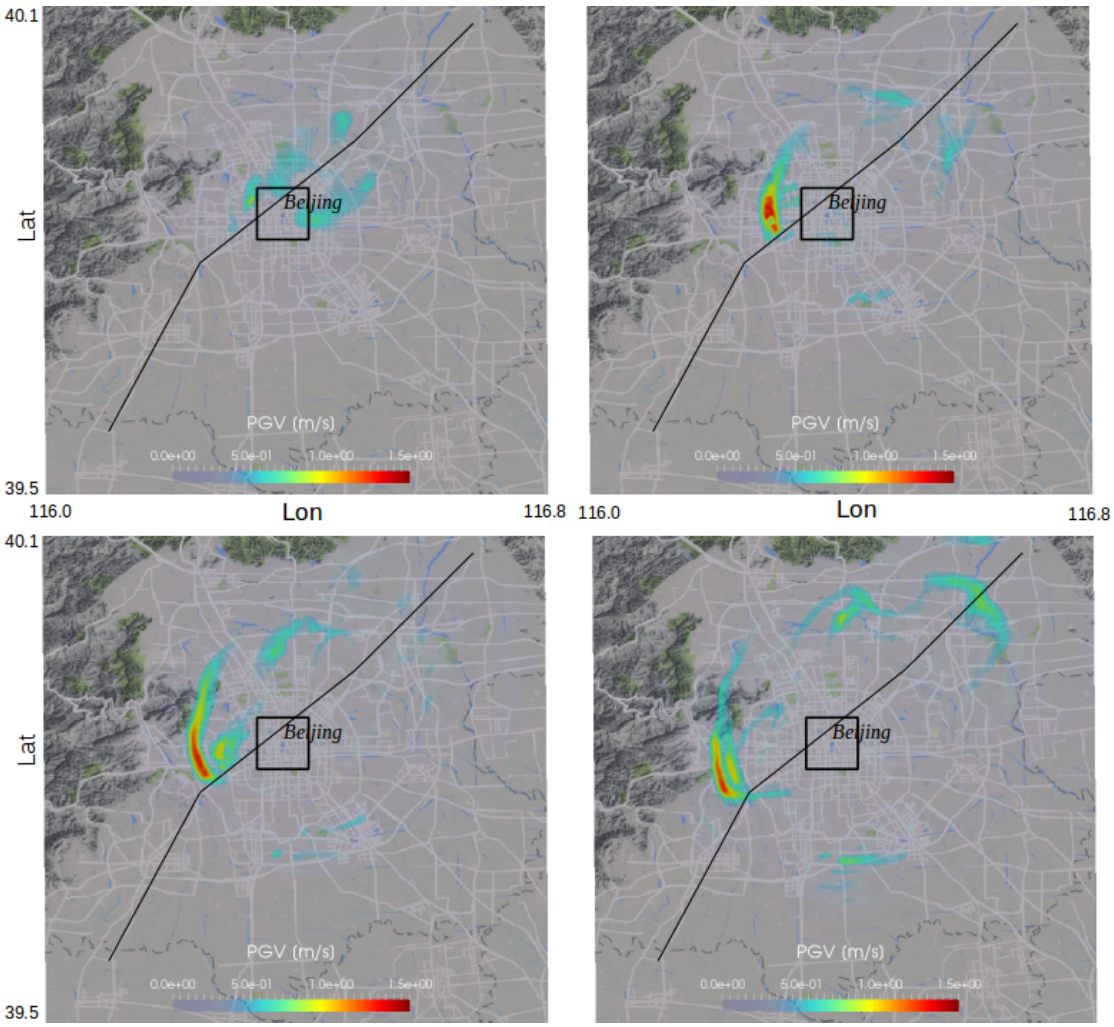

Figure 3.8. Snapshots of the PGV obtained for a scenario with Mw 7.3. Top-left: t = 8 s, top-right: t = 9 s, bottom-left: t = 10 s, bottom-right: t = 11 s.

Scenarios of maps shows the location of the hypocenter and fault, considering the distribution of PGA, PGV, PGD, and SA at certain vibration period, see the following figures.

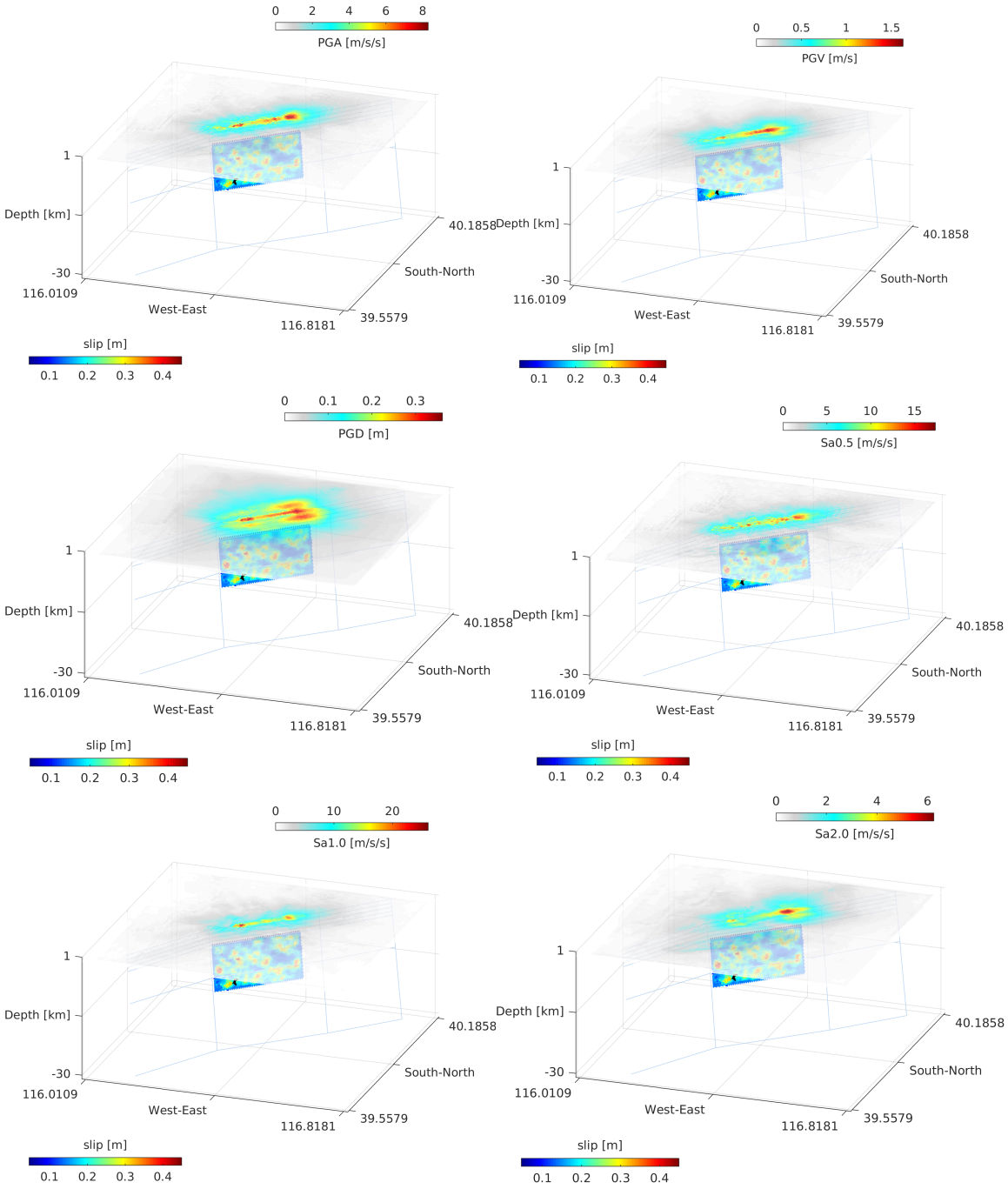

Figure 3.9 Plots of Scenario 1(Mw6.5). From right top to left bottom are the maps of relationship between depth and PGA, PGV, PGD, Spectral Acceleration（SA）(T=0.5s), SD(T=1s), SA(T=2s).

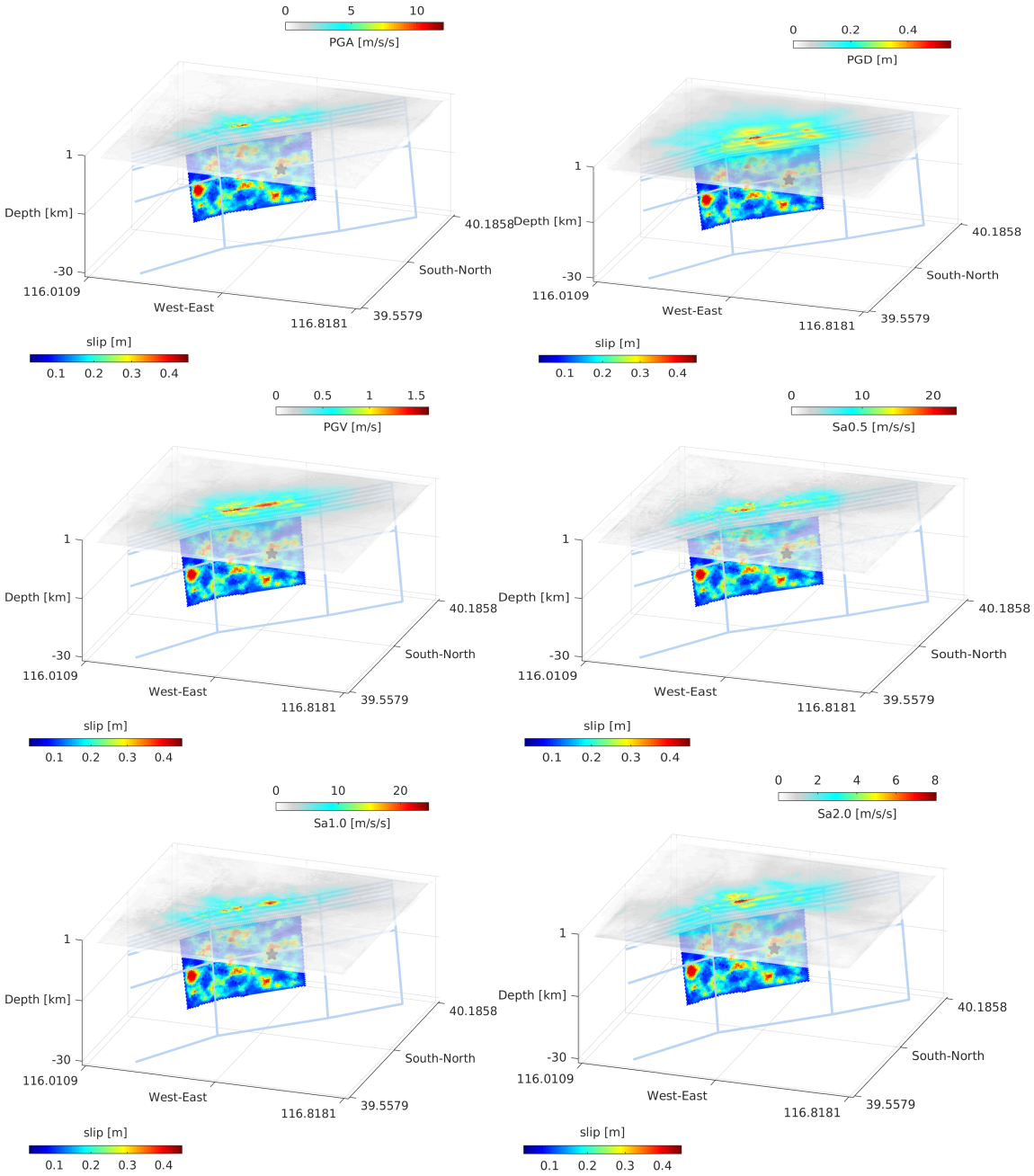

Figure 3.10 Plots of Scenario 14(Mw 6.9). From right top to left bottom are the maps of relationship between depth and PGA, PGV, PGD, Spectral Acceleration（SA）(T=0.5s), SD(T=1s), SA(T=2s).

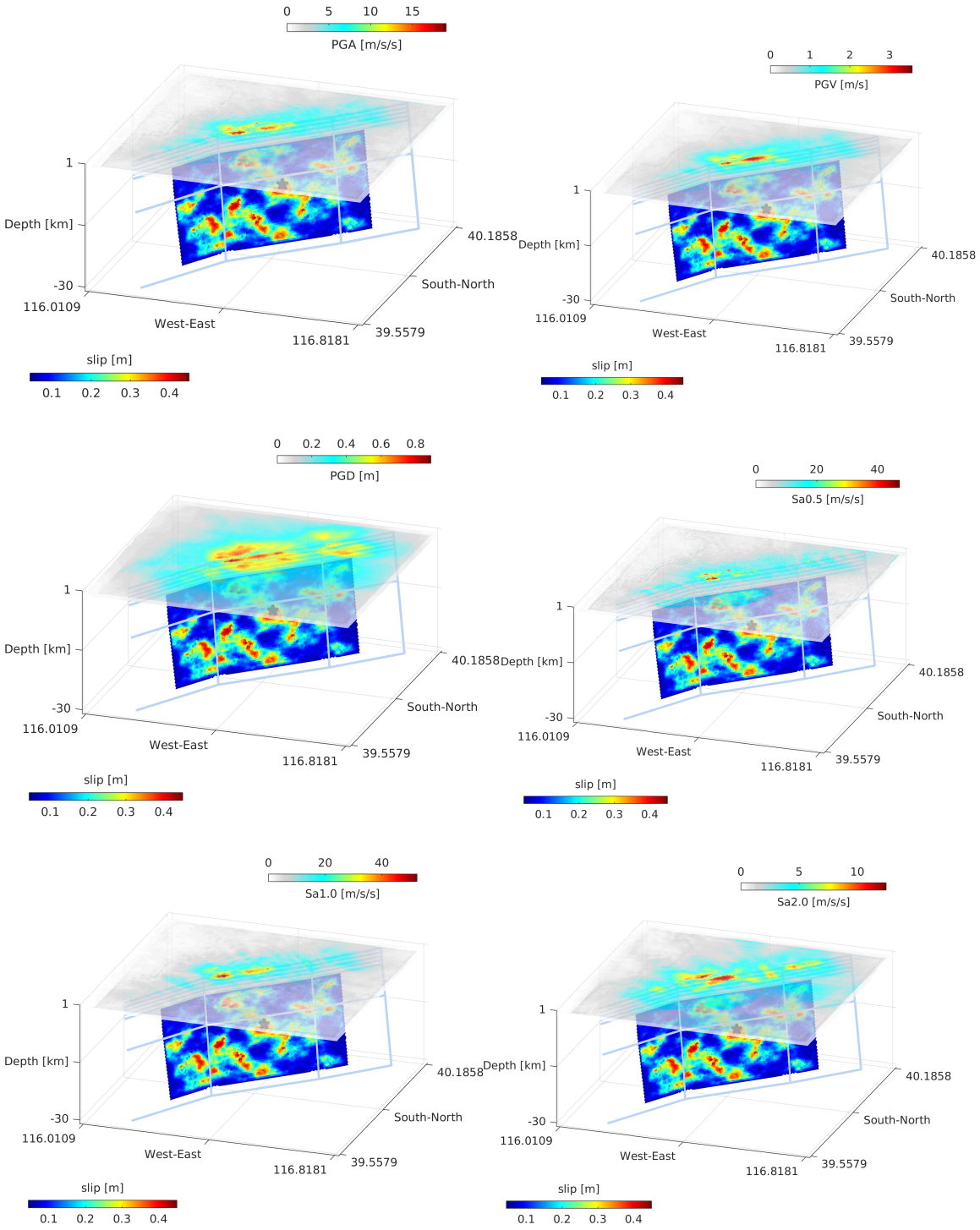

Figure 3.11 Plots of Scenario 22(Mw 7.3). From right top to left bottom are the maps of relationship between depth and PGA, PGV, PGD, Spectral Acceleration（SA）(T=0.5s), SD(T=1s), SA(T=2s).

The scenarios provided from the SPEED code is very useful for the description of characteristics of strong ground motion. Distribution of SD for different scenarios at different magnitudes were carried out, see Figure 3.12. The left part shows that the distribution of Sd at T=3s for Scenario 1 Mw6.5, the right part shows the relationship between Sd ad vibration period from 0 to 5 s for selected locations.

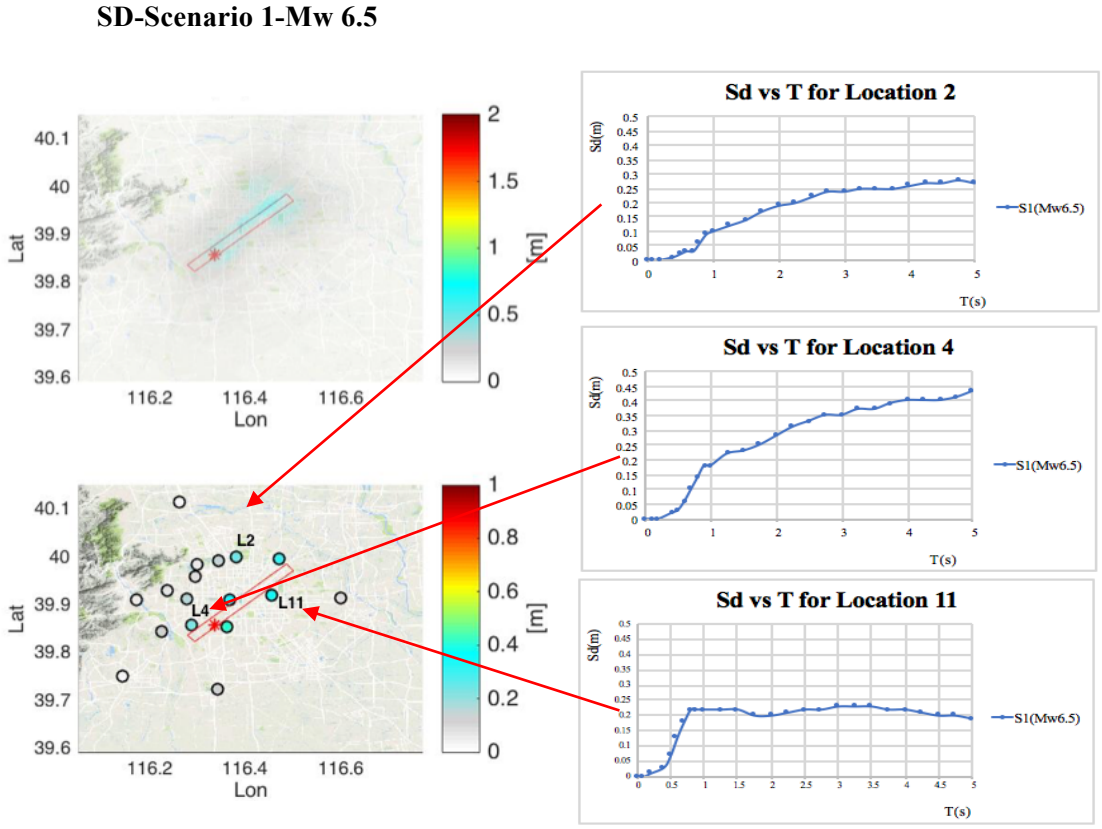

Figure 3.12 The left figure shows the distribution of SD(T=3s) for Scenario 1Mw6.5, the right part Sd vs T for selected locations

The following figures also illustrated for Mw 6.9 and Mw7.3 SD(T=3s) distribution.

SD-Scenario 14-Mw 6.9

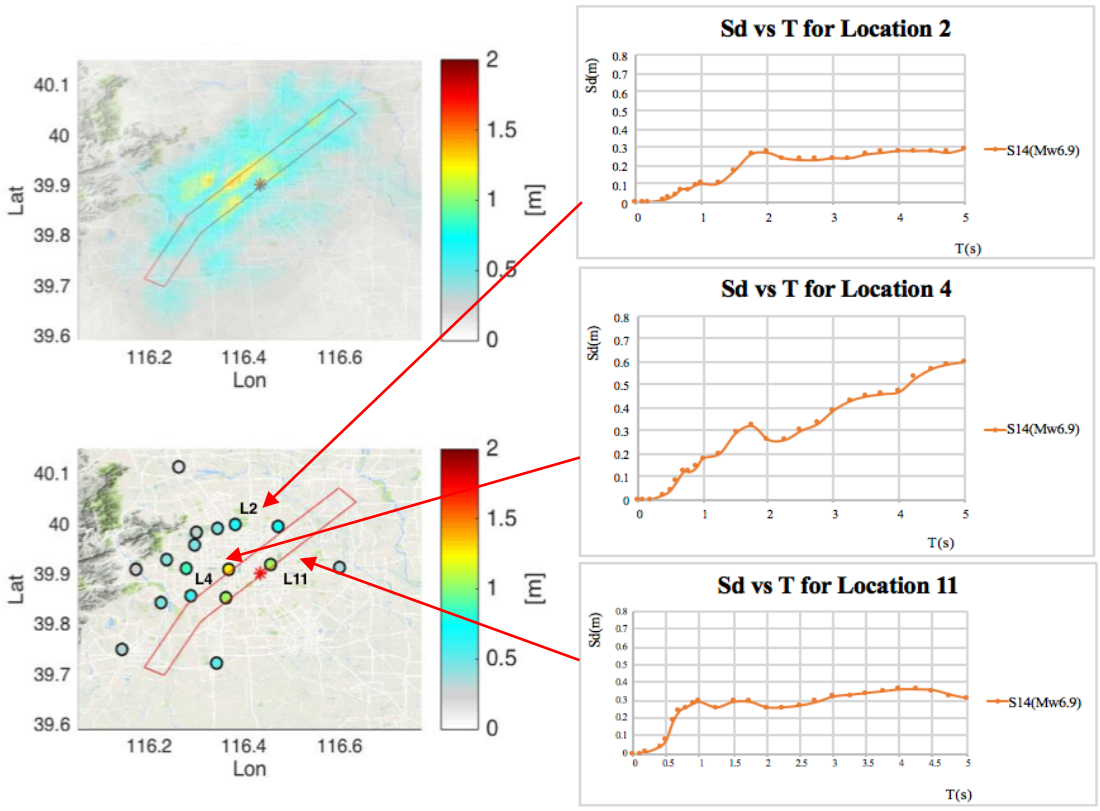

Figure 3.13 The left figure shows the distribution of SD(T=3s) for Scenario 14 Mw6.9, the right part Sd vs T for selected locations

SD-Scenario 22-Mw 7.3

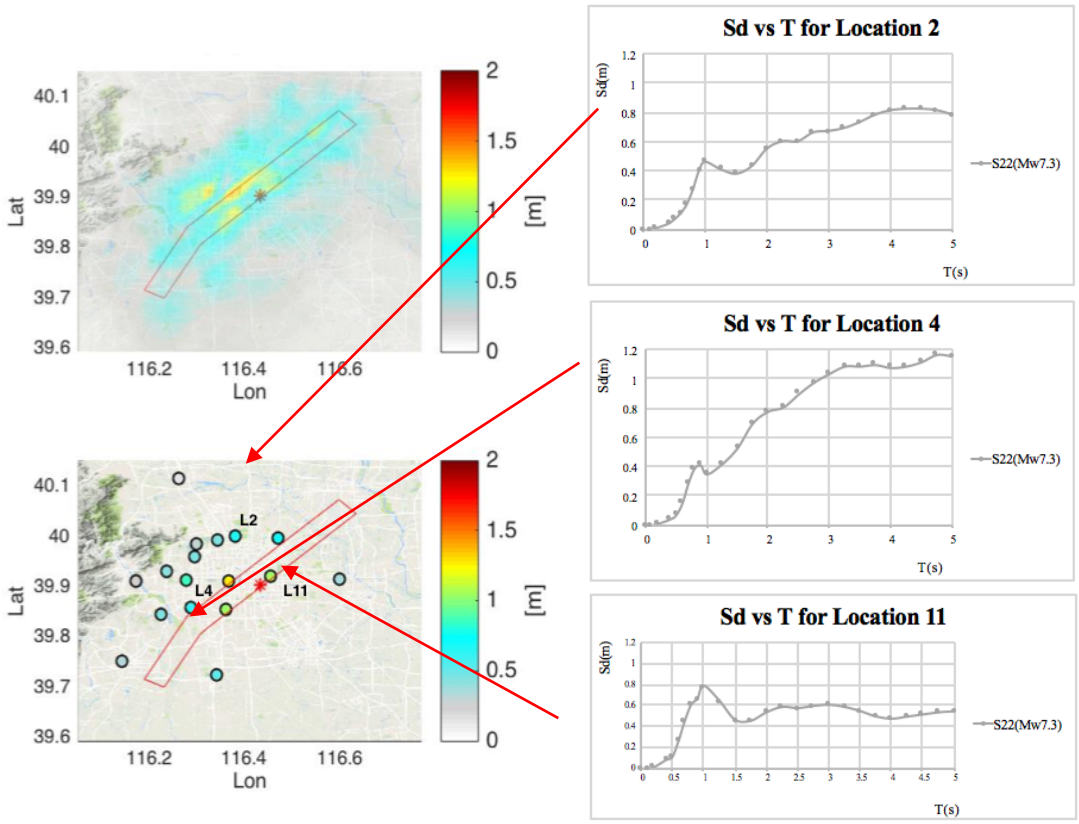

Figure 3.14 The left figure shows the distribution of SD(T=3s) for Scenario 22 Mw7.3, the right part Sd vs T for selected locations

4. Fragility curves for high-rise buildings

4.1 Fragility curve and fragility function

Seismic vulnerability assessment needs to be carried out for a particular characteristic of the ground motion, which will represent the seismic demand on the buildings. Vulnerability models aim at establishing a correlation between the ground motion intensity and the damage to the building Fragility curves represent a particular class of vulnerability models (see Chapter 2) and express a non-linear and continuous relationships between a ground motion intensity measure (IM) and the exceeding probability of damage states. A fragility curve defines the probability of exceedance of a given damage state (e.g. collapse) conditioned on the occurrence of a given level of ground motion, expressed by a specific intensity measure. In most cases, peak ground acceleration and response spectral acceleration at specific vibration periods are used as intensity measures.

To derive the fragility curve, first we have to define the fragility function. The most common form of fragility function for seismic assessment is the lognormal cumulative distribution function (CDF).

$$F_d(x) = P[D \geq d | X = x] \quad d \in \{1,2, \dots N_d\}$$

$$= \Phi\left(\frac{ln\,(x/\theta_d}{\beta_d}\right)$$

where

P[A|B] is the conditional probability of A with respect to B

D is the aleatory variable for the damage state of a particular component.

d means a particular value of D.

nD is the number of possible damage states.

X is the aleatory variable representing the excitation, i.e. the ground motion, herein the excitation is called demand parameter (DP).

x is a particular value of X

Fd(x) is a fragility function for damage state d evaluated at x.

$\Phi(s)$ is the standard normal cumulative distribution function (often called the Gaussian) evaluated at s,

ln(s) is the natural logarithm of s

θd represents the median capacity of the asset to resist damage state d measured in the same units as X.

βd is the standard deviation of the natural logarithm of the capacity of the asset to resist damage state d.

After obtaining the fragility functions, according to exceeding probability in terms of the intensity measures for the different damage states, the fragility curve is available to plot.

The following Figure 4.1 shows one general model of fragility curve, where the exceeding damage probabilities are given as a function of a generic intensity measure for 4 damage states. Therefore, the x coordinate is intensity measure, y coordinates is exceeding probability, and the maximum exceeding damage probability is 1.

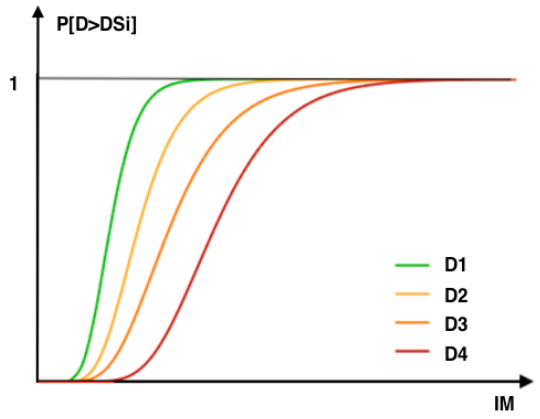

Figure 4.1 Example of vulnerability curves

4.2 Overview of literature studies

To perform the seismic risk assessment in Beijing, as a first step, a literature review has been carried out to identify the fragility curves which are suitable for the area urban study. In general, there are a few studies regarding the vulnerability assessment of high-rise buildings. In the following, the most salient publications concerning the fragility assessment of medium-rise or high-rise buildings are listed and described, see Figure 4.1. Different intensity measures are used for different references, such as Peak Ground Acceleration (PGA), Spectral Acceleration (Sa), Spectral Displacement (Sd).

Overview of fragility curves for high-rise buildings from literature review.								
	Title	**Authors**	**Geographic area of the building**	**Structure material**	**Damage State**	**Parameters**	**Story**	**Index**
1	Seismic fragility assessment for reinforced concrete high-rise buildings in Southern Euro-Mediterranean zone	Jelena Pejovic, Srdjan Jankovic	In Southern Euro-Mediterranean zone, high seismic hazard zone	RC high-rise building	4	Yes	20,30,40	PGA
2	Analytical Vulnerability Assessment of Modern Highrise RC Moment-resisting Frame Buildings in the Western USA for the Global Earthquake Model	Athanasia Kazantzi, Dimitrios Vamvatsikos, Keith Porter, In Ho Cho	In western United States, high seismic hazard area	RC tall building	4	No	7-20 story	Sa(1s)
3	Building Seismic Vulnerability Study for China High Rises	Fan Wu, Ming Wang, Xinyuan Yang	In china , high seismic hazard area	RC high-rise building	4	No	larger than 200 m; smaller than 200m.	Sd(2s)
4	An analytical framework for seismic fragility analysis of RC high-rise buildings.	Jun Ji, Amr S. Elnashai, Daniel A. Kuchma	In Jumerah beach Tower C03, low seismic hazard area	RC building	4	Yes	54	Sa(1s)
5	A procedure for establishing fragility functions for seismic loss estimate of existing buildings based on nonlinear pushover analysis.	Xiaonian Duan and Jack W. Pappin	In moderate seismic hazard zone	RC building	4	No	8-15 stories, intermediate high-rise buildings	Sd(1s)
6	Preliminary Study on the Fragility Curves for Steel Structures in Taipei.	Rwey-Hua Cherng	in Taipei, high seismic hazard zone	Steel Structure	4	No	69-103 m	Sd(3s)

Table 4.1 Overview of fragility curves for high-rise buildings from literature review (1)

Overview of fragility curves for high-rise buildings from literature review.								
	Title	**Authors**	**Geographic area of the building**	**Structure material**	**Damage State**	**Parameters**	**Story**	**Index**
7	Fragility analysis of high-rise building structure.	Sumit.A.Patel, Prof. A.R.Darji, Prof Dr. K.B. Parikh, Prof. Bhavik.R.Patel	unknown, developed country, maybe in india	RC buidling	4	NO	20	PGA
8	Performance-based Seismic Fragility Analysis of Tall Hybrid Structures	He Yi-bin , LI Yan , Shen Pu-sheng	In China	Steel frame-concrete core-wall structures	4	No	15 stories, 54m	PGA
9	Probabilistic Damage Assessment and Fragility Functions of Tall Buildings in Istanbul	Sinan Akkar,Ömer Odabaşı	Istanbul, Turkey, high seismic hazard area	RC buidling	4	No	Group 1: 15, Group 2: 25	Sa
10	Seismic Fragility Assessment for Reinforced Concrete High-Rise Buildings	Jun Ji, Amr S. Elnashai, Daniel A. Kuchma	Tower C03, in the Jumerirah Beach development, Dubai,low seismic hazard area	RC building	4	Yes (Page184)	54 stories, 184m	PGA
11	Assessment of performance of Peruvian high-rise thin RC wall buildings using numerical fragility functions	Luis G. Quiroz, Yoshihisa Maruyama	In Lima, Peru	Thin RC wall buildings	4	No	10 stories	PGA
12	Seismic Fragility And Relationships Of High-Rise Reinforced Concrete Buildings	Qaiser uz Zaman Khan, Nazakat Ali, Muhammad Yaqub, Fiaz Tahir, Mohammad Saad	In Pakistan	RC building	4	No	15, 25, ,25	PGA

Table 4.2 Overview of fragility curves for high-rise buildings from literature review (2).

4.2.1 Fragility curve as a function of PGA

The first reference focus on the study of the Seismic fragility assessment for reinforced concrete high-rise buildings in Southern Euro-Mediterranean zone, by *Pejovi J., Jankovic S.* (2016), where the PGA has been as the intensity measure. The structure material is reinforcement concrete and the analysis buildings are 20, 30, and 40 floors. The damage state is divided by no damage, slight damage, moderate damage, extensive damage and complete damage state. The details of the paper are as follows.

Reference Name.	**Seismic fragility assessment for reinforced concrete high-rise buildings in Southern Euro-Mediterranean zone**
Material	RC high-rise building
Floors	20,30,40
Damage State	5 States.
Geographical Area	In Southern Euro-Mediterranean zone, high seismic hazard zone
Intensity Measure	PGA
Parameter (Mean and Standard deviation)	Given

Table 4.3 The details of Pejovic & Jankvic (2016).

The fragility curve obtained in this reference as followings are for three different classes of buildings, 20-story building,30-story building and 40 story building and for five damage limit states (including no damage).

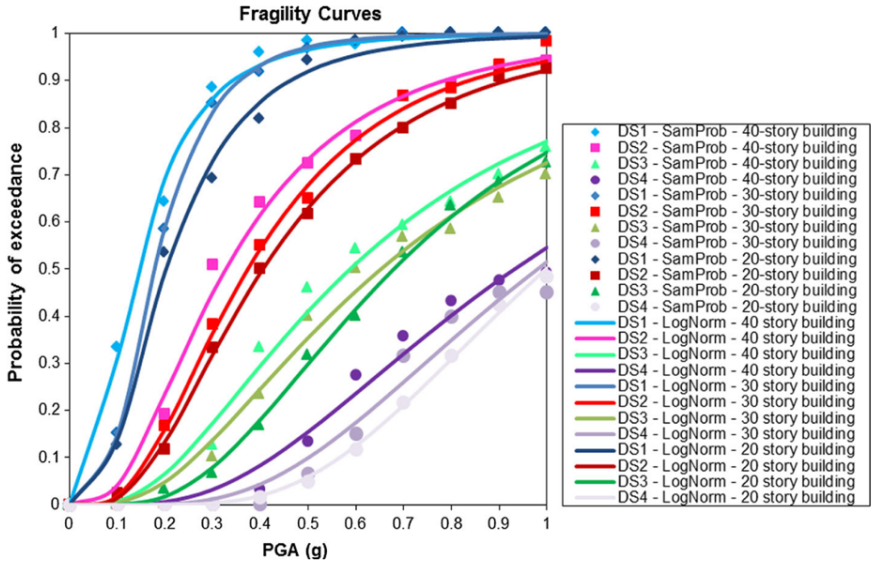

Figure 4.3 The fragility curve of Pejovic & Jankvic (2016).

Another good reference is written by Quiroz L.G. and Maruyama Y. (2014) about the assessment of Peruvian high-rise thin RC wall buildings with 10 stories. The details and fragility curve are given below.

Reference Name	**Assessment of performance of Peruvian high-rise thin RC wall buildings using numerical fragility functions**
Material	Reinforcement Concrete
Floors	10 stories
Damage State	5 States.
Geographical Area	In Lima, Peru, high seismic hazard area
Intensity Measure	PGA
Parameter (Mean and Standard deviation)	Not given

Table 4.4 The details of Quiroz & Maruyama (2014).

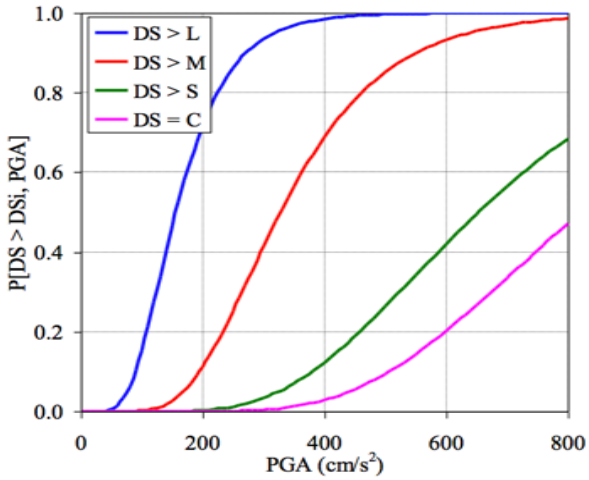

Figure 4.4 The fragility curve of Quiroz & Maruyama (2014).

4.2.2 Fragility curves as a function of Sa

The Spectral Acceleration with respect to specific time period could be a good intensity measure for the seismic risk assessment. There are some good references using Sa as the intensity measure. The first one to introduce here is the work performed by Akkar &Odabasi (2017) for damage assessment of tall buildings in Istanbul. Two different groups of buildings divided by 15-story building and 25 story-building with three different shear wall ratios are considered. Fragility curve with 25 story-building is shown as follows.

Reference Name	**ROBABILISTIC DAMAGE ASSESSMENT AND FRAGILITY FUNCTIONS OF TALL BUILDINGS IN ISTANBUL HYBRID STRUCTURES (Group 1: T= 2.25-3.3s; Group 2 :3.0-4.35s.)**
Material	Reinforcement Concrete
Floors	Group 1: 15, Group 2: 25
Damage State	5 States.
Geographical Area	Istanbul, Turkey, high seismic hazard area
Intensity Measure	Sa
Parameter (Mean and Standard deviation)	Not given

Table 4.5 Details of Akkar &Odabasi (2017)

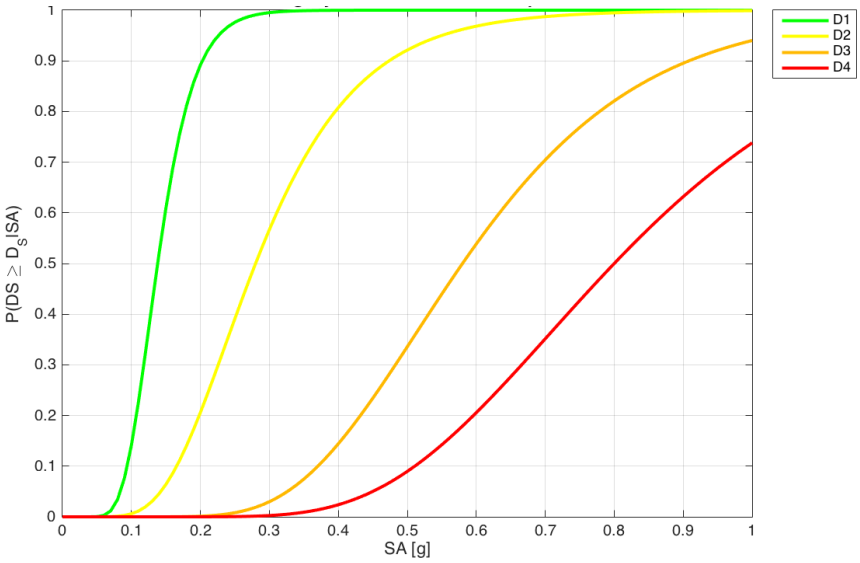

Figure 4.5 The fragility curve of Akkar &Odabasi (2017).

The other reference is about the seismic fragility analysis of RC high-rise buildings in Dubai, including the Jumerah Beach Tower C03 and is a new model high-rise building. Considering the unique structural configurations and seismic behavior m the limit damage states are defined by LS1(Serviceability), LS2(Damage Control) and LS3(Collapse Prevention). The intensity measure is the spectral acceleration at vibration period of 1 s. However, Dubai is located in a low seismic hazardous area, therefore, the reference is not as much significant as other references for our case study. And the details and fragility curve are shown in the following.

Reference Name	**An analytical framework for seismic fragility analysis of RC high-rise buildings. (T=1s)**
Material	RC high-rise building
Floors	54
Damage State	4 States.
Geographical Area	In Jumerah beach Tower C03, low seismic hazard area
Intensity Measure	Sa
Parameter (Mean and Standard deviation)	Given

Table 4.6 The details of Ji L et al. (2007).

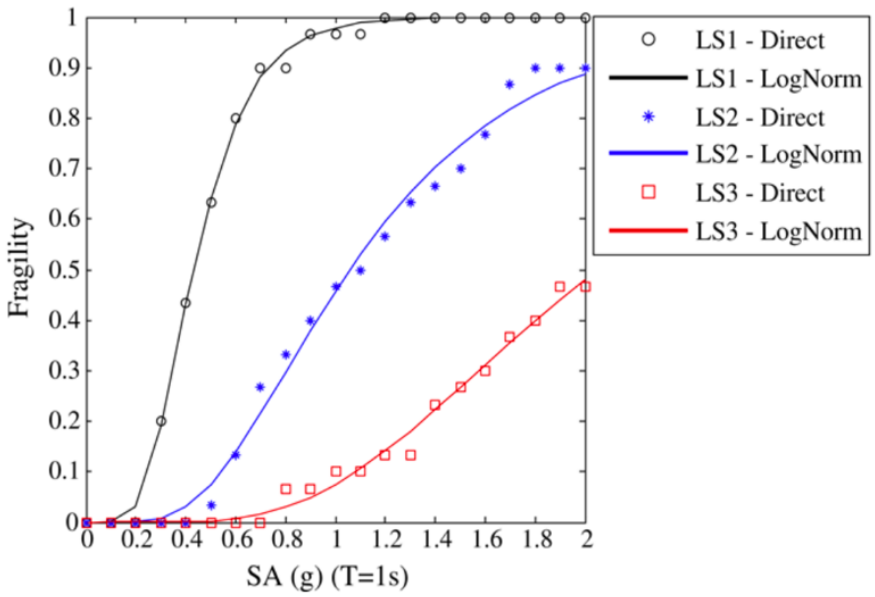

Figure 4.6 The fragility curve of of Ji L et al. (2007).

4.2.3 Fragility curve as a function of Sd

Spectral Displacement is a good intensity measure for fragility curve of high-rise buildings since the high-rise structures have long periods of vibrations. For instance, the following fragility curve for high-rise buildings in China is a pretty good reference which based on the published data of more than 50 high-rise and super-rise buildings. The fragility curve could be used to estimate well the economic loss for high-rise buildings under earthquake ground motion.

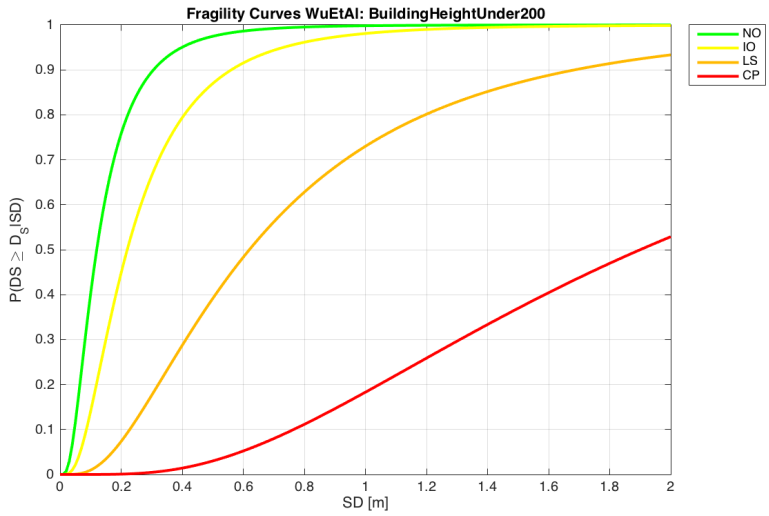

Figure 4.7 The fragility curve of height< 200 m in low code Wu et al (2013).

In another paper *Preliminary Study on the Fragility Curves for Steel Structures in Taipei (*Cherng, 2001), the study of fragility curve is evaluated by using the nonlinear state analysis method for steel structure in Taipei, since there are too many high-rise steel structures in Taipei. In this study, the author carried out the fragility curve for two sets of buildings, which were designed to resist lateral loads by Special Moment Resisting Frames (SMRF) and Special Moment Resisting Braced Frames (SMEBF) according to the Taiwan seismic code prior to Chi-Chi earthquake.

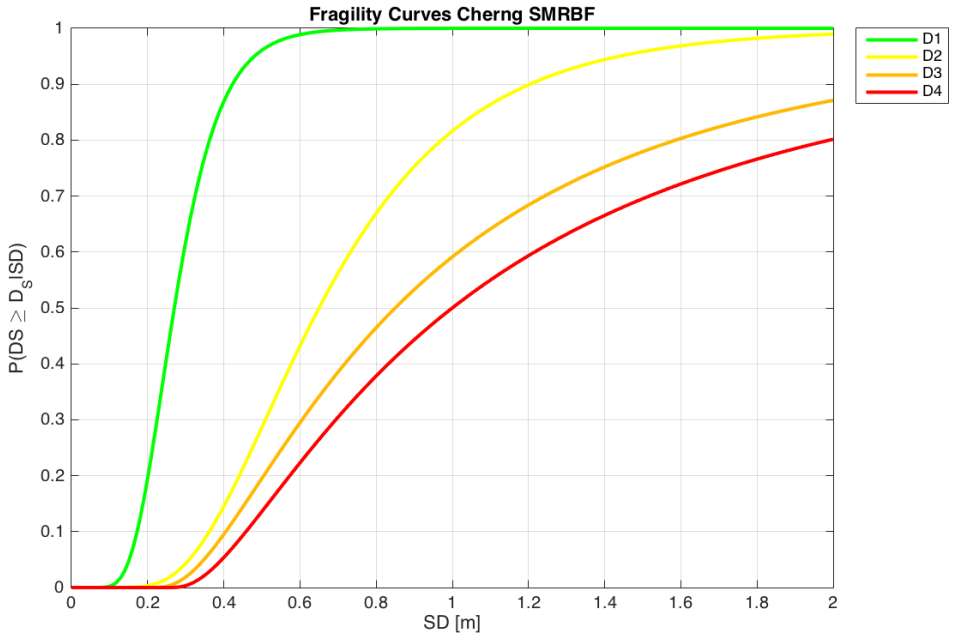

Figure 4.8 Fragility curves for SMRBF in Taipei Cherng. (2011)

The damage state in this study are defined into four groups, including D1(slight damage), D2(moderate damage), D3(extensive damage), and D4(complete damage). The computed fragility curves for SMRF and SMRBF are obtained by using Monte-Carlo simulation analysis, which employs the spectral displacement (SD) as the intensity measure (T=3s). Here the fragility curves for SMRBF is shown in Figure 4.8.

Among these literature studies, two fragility functions have been selected to be used for the seismic risk assessment in Beijing area shown in the following chapters. The preferred fragility curve is WU13 as it refers to high-rise buildings in China. Akkar17 has been selected to perform some sensitivity analysis. These two models are listed in the following table and more details will be described afterwards.

	Title	Authors
1	Building Seismic Vulnerability Study for China High Rises (2013)	Fan Wu, Ming Wang, And Xinyuan Yang
2	Probabilistic Damage Assessment and Fragility Functions of Tall Buildings in Istanbul(2017)	Sinan Akkar,Ömer OdabaşI

Table 4.7 The main two references used in this study

NO.	Reference	Condition	Fragiltiy curve parameters		
			Damage State	Median Value	β_s
1	WU13	H<200m	D1(NO)	10	0.93
			D2(IO)	2.2	0.83
			D3(LS)	0.68	0.73
			D4(CP)	0.3	0.85
		H>200m	D1(NO)	0.12	0.73
			D2(IO)	0.22	0.73
			D3(LS)	0.62	0.78
			D4(CP)	1.9	0.72
2	Akkar17	Group 2	D1(NO)	0.138	0.3
			D2(IO)	0.28	0.41
			D3(LS)	0.58	0.35
			D4(CP)	0.8	0.35

Table 4.8 Parameters of the fragility curves two references

4.3 Fragility curve of WU13

The first reference discusses about the high-rise building seismic vulnerability WU13. In this reference, more than 50 high-rise buildings are separated into two groups, whose height smaller than 200 m and height larger than 200 m. The building structure information including the natural period is illustrated in the Table 4.8.

Building Height (m)	Quantity	Representative buildings	Period Tn(s) Mode I/II/III
100-200	32	Gaobao Tower, Shanxi Information Tower	2~5/2~5/2~3
200+	24	Guangsheng International Building, New CCTV building,Shanghai World Financial Center, Shanghai Center Tower	5~7/5~6/~3

Table 4.9Building Structure Information

Data from structural analyses in terms of maximum story drift ratio δ , selected as overall performance index, and spectral displacement were selected to derive fragility curve since the structures have comparatively long natural period. Based on statistics and regression analysis, the relationship between the maximum story drift ratio and response spectrum displacement could be obtained. According to the height groups and earthquake design codes, the fragility curves can be developed. For this purpose, a cumulative lognormal distribution has been assumed and maximum-likelihood method has been adopted. For the given under a certain Sd value, the structure damage under the ground motion, the probability exceeding the threshold drift ration LSi, could be evaluated using the following Equation.

$$P(\mu/S_d > LSi) = 1 - \Phi(\frac{ln(LSi/\delta)}{\beta_s})$$

$$\beta_s = \sqrt{{\beta_c}^2 + {\beta_m}^2 + {\beta_d}^2}$$

where,

β_S is the total variability for structural damage state in natural logarithm. It is a combination of three contributors to structural damage variability.

β_c, related to the variability of the building capacity curve, $\beta_c = 0.25$ for all Coded buildings.

β_d is the standard deviation of δ.

β_m, related to the uncertainty in the estimate of the median value of the threshold of structural damage state. and $\beta_m = 0.4$ for all structural damage states and building types.

Then according to the fragility function, two fragility curves are obtained considering two different groups of buildings heights, below and above 200 m, and different levels of seismic codes, Low, Medium and High.

Here the fragility curve of the WU13 of building height under 200 m for low code is shown. Damage states are classified into four categories, including normal operation (NO), immediate occupancy (IO), life safe (LF) and collapse (C).

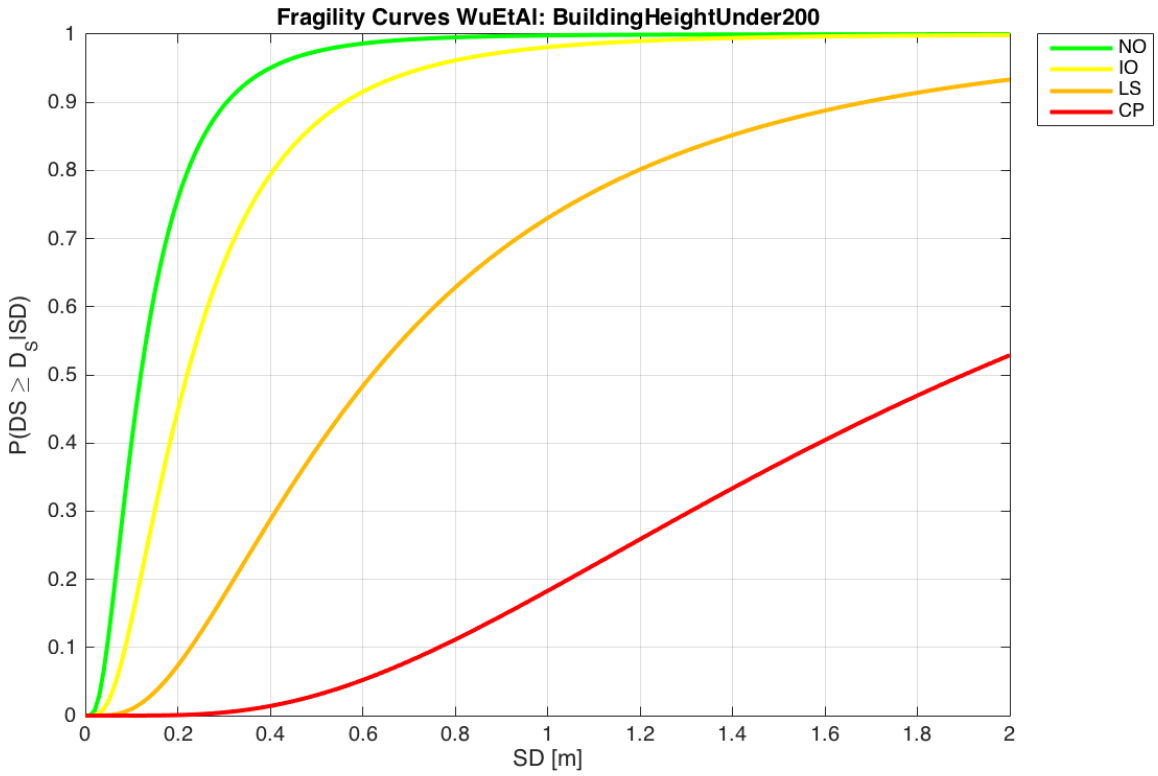

Figure 4.9 Fragility curves for low design code height under 200 m

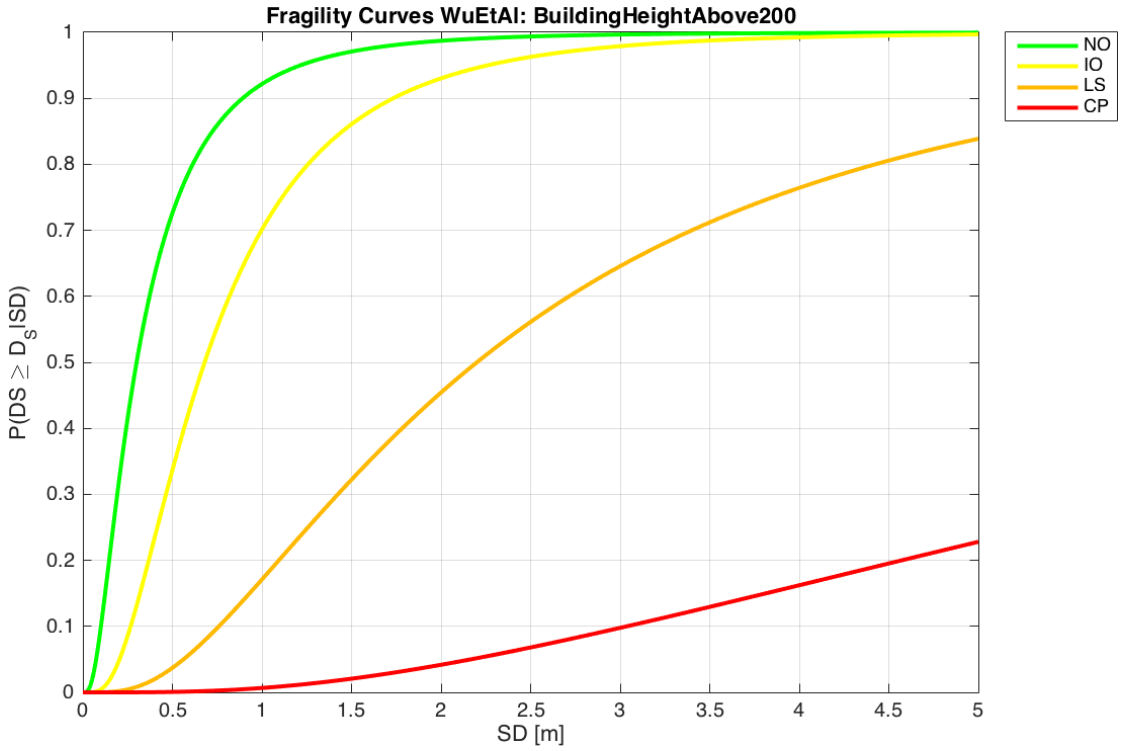

Figure 4.10 Fragility curves for low design code height above 200 m

Generally, we could draw the conclusions from the curves that under a comparatively large response spectrum displacement like smaller than 0.2 m, for the damage state of life safe (LF) and collapse (C), the exceeding probability is very low, and for immediate occupancy (IO) some little damages might be happened.

4.4 Fragility curve of Akkar17 (Instabul)

In this part, the paper *Probabilistic damage assessment and fragility functions of tall buildings in Istanbul* Akkar17 were introduced to study about high-rise reinforced concrete shear wall buildings having 10 to 30 stories in metropolitan cities of Turkey. The results could be considered as a reference in terms of estimating cost-effectiveness and vulnerability functions of high-rise building stock in high seismic zone of Turkey. The author has studied two groups of buildings, 15 stories and 25 stories buildings. There are submodels under each major group which are categorized the buildings according to their shear wall area or floor plan area ratios (SW ratio). Details of the groups are listed in the table below.

Group	Subtype(Model Name)	Shear Wall Ratio-Long Direction*	Shear Wall Ratio-Short Direction*
1	1A	0.45%	1.54%
	1B	0.78%	1.47%
	1C	1.22%	1.93%
2	2A	0.63%	1.05%
	2B	1.56%	1.19%
	2C	2.93%	2.03%

Table 4.10 Details of groups and shear wall reinforcement Akkar17.

Tall building fragility curves has been developed referring to the analytical method proposed by Baker (2015) which assesses the exceedance probability of a certain damage state under a ground-motion intensity measure (IM). In this reference Sa, at the average horizontal fundamental period of vibration of the structure, has been considered as intensity measure. Since the goal is to evaluate the seismic risk of tall buildings in Beijing area and the building stories are usually much higher than 15 or 25, we consider the Group 2C fragility curve. Given the hazard levels, the probabilities of observing damage states (no damage, slightly damage, moderate damage, severe damage and complete damage) are computed from the fragility functions shown in the previous section.

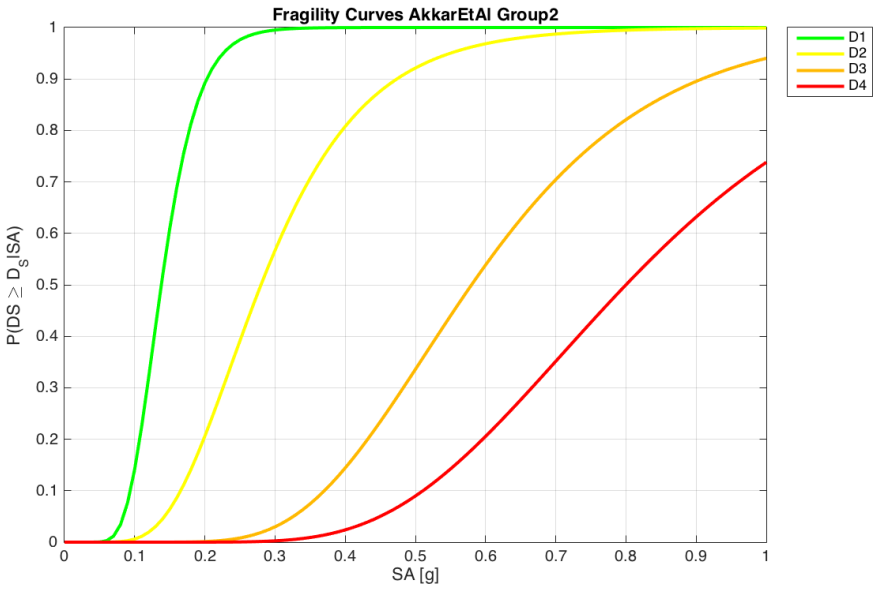

Figure 4.10 Fragility curves for Group2 Akkar &Odabasi (2017)

5. Analysis and comparison of the results from the selected fragility curves

5.1 Introduction

This chapter illustrates the main results of the seismic risk analyses which have been performed for the high-rise building in the urban area of Beijing. Initially some representative sites of high-rise buildings are selected to identify those locations where seismic damage assessment will be illustrated in detail. WU13 (Wu et al. 2013) has been considered the default fragility model for high-rise buildings. Different scenarios of the corresponding magnitude obtained from 3DPBNS were introduced to carry out the analysis. Comparisons of damage scenarios resulting from earthquakes with equal magnitude as well as of damage scenarios resulting from earthquakes with different magnitude (Mw6.5, Mw 6.9 and Mw 7.3) will be shown. Results of damage assessment will be expressed in terms: damage pie diagram at selected locations, probability of damage states and mean damage ratio as a function of the distance from the fault.

Generally, seismic hazard assessment is analyzed by GMPEs and 3D physic-based numerical approaches. In this chapter, we also perform a comparison of results between these two approaches. Furthermore, the sensitivity of results with respect to the fragility curves will be also addressed to check the variability of the seismic risk assessment with respect to the vulnerability model, considering the work by Akkar17.

5.1.1 Selected locations in Beijing area

To study the seismic risk for Beijing area, 17 representative locations of existing high-rise buildings are selected, see Figure 5.1 and Table 5.1, which shows the representative locations and coordinates of hypocenter and fault for Scenario 1 Mw6.5. It is obvious to observe that the hypocenter is inside the fault in the x-y projection view and the studying points are scattered around the fault. Some locations such as Location 7 and Location 11 are very close to the fault and some locations are far from the fault like Location 8 and Location 12. We note that the distance metric used here is Rrupt. (rupture distance, closest distance to the fault rupture) and for Scenario 1 Rupture distance for each location is shown in the table besides the figure.

NO.	Cities	Rrupt[km]
1	Beijing_Lang.&Cult._University	10
2	Nat._Conv._Center_Grand_Hotel	8
3	Haidian_New_Tech._Build.	11
4	Beijing_Guangzhou_Center_Build.	5
5	Building_Amp_Sky	10
6	Peking_Shopping_Mall	4
7	Soubao_Business_Center	5
8	Changping_District	24
9	Daxing_District	14
10	Fangshan_District	16
11	Fengtai_East_Street	4
12	Guanzhuang_Village	13
13	Qiaoxi_Street	6
14	Shijingshan_District_1	11
15	Shijingshan_District_2	13
16	Wangjing_Street	4
17	Wukesong_Area	7

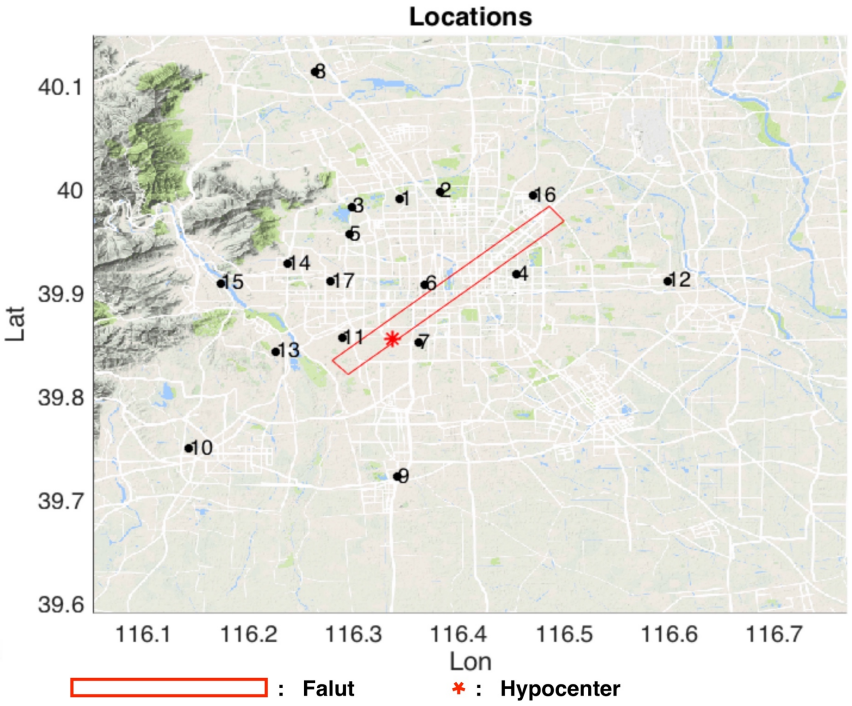

Figure 5.1 Overview of the selected locations for analysis, hypocenter and fault for Scenario 1 Mw 6.5. The selected locations are represented by black dots. The red star shows the projection of hypocenter and the red rectangular represents the projection of the fault.

Cities	Lat	Lon
Beijing_Lang.&Cult._University	39.9926	116.3435
Natl._Conv._Center_Grand_Hotel	40.0000	116.3815
Haidian_New_Tech._Build.	39.9850	116.2984
Beijing_Guangzhou_Center_Build.	39.9196	116.4550
Building_Amp_Sky	39.9586	116.2952
Peking_Shopping_Mall	39.9102	116.3673
Soubao_Business_Center	39.8537	116.3613
Changping_District	40.1152	116.2623
Daxing_District	39.7244	116.3415
Fangshan_District	39.7515	116.1427
Fengtai_East_Street	39.8587	116.2884
Guanzhuang_Village	39.9137	116.5987
Qiaoxi_Street	39.8455	116.2253
Shijingshan_District_1	39.9302	116.2362
Shijingshan_District_2	39.9113	116.1726
Wangjing_Street	39.9957	116.4704
Wukesong_Area	39.9129	116.2779

Table 5.1 Coordinates of the selected locations for analysis.

5.2 Vulnerability Model: fragility curve by WU13

As we discussed previously, fragility curves can be used for the assessment of seismic vulnerability assessment, which generally provides estimation for the probability of a structure reaching or exceeding a limit damage state at a given level of ground motion. For the case of seismic risk assessment of Chinese high-rise buildings, WU13 is solid reference as it is specifically focused on the seismic vulnerability of high-rise buildings in China. For the analyses shown in this thesis, the WU13 fragility curves for height < 200 m and low code have been considered as the vulnerability model, see Figure 5.2.

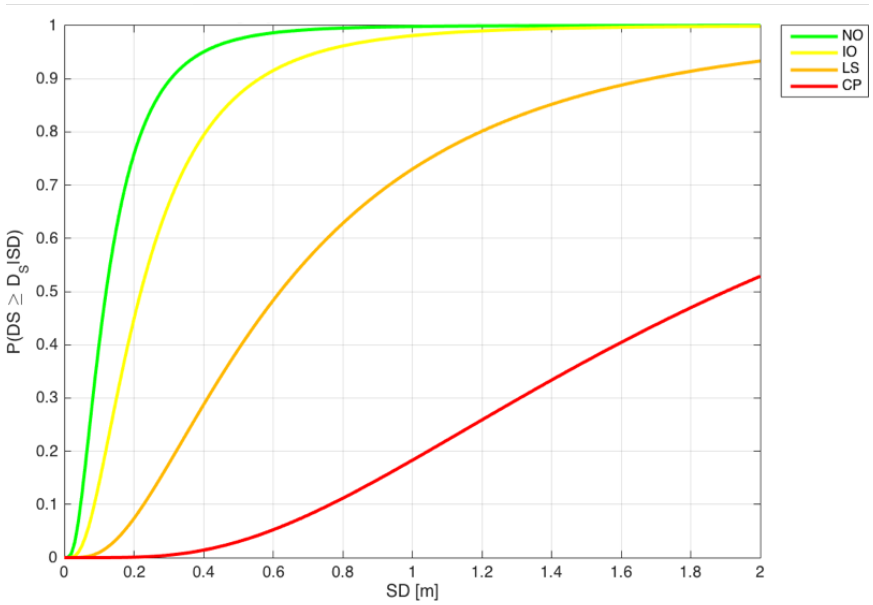

Figure 5.2 Fragility curve WU13 of buildings height under 200m in Low Code

In order to compute the values of intensity measure, spectral displacement, to provide as input for vulnerability assessment, the vibration period at which the response spectral displacement is computed should be defined. The relationship between natural vibration periods and structural heights for high-rise buildings in China and its range have been analyzed by Xu et al. (2014), based on analysis of 414 high-rise buildings completed or passed over-limit approval in China. The analyzed building structures are reinforcement concrete structures or composite structures excluding pure steel structures. Besides the structure types are frame-core tube structure, frame-shear wall structure and shear wall structure.

According to their study, the relationship between the structural height of

high-rise buildings in China and the fundamental period T_1 doesn't follow a linear trend, see Figure 5.3. Based on the characteristics of the data and clssifications rules for concrete structures of high-rise builidngs etc, the rules could be described. Here due to the analyzed height of the high-rise budlings less than 200 m, we only introduce the rules of height between 100 m and 200 m. When 100 m $\leqslant$ H $<$ 150 m, the reference range is between $0.2\sqrt{H}$ and $0.35\sqrt{H}$. for stiff structure, T_1 is smaller than $0.2\sqrt{H}$ and for flexible structure, T_1 is larger than $0.35\sqrt{H}$.

Therefore, when H is 100 m, 2s $<T_1<$ 3.5s; and when H is 150 m, 2.45s $<T_1<$4.28s. The fundamental natural period should be between 2s and 4.28s, as shown by the purple points in the Figure 5.3. All above, T_1 equal to 3s has been chosen as the natural vbiration period in our further analysis.

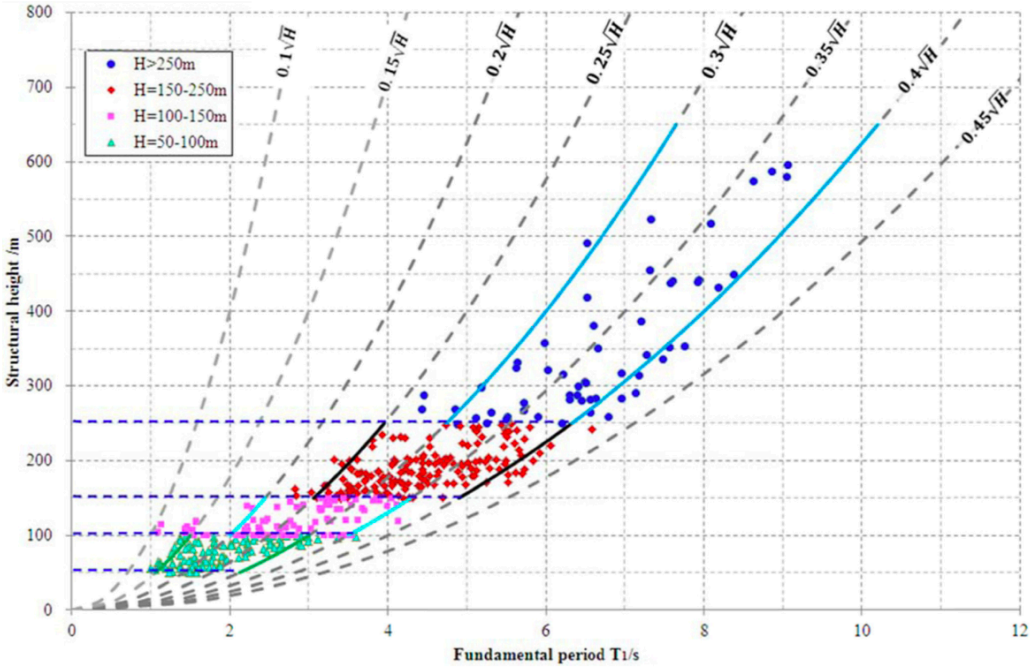

Figure 5.3 Relationship between fundamental periods T_1 and structural heights H for Chinese buildings (Xu et al. 2006).

5.3 Seismic damage scenarios for selected earthquakes

For all the scenarios obtained from 3D physics-based numerical simulation methods, several seismic damage scenario maps can be obtained considering the evaluation of the specific seismic hazard analysis and seismic vulnerability analysis. Initially we concentrate on analysis for one specific case, Seismic damage Scenario 1 Mw 6.5.

5.3.1 Seismic damage Scenario 1 Mw 6.5

Obviously, each location will have a specific distance from the fault and spectral displacement value at T=3 seconds. Therefore, distribution of spectral displacement in Beijing area for Scenario 1 is shown in the Figure 5.4, from which we could observe in some locations the spectral displacements are pretty high near the fault, and for the locations far away from the fault, the spectral displacements are almost zero.

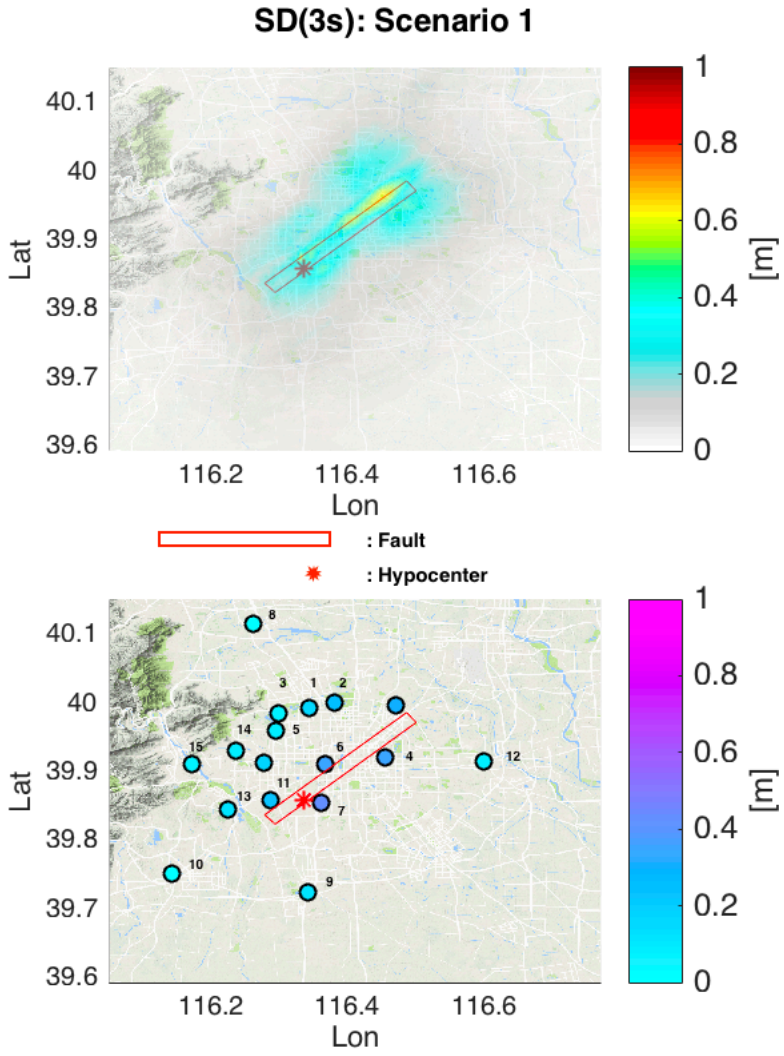

Figure 5.4 Distribution of SD (3S) in Beijing area for Scenario 1. The selected locations are represented by circles. The red star shows the projection of hypocenter and the red rectangular represents the projection of the fault.

Combining the values of SD(3s) at the selected locations with the fragility curve WU13, the probabilities at different damage states for Scenario 1 can

be computed, see Table 5.1. In the table, different color represents different damage states, D0 means No Damage state in white color; D1 represents Slight Damage state, corresponding to Normal Operation (NO) state for WU13 in green color; D2 represents Moderate Damage state, Immediate Occupancy(IO) for WU13 in yellow color; D3 represents Severe Damage state, Life Safe(LF) for WU13 in orange; D4 means Complete Damage, Collapse Prevention (CP) in red. For each location, 5 probability values for corresponding damage states have been obtained, nevertheless, the sum of the 5 damage state values is equal to 1.

Location	Sd[m]	D0	D1	D2	D3	D4
L1	0.15	0.390	0.319	0.258	0.032	0.000
L2	0.24	0.169	0.280	0.438	0.112	0.002
L3	0.05	0.871	0.104	0.024	0.001	0.000
L4	0.35	0.071	0.191	0.506	0.224	0.009
L5	0.08	0.718	0.203	0.076	0.004	0.000
L6	0.36	0.068	0.187	0.507	0.229	0.009
L7	0.41	0.046	0.150	0.505	0.284	0.016
L8	0.02	0.992	0.007	0.001	0.000	0.000
L9	0.11	0.538	0.285	0.163	0.014	0.000
L10	0.03	0.971	0.026	0.003	0.000	0.000
L11	0.23	0.182	0.287	0.426	0.103	0.002
L12	0.09	0.645	0.240	0.108	0.007	0.000
L13	0.11	0.528	0.288	0.169	0.015	0.000
L14	0.07	0.757	0.180	0.061	0.003	0.000
L15	0.06	0.856	0.115	0.028	0.001	0.000
L16	0.30	0.106	0.232	0.488	0.170	0.005
L17	0.16	0.333	0.322	0.301	0.044	0.000
Comments	Different color represents different damage states, D0 means No Damage state in white color; D1 represents Slight Damage state, corresponding to Normal Operation (NO) state for WU13 in green color; D2 represents Moderate Damage state, Immediate Occupancy(IO) for WU13 in yellow color; D3 represents Severe Damage state, Life Safe(LF) for WU13 in orange; D4 means Complete Damage, Collapse Prevention (CP) in red.					

Table 5.2 The damage value for different damage states at different locations Scenario 1 Mw6.5

Afterwards the damage pie plot and damage histogram for each scenario can be obtained easily by adopting the damage values above, see Figure 5.5, where the different color means different damage states. The left corner table shows the rupture distances and SD values for the corresponding locations. It is feasible to observe that for some locations with smaller Rrupt. could have comparative larger values of SD. For the comparative large value of spectral displacement usually represents large damage probability value at complete damage state and severe damage state.

From the damage pie diagram, among the selected locations, Location 4, Location 6, Location 7, Location 11 and Location 16 and Location 17 are the ones exhibiting the largest damages during the selected earthquake of Magnitude 6.5, owing to the proximity to seismic fault. For other locations with larger rupture distance, such as for Location 3 there is only slightly damage and moreover there is almost no damage for Locations 8 if earthquake occurs. Some further comparisons will be carried out in the following parts.

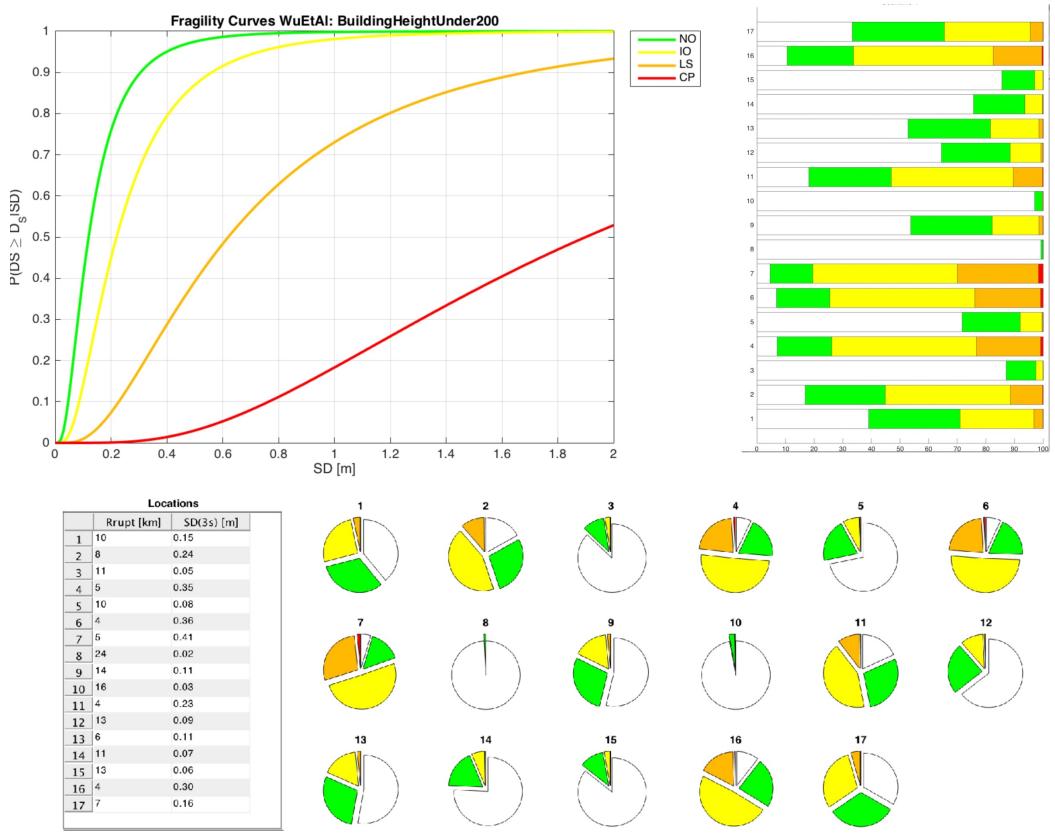

Figure 5.5 The damage pie diagram and histogram WU13 Scenario 1 Mw 6.5

Moreover, through analysis of the fragility curve, probability of exceedance at four damage states regarding rupture distances can be calculated for Scenario 1 Mw 6.5, see Figure 5.6. It can be observed in general that the exceeding probability at a certain damage state has a non-linear relationship with rupture distance, and as rupture distance increase, the corresponding probability value of exceedance decreases. Exceeding probability at slight damage state (D1) is higher than that of at moderate damage state (D2) and severe damage state (D3) considering the same rupture distance. Besides, the probability of exceedance at complete damage is pretty little or nil.

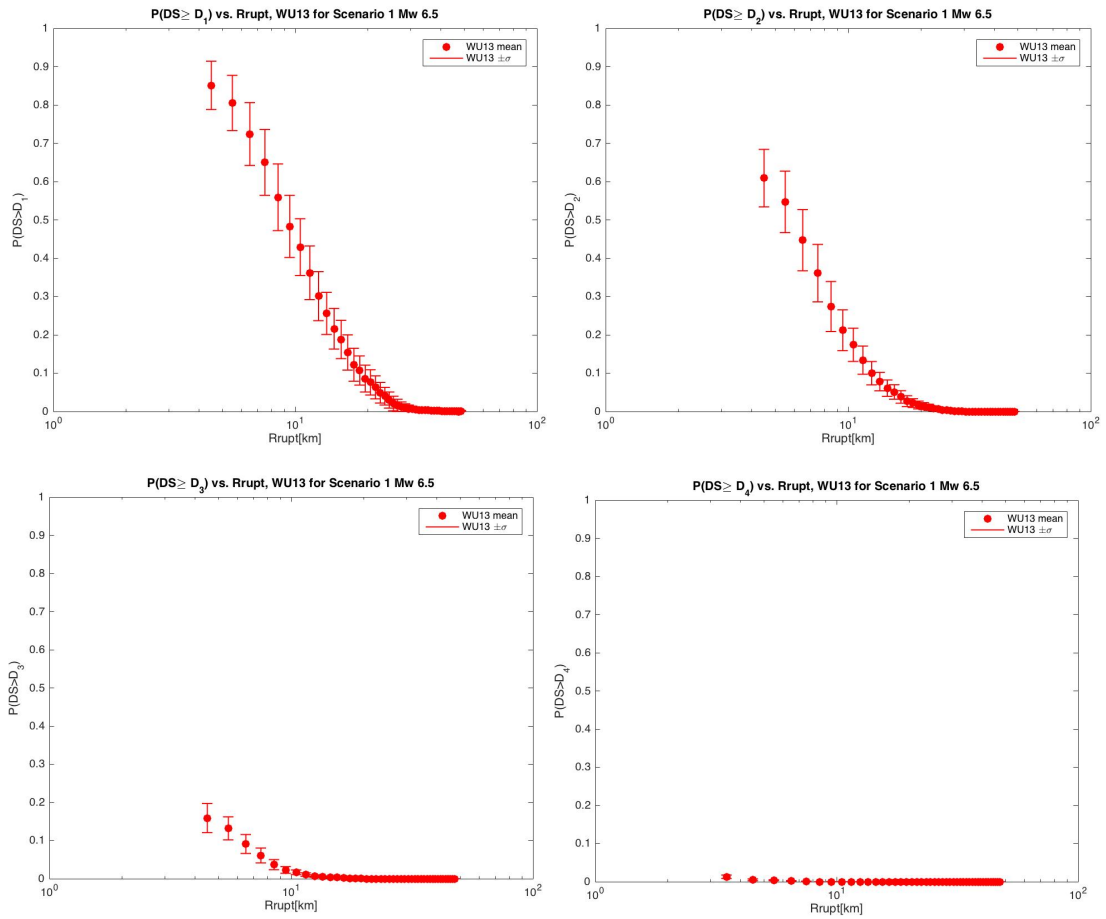

Figure 5.6 Exceedance Probability vs Rrupt at different damage state for Scenario 1 Mw 6.5. The red dot simply represents the mean of exceeding probability at certain damage state for Scenario 1 and the bar by the dispersion around that value.

All above the exceedance probabilities at different damage states with respect to rupture distances are expressed in different color, see Figure 5.7, from which it is easy to obtain and compare the damage contents at different damage states at one specific location. Furthermore, the exceeding probability at one specific damage state differs from the magnitude of the selected scenarios.

The black dot simply represents the mean of exceeding probability at certain damage state for Scenario 1 and the bar shows the standard deviation around the mean. It is worth to note that the large dispersion around the mean value and the extremely rapid decrease of the probabilities associated to different damage state with respect to the Rupt.

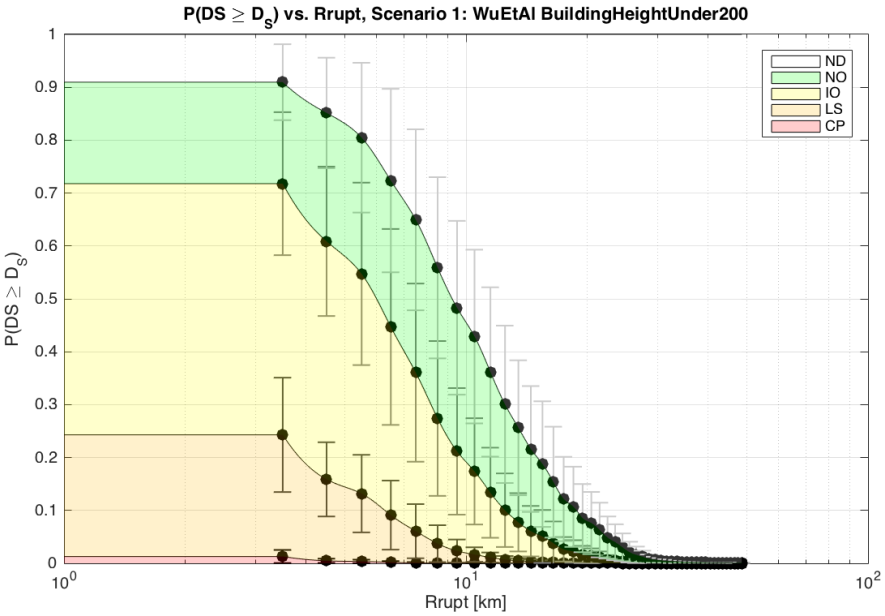

Figure 5.7 Exceedance Probability vs Rrupt. The black dot simply represents the mean of exceeding probability at certain damage state for Scenario 1 and the bar by the dispersion around that value.

In order to capture this variability in damage, we focus on not only at a single value for the damage ratio, but at a whole distribution of possible damage values. Therefore, the mean damage ratio (MDR) is a good reference to be considered, which is defined as the mean of the damage distribution. Nevertheless, initially damage parameters have to be assumed, see Table 5.3.

Damage State	Damage State (WU13)	Damage Grade Value Li
D0 (No Damage)	-	0.00
D1(Slight Damage)	NO	0.10
D2(Slight Damage)	IO	0.50
D3(Severe Damage)	LS	0.70
D4(Complete Damage)	CP	1.00

Table 5.3 Overview of the damage grade parameters

Mean damage ratio can be defined using the formula below based on fragility curve.

$$MDR = \sum L_i * Pd_i$$

Where,

Li is the assumed damage grade value for the damage state; *Pdi*, the probability of exceedance at the corresponding damage state.

Therefore, MDR curve with respect to spectral displacement at T=3s for building height under 200 m WU13 can be obtained, see Figure 5.8. It is not difficult to observe that the relationship between two parameters has a non-linear trend and the curve is increasing as SD increases. Moreover, it is possible to estimate the economic damage by obtaining the MDR value for a given spectral displacement (SD) based on the MDR curve.

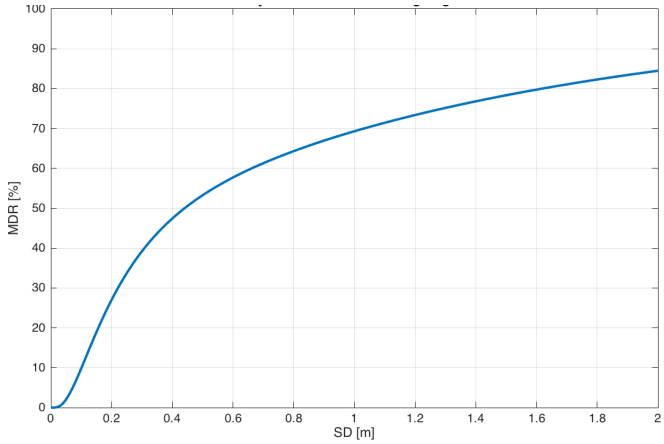

Figure 5.8 MDR curve of building height under 200 m WU13

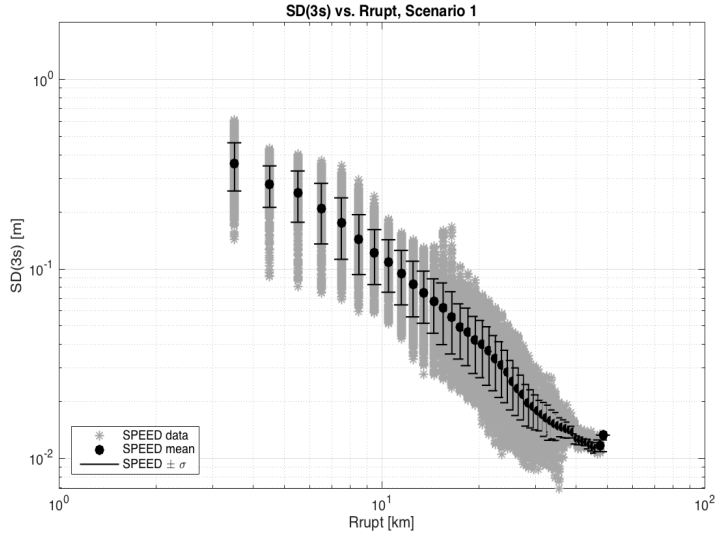

Figure 5.9 SD(T=3s) distribution vs Rupture Distance for Scenario 1 Mw 6.5: for each distance bin, the grey stars show the SD simulated for Scenario 1, while the filled black dot simply represents the mean value and the bar represents the standard deviation.

Another observation is that since distribution of SD regarding different rupture distances can be expressed, see Figure 5.9, and for each distance bin, the grey stars show the SD simulated for Scenario 1. While, the filled black dot simply represents the mean value and the bar represents the standard deviation. It is easy to figure out that as the rupture distance increases, SD decreases.

Moreover, by using the MDR vs. SD curve, the relationship between Rrupt and MDR can be obtained, see Figure 5.10, here for each distance bin, the grey stars representing the MDR for Scenario 1, while the filled black dots with bars representing the mean value and the corresponding standard deviation. It can be see that as the rupture distance increases, the average values of MDR decreases, which means that when the locations of high-rise buildings are comparative far from fault, only little damage or no damage could occur when facing the seismic hazard Scenario 1 Mw 6.5 based on WU13 fragility model, since they are less exposed to the seismic hazard.

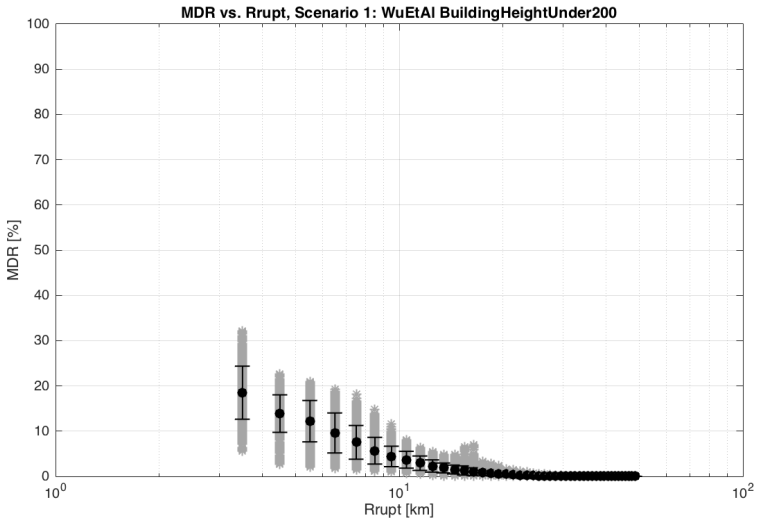

Figure 5.10 MDR distribution considering the rupture distance for Scenario 1 Mw 6.5: for each distance bin, the grey stars show the MDR for Scenario 1, while the filled black dots with bars represent the mean value and the corresponding standard deviation.

5.3.2 Comparison of results for different locations

Specially, four locations, L2, L4, L11, L12 have been chosen for further analysis, see Figure 5.11. It can be observed that L11 is near the hypocenter, L12 and L4 is near the fault, while L12 is far away from the fault. Since the value Sd of L4 is larger than that of L2, according to the fragility curve, the value of exceeding probability at Damage State 1 and Damage State 2 for L4

is smaller than that for L2， which means considering a comparatively large SD, the exceeding probability for the damage limit state is larger. Damage pie plot can show clearly the damage distribution for different location by using different color, see Figure 5.12, which no damage state is represented in white; slight damage state is in green; moderate damage state in yellow; severe damage state is in orange and complete damage state is in red.

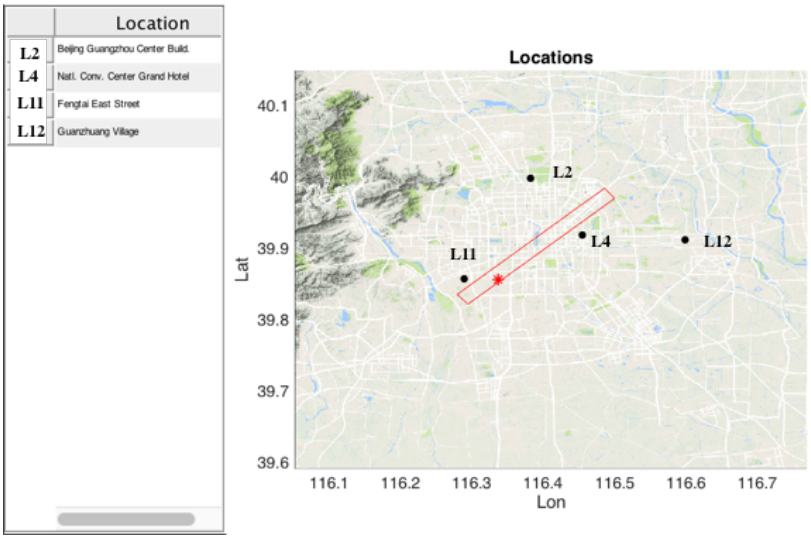

Figure 5.11 Distribution of Selected locations. The selected locations are represented by black dots. The red star shows the projection of hypocenter and the red rectangular represents the projection of the fault.

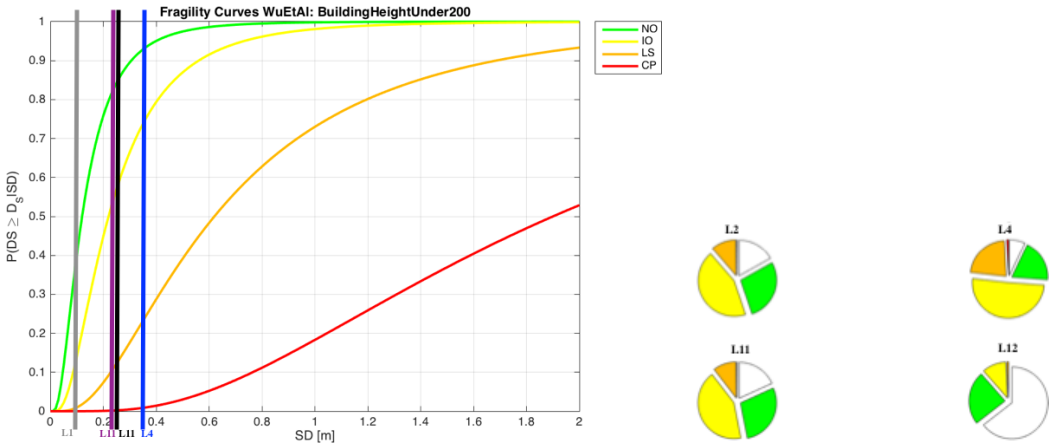

Figure 5.12 Damage comparison of L2, L4, L11, L12 Scenario 1

5.3.3 Comparison of scenarios of equal magnitude Mw 6.5

In this section, comparison of scenarios of equal magnitude Mw 6.5 has been carried out in order to check the variation of the simulated scenarios. Specially

There are two selected scenarios presented to carry out the comparison Scenario 1 and Scenario 11. First of all, the hypocenter information about two scenarios has been illustrated and compared in the Table 5.4.

Senario ID	Mw	Hypocenter		
		Lon(degree)	Lat(degree)	Z(m)
S1	6.5	116.34	39.86	-13560.73
S11	6.5	116.46	39.96	-9885.77

Table 5.4 Main features of the sample of scenarios considered.

The maps of seismic shaking were produced by 3D physics-based numerical simulations illustrated by the ground shaking maps in terms of Peak Ground Acceleration (PGA), Peak Ground Velocity(PGV), Peak Ground Displacement(PGD) and Spectral Acceleration (SA) at specified vibration periods, ranging from 0.5s to 2s for the two scenarios under consideration.

The physics-based numerical simulations were realized by using the open code SPEED developed by Politecnio di Milano, which can quantify the spatial variability of ground motion at large period T and has been extensive proven in other study, such as Smerzini et al. (2010), Paolucci et al. (2010). In terms of spatial variability of earthquake ground motion having a more accurate characterization of the seismic wave field on a wide scale, improved results are obtained. Besides, it comprises all the factors that can affect seismic motion from the source to the site such as azimuthal of ground motion because of certain details of focal mechanism, topographic effects, 3D site effects and fault rupture process, which GMPEs cannot take account into. Furthermore, the proposed ANN-based approach could be applied into the results obtained from SPEED, which allows to get simulated scenarios in terms of broadband ground motions.

Some results of Scenario 1 and Scenario 11 are presented in this section. The main features of the simulations are listed in Table 4.1 and the scenarios map with respect to PGA, PGV, PGD, SA (T=0.5), SA(T=1s), SA(T=2s) are represented, see Figure 5.13, Figure 5.14, from where it is easy to see the distribution of intensity measures and can be the basic the further analyses.

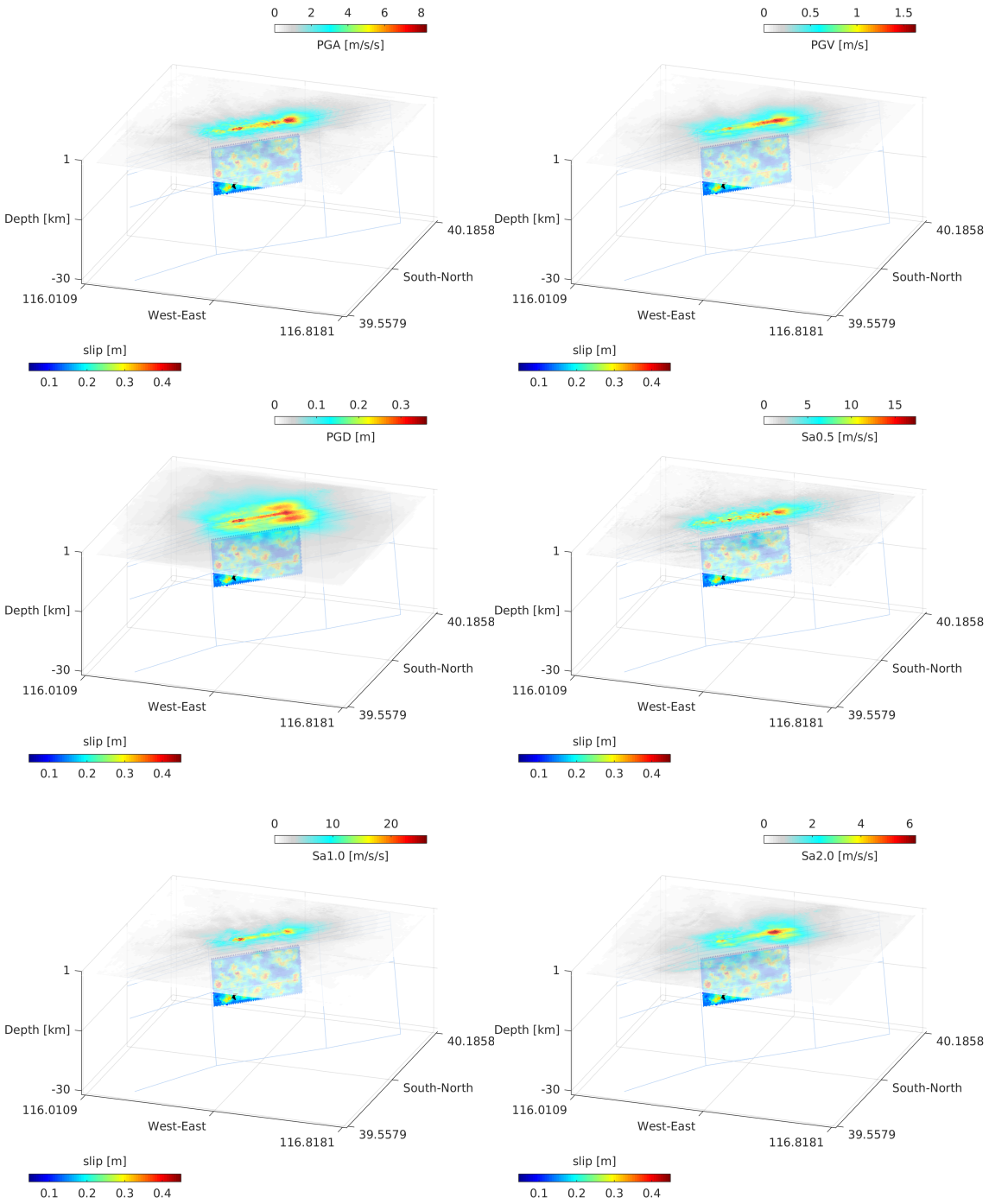

Figure 5.13 From left top to right bottom: PGA, PGV, PGD, SA at 0.5s, Sa at 1s, and Sa at 2s maps obtained at S1. The hypocenter is represented in a black star.

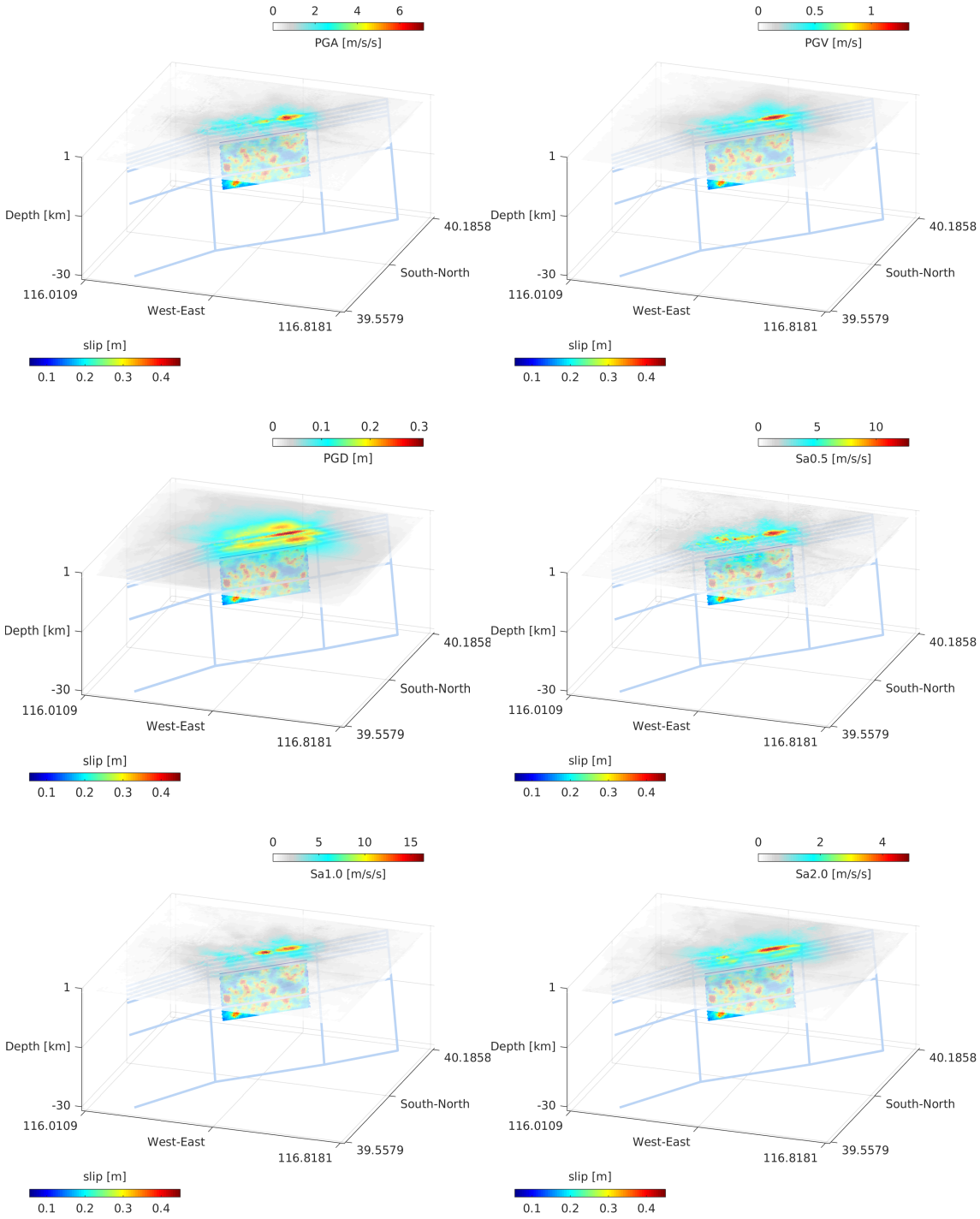

Figure 5.14 From left top to right bottom: PGA, PGV, PGD, SA at 0.5s, Sa at 1s, and Sa at 2s maps obtained at S11. The hypocenter is represented in a black star.

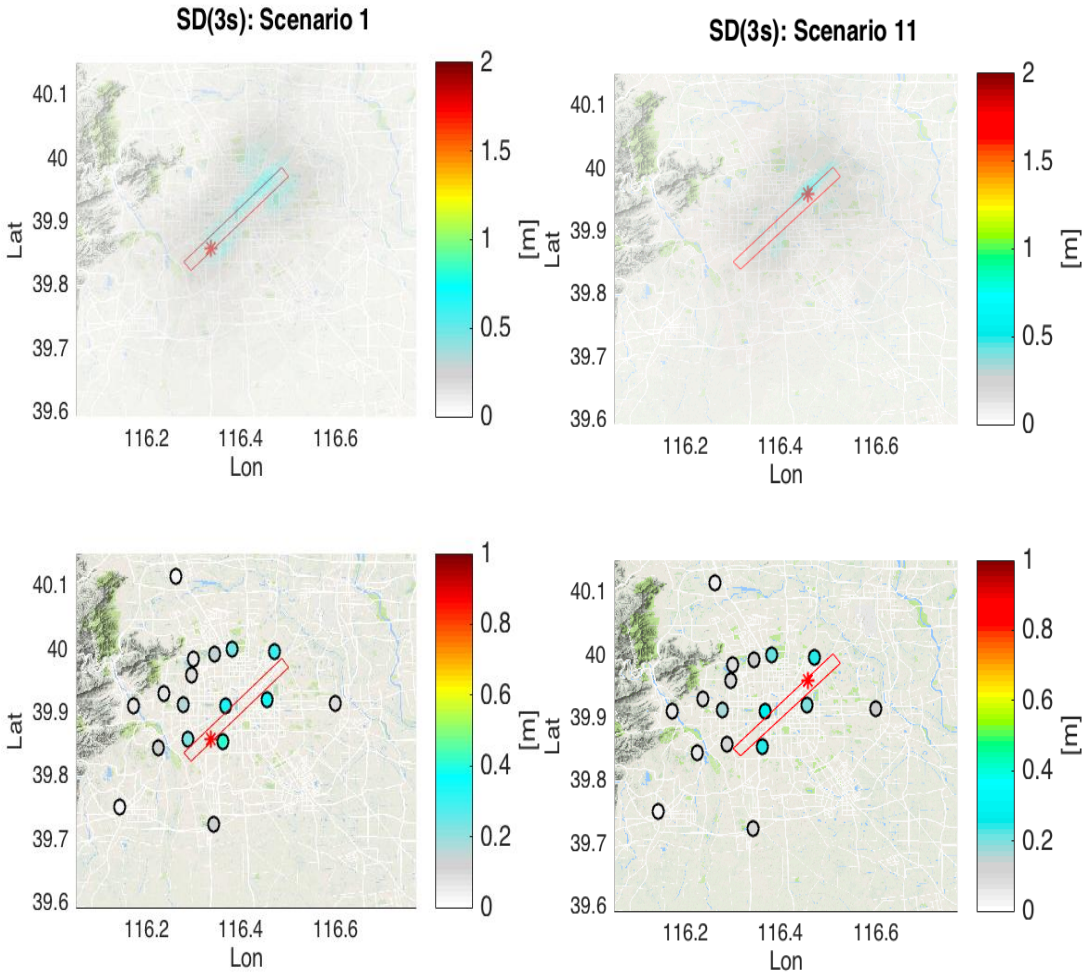

Figure 5.15 Comparison of SD (T=3s) for Scenario 1 and Scenario 30 in selected locations. The circles represent the selected locations. The red star shows the projection of hypocenter and the red rectangular represents the projection of the fault.

As we introduced the procedure before, distribution of SD (T=3s) for Scenario 1 and Scenario 11 can be obtained in Beijing area, see Figure 5.15, which uses color bar to demonstrate the SD value at T=3s in the region and also the selected locations for Scenario 1 and Scenario 11. The circles represent the selected locations. The red star shows the projection of hypocenter and the red rectangular represents the projection of the fault. It can be observed the large difference of the SD between the two magnitude 6.5 events selected. The locations which are near the fault have comparable higher values compared to other locations. However, it is not clear to observe the differences of the SD for Scenario 1 and Scenario 11 from Figure 5.15.

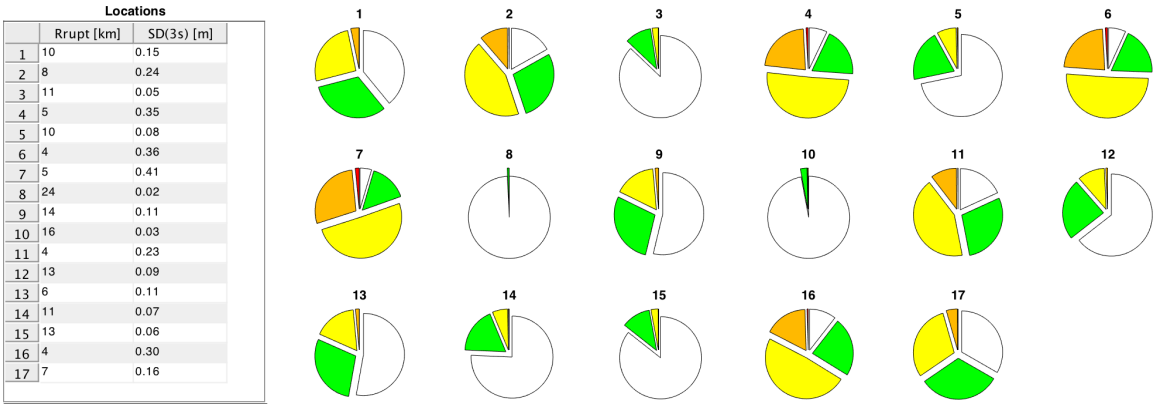

Locations

	Rrupt [km]	SD(3s) [m]
1	10	0.15
2	8	0.24
3	11	0.05
4	5	0.35
5	10	0.08
6	4	0.36
7	5	0.41
8	24	0.02
9	14	0.11
10	16	0.03
11	4	0.23
12	13	0.09
13	6	0.11
14	11	0.07
15	13	0.06
16	4	0.30
17	7	0.16

Scenario 1

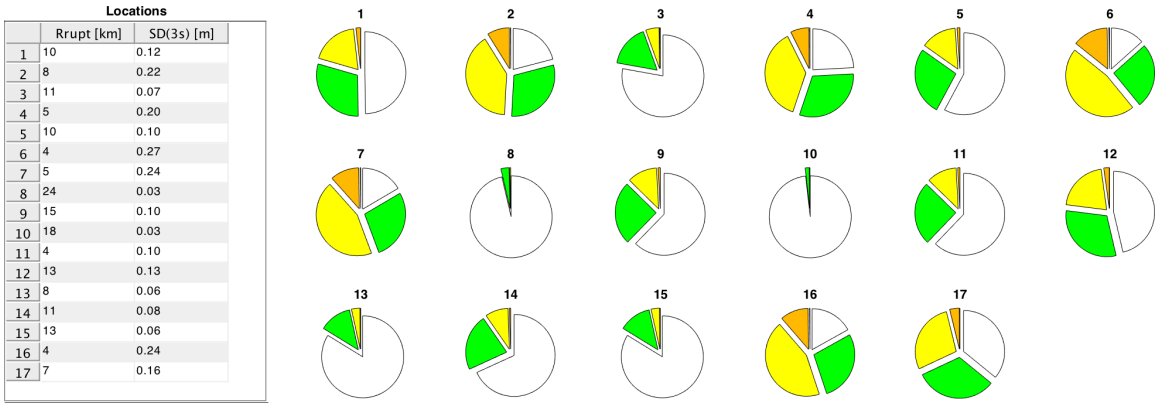

Locations

	Rrupt [km]	SD(3s) [m]
1	10	0.12
2	8	0.22
3	11	0.07
4	5	0.20
5	10	0.10
6	4	0.27
7	5	0.24
8	24	0.03
9	15	0.10
10	18	0.03
11	4	0.10
12	13	0.13
13	8	0.06
14	11	0.08
15	13	0.06
16	4	0.24
17	7	0.16

Scenario 11

Figure 5.16 Comparison of pie diagram between Scenario 1 and Scenario 11.

Apparently, different spectral displacements can be obtained for different selected locations at T=3s, as well as different rupture distances. Furthermore, according to the fragility curve, probabilities of exceedance at four damage states can be expressed in pie diagram, which clearly demonstrates the probability distribution in each location for one specific scenario. Scenario 1 and Scenario 11 have two different distribution of damage pie diagram and it can be figured out that for some locations when rupture distance is very large such as L8, L10, SD value will be usually low, which means contributes to be at no damage state and to have a low or negligible probability at all the other damage states. Nevertheless, for the locations with short source-to-site distance such as L6, L7 and L11, the probability of Damage State 2(Moderate Damage), Damage State 3(Severe Damage) and Damage State 4(Complete Damage) is much higher than those of other locations, but it is not an easy task to compare the damage situation in these three locations due to corresponding hypocenter and fault location for two scenarios.

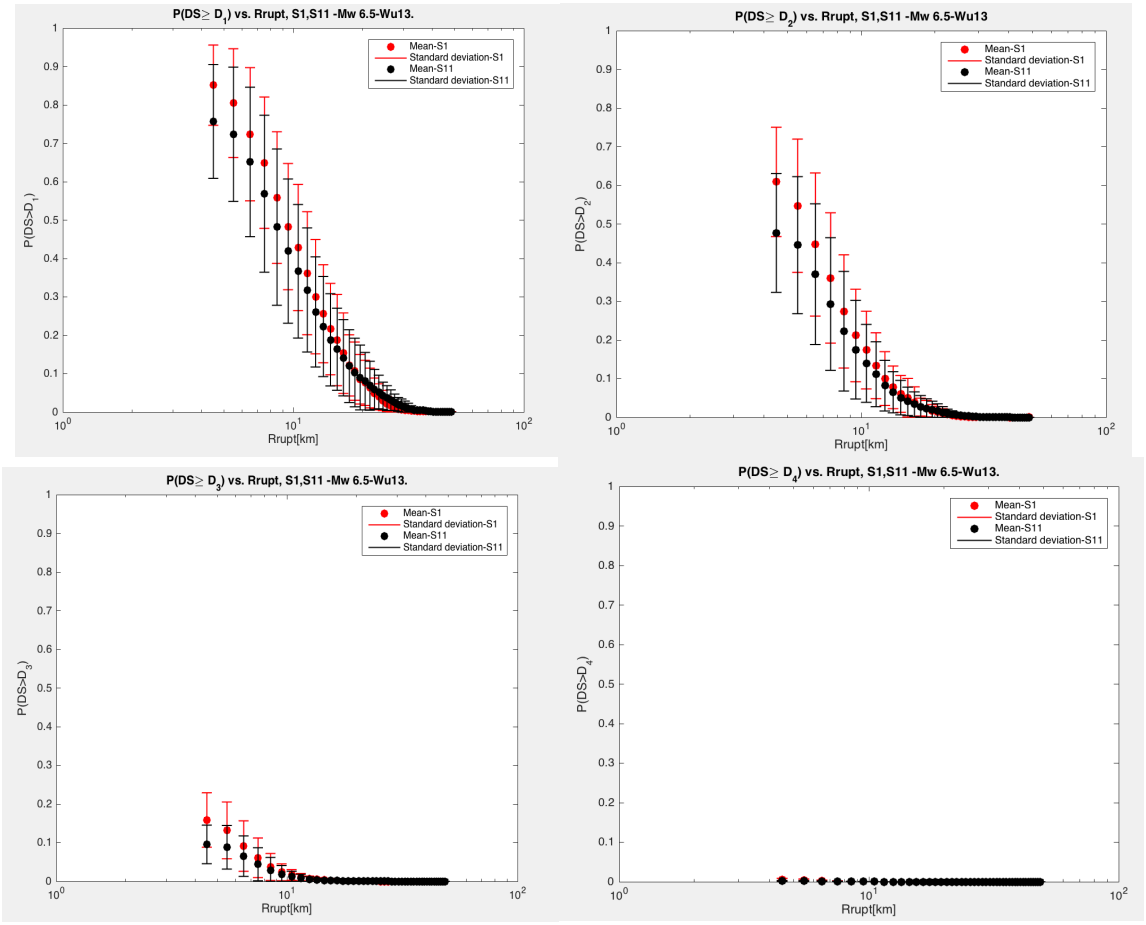

Figure 5.17. Comparison of exceeding probability vs Rupt. at four damage states for Scenario 1 and Scenario 11 Mw6.5. From top left to right bottom are P(DS>D1) vs Rrupt,; P(DS>D2) vs Rrupt,; P(DS>D3) vs Rrupt,; P(DS>D4) vs Rrupt. The dot simply represents the mean of exceeding probability at certain damage state for scenarios and the bar by the dispersion around that value.

Comparison of the exceeding probability with respect to Rrupt. at different damage states has been carried out, see Figure 5.17. It could be observed that for the exceeding probability at D1(Slight damage state), D2(Moderate damage state), D3(Severe damage state), Scenario 1 has higher values than Scenario 11, which represents Scenario 1 provides an overestimated result for exceeding probability at slight damage state.

For the exceeding probability at Damage State 4, for both Scenario 1 and Scenario 11 they are almost zero, which represents it is difficult to get probability of exceedance at complete damage state, or in other words the high-rise buildings for both scenarios cannot be complete damaged.

All above, it is not difficult to conclude that the probability of exceedance at a certain damage state is closely associated with the characteristics of the selected scenarios, precisely the location of the hypocenter and faults.

Location	Rrupt. [km]	SD(3S) [m]
L2	8	0.24
L4	5	0.35
L11	4	0.23
L12	13	0.09

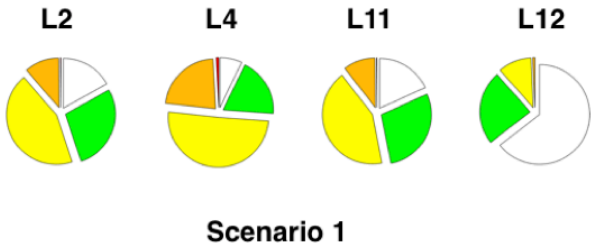

Scenario 1

Location	Rrupt. [km]	SD(3S) [m]
L2	8	0.22
L4	5	0.20
L11	4	0.10
L12	13	0.13

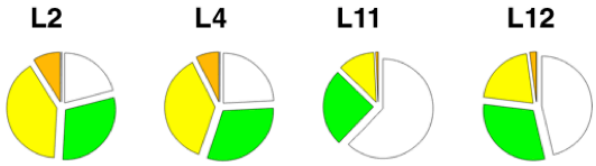

Scenario 11

Figure 5.18 Comparison between Scenario 1 and Scenario 11 for selected locations.

Scenario	Location	SD	Rrupt.[km]	D0	D1	D2	D3	D4
Scenario 1	L2	0.24	8	0.169	0.280	0.438	0.112	0.002
	L4	0.35	5	0.071	0.191	0.506	0.224	0.009
	L11	0.23	4	0.182	0.287	0.426	0.103	0.002
	L12	0.09	13	0.645	0.240	0.108	0.007	0.000
Scenario 11	L2	0.22	8	0.209	0.299	0.403	0.088	0.001
	L4	0.20	5	0.242	0.310	0.375	0.073	0.001
	L11	0.10	4	0.622	0.251	0.119	0.008	0.000
	L12	0.13	13	0.464	0.306	0.208	0.022	0.000

Table 5.5 Comparison values between Scenario 1 and Scenario 11 for selected locations.

Figure 5.18 shows the comparison of pie diagram at four selected locations for both scenarios and corresponding Rrupt. values and SD values at 3 seconds are below, see Table 5.5. It is easy to notic that different locations have different spectral displacements in terms of corresponding rupture distances. For Scenario 11 at L2 has larger Rrupt. and smaller SD, which results to a higher value than Scenario 1 at D0 (No damage state) and D1(Slight damage state), and in the contrary Scenario 11 has lower values for the other damage states.

5.3.4 Comparison among scenarios of variable magnitudes: Mw6.5 vs6.9vs 7.3

In the previous study, comparison among scenarios of same magnitude has been carried out. However, in this part, we focus on the comparison among scenarios of different magnitude such as Scenario 1（Mw 6.5），Scenario 14(Mw6.9) and Scenario 22(Mw7.5). in principle, comparison among scenarios of SD distribution, damage pie diagram, and probability of exceedance at a certain damage state.

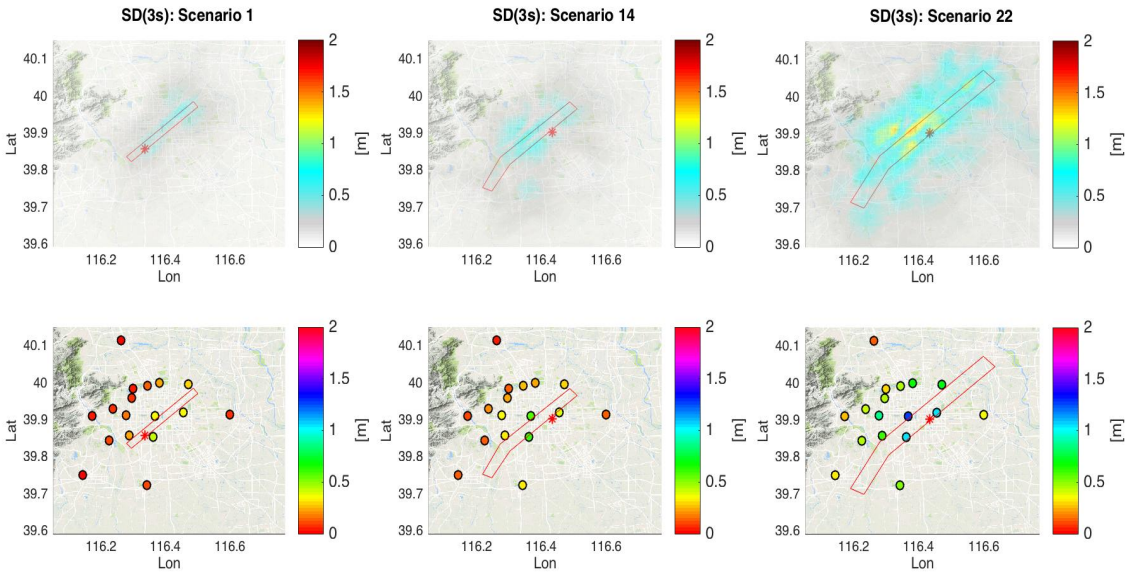

Figure 5.19 SD(3s) distribution of different magnitude Mw 6.5, Mw 6.9, Mw 7.5. The selected locations are represented by circles. The red star shows the projection of hypocenter and the red rectangular represents the projection of the fault.

Different scenarios representing different magnitudes have been illustrated, see Figure 5.19, from which it is obvious to see that Scenario 22 has much larger SD distribution compared to the other two scenarios. Probability at each damage state at each location is represented by damage pie diagram in Figure 5.20. It shows that when the rupture distance is smaller, the spectral displacement is larger, then the probability of damage at more serious damage state become higher. Beijing urban area is affected by very high values of ground motion and the values increase as the magnitude increases.

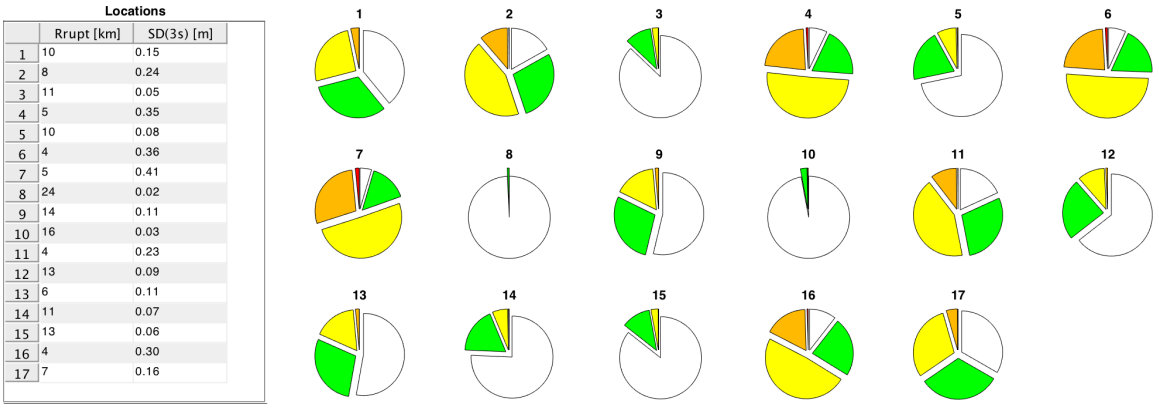

Locations

	Rrupt [km]	SD(3s) [m]
1	10	0.15
2	8	0.24
3	11	0.05
4	5	0.35
5	10	0.08
6	4	0.36
7	5	0.41
8	24	0.02
9	14	0.11
10	16	0.03
11	4	0.23
12	13	0.09
13	6	0.11
14	11	0.07
15	13	0.06
16	4	0.30
17	7	0.16

Scenario 1-Mw 6.5

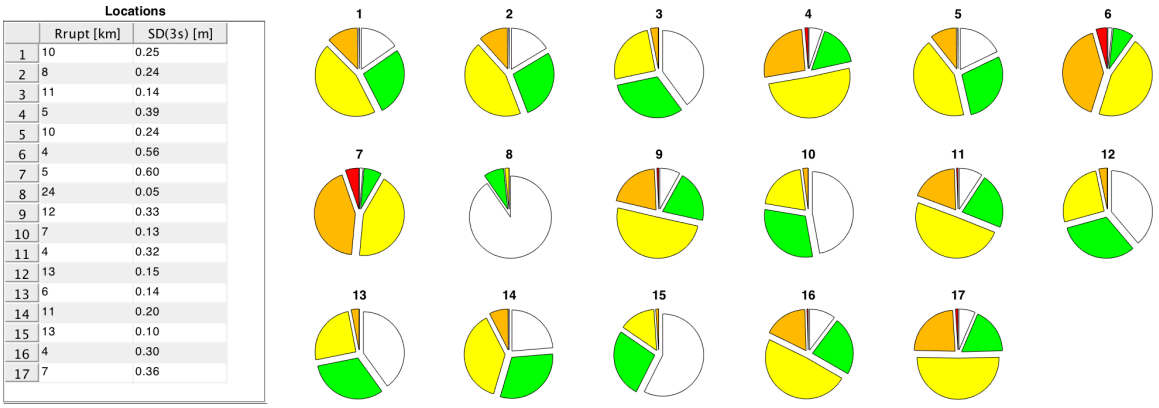

Locations

	Rrupt [km]	SD(3s) [m]
1	10	0.25
2	8	0.24
3	11	0.14
4	5	0.39
5	10	0.24
6	4	0.56
7	5	0.60
8	24	0.05
9	12	0.33
10	7	0.13
11	4	0.32
12	13	0.15
13	6	0.14
14	11	0.20
15	13	0.10
16	4	0.30
17	7	0.36

Scenario 14-Mw 6.9

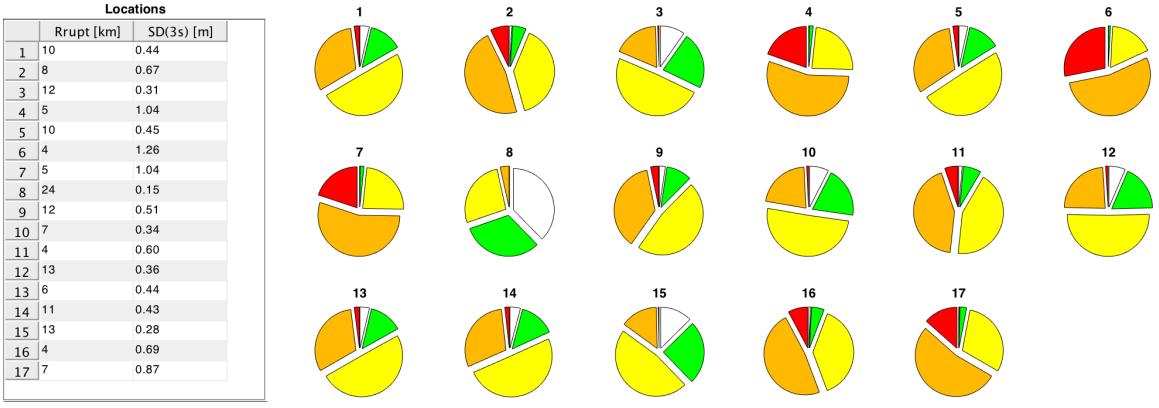

Locations

	Rrupt [km]	SD(3s) [m]
1	10	0.44
2	8	0.67
3	12	0.31
4	5	1.04
5	10	0.45
6	4	1.26
7	5	1.04
8	24	0.15
9	12	0.51
10	7	0.34
11	4	0.60
12	13	0.36
13	6	0.44
14	11	0.43
15	13	0.28
16	4	0.69
17	7	0.87

Scenario 22-Mw 7.3

Figure 5.20 comparison of pie damage diagrams for different scenarios with respect to corresponding magnitudes.

Finally, comparison of exceeding probability at each damage state vs Rrupt. among three scenarios S1, S14, S22 has been carried out, see Figure 5.21,

from which, it can be figured out that the relationship between exceeding probability at certain damage state and Rrupt. has a non-linear trend. Moreover, for each exceeding probability at one specified damage state with respect to the same Rrupt. value, S22 has the largest values, then S14 and S1, which corresponds to the distribution of SD.

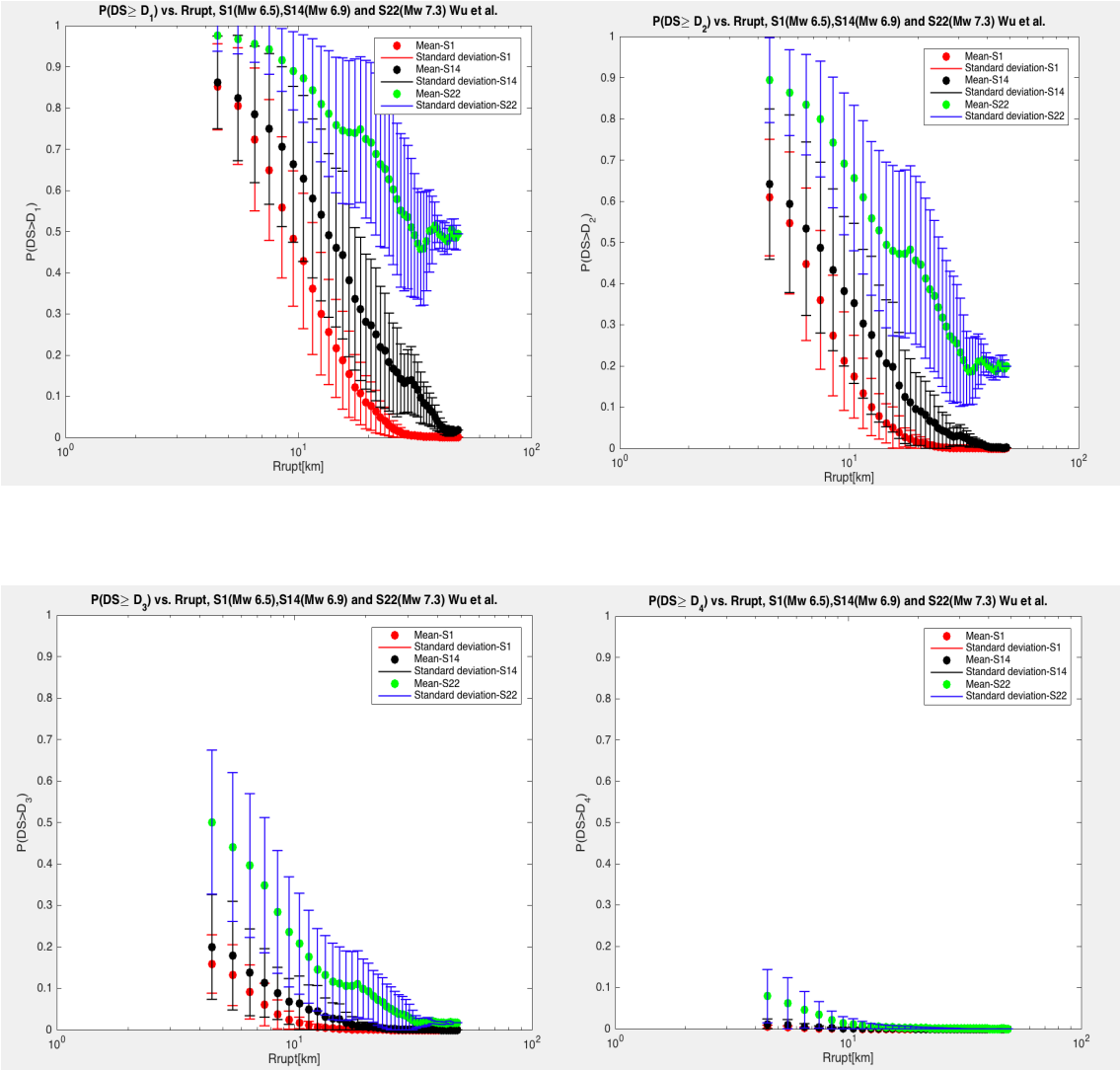

Figure 5.21 Comparison of exceeding probability at four damage states for Scenario1, Scenario14, Scenario 22. The dots simply represent the mean of exceeding probability at certain damage state for scenarios and the bars represent the corresponding standard deviation.

5.4. Comparison of the results obtained from 3D physics-based numerical simulation methods and GMPE methods

As we mentioned in previous chapters, GMPEs and 3D physic-based numerical methods are two main approaches to predict the earthquake ground motion and afterwards for further seismic hazard analysis. In general, GMPEs are efficiently used to estimate ground motions in both deterministic and probabilistic seismic hazard studies and have some limitations about some conditions such as near-source with large earthquake magnitude, complex topographic etc. However, 3D physic-based numerical simulation methods are deterministic simulations of seismic wave propagation including a complete 3D model of seismic fault rupture, complex geological environments and source-to-site propagation.

In this section, the results are compared with the estimations derived from the GMPEs of Cauzzi et al. 2015(hereinafter CAEA15), which provides ground motion intensity measure as a function of some parameters like earthquake magnitude, fault type, $V_{S,30}$ and Rupture distance. Here we estimate only for an average value of about 235 m/s (corresponding roughly to the average Vs30 of central Beijing) against the synthetic recordings. In order to present an average trend of the synthetics, these latter have been grouped adopting a sampling rate of 1 km. For the sake of brevity, no plots regarding one specific Vs30 is here proposed, nevertheless it is worth noting that our region of interest roughly correspond to the aforementioned 250 m/s and therefore we are confident of the relevance of the plots.

According to the previous studies, results in terms of exceeding probability diagram at certain damage states versus Rupt. and MDR versus Rupt. have been obtained from 3D physics-based numerical simulation methods. In this section, GMPEs are also used as an alternative method to carry out the simulation, then comparison between the two methods will be carried out as follows.

The numerical results of ground motion intensity measure SD versus Rrupt. have been obtained by the two methods.

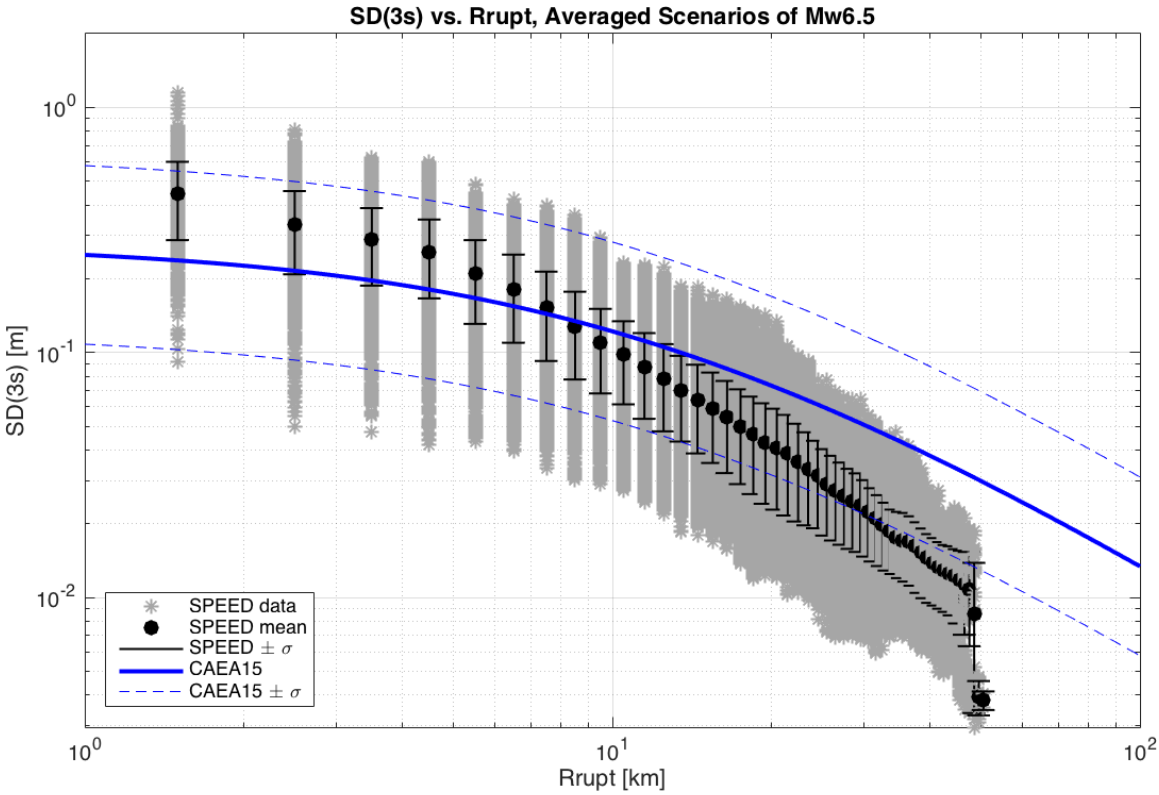

Figure 5.22. Comparison of SD(3S) vs.Rrupt. obtained from GMPES by Cauzzi et al.(2015) against 3DPBNS for Mw 6.5. The grey stars show the SD simulated for receivers and scenarios, while the black dot simply represents the mean and the bar by the dispersion around the value.

The relationship between Rupture distance and SD from GMPEs and 3D physics-based numerical simulation methods for Mw 6.5 has been plotted, see Figure 5.22. Spectral Displacement of 3DPBNS using codes SPEED is the average values for all the scenarios in Mw6.5 in terms of vibration period is 3s, while SD of GMPEs are obtained from CAEA15. The numerical results obtained by 3DPBNS are substantially inn agreement with the proposed GMPEs.

However, it could be figured out that synthetic scenarios obtained by SPEED produce higher SDs for short rupture distance, while GMPEs tends to underestimate SDs. This phenomenon has already been discussed in many recent works (such as Paolucci et al. 2014), which may play an important role in seismic hazard assessment.

However, the 3DPBNS gives lower values of SD than those from GMPEs when the rupture distances are long. It exactly verifies that GMPEs have a limitation for near source-to-site distance, while 3DPBNS could provide a

complete scenario of seismic waves of source-to-wave propagation.

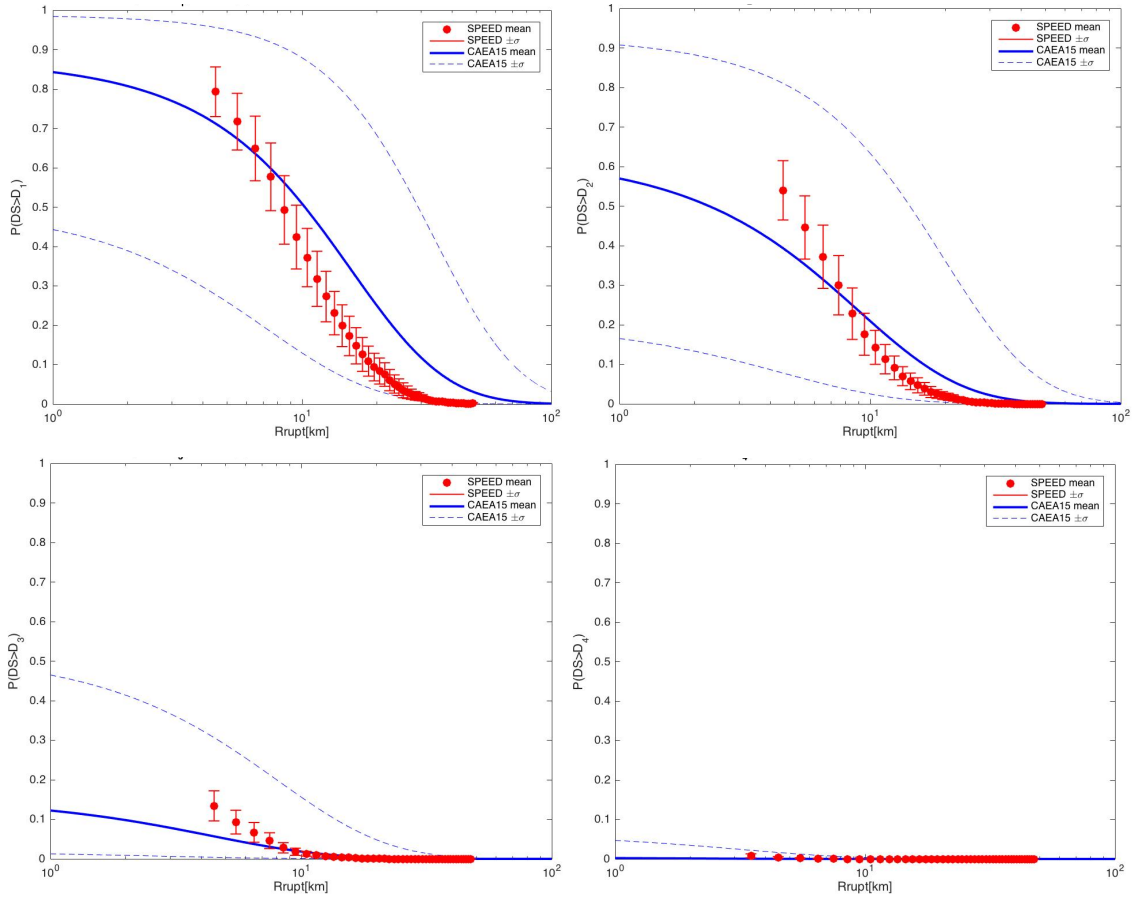

Figure 5.23 Comparison of exceeding probability at different damage states between the results obtained from 3DPBNS(SPEED) and GMPEs(CAEA15) Mw 6.5. Form left top to right bottom, exceeding probability of D1, D2, D3, D4. The red dot simply represents the mean obtained by SPEED and the bar by the dispersion around the value. The blue line shows the mean obtained by GMPEs (CAEA15) and the dashed blue lines shows the dispersion around the value.

Figure 5.23 shows the probability of exceedance at certain damage states versus the closest distance to the fault rupture (Rrupt). The red dot simply represents the mean obtained by SPEED and the bar by the dispersion around the value. The blue line shows the mean obtained by GMPEs (CAEA15) and the dashed blue lines shows the dispersion around the value.

Consistently with Figure 5.22, the probability of exceedance at different damage states can be obtained, and it decreases as Rrupt. increases. At damage state 3(Severe damage state), the exceeding probability decreases significantly at Rrupt around 10 km but remains dangerously high at low

distances.

The comparison diagrams of exceeding probability of damage states have similar behavior as the diagram of SD. For damage state 1(slight damage state), GMPEs provides lower values of the exceeding probability of near source distance, while 3DPBNS produce higher values for near source distance estimation, which proves that 3DPBNS may have a great impact on seismic hazard estimates, as standard GMPEs cannot account for such effects.

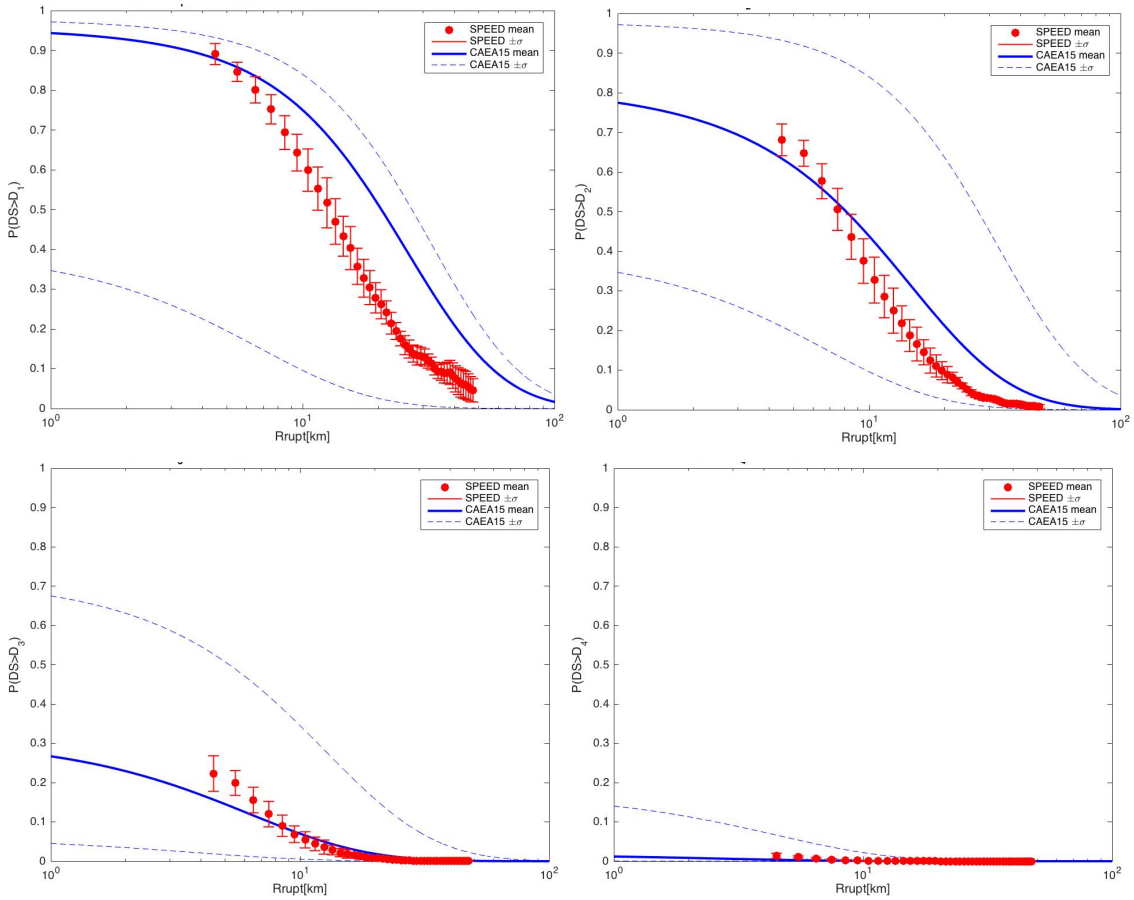

Figure 5.24 Comparison of exceeding probability at different damage states between the results obtained from 3DPBNS(SPEED) and GMPEs(CAEA15) Mw 6.9. Form left top to right bottom, exceeding probability of D1, D2, D3, D4. The red dot simply represents the mean obtained by SPEED and the bar by the dispersion around the value. The blue line shows the mean obtained by GMPEs (CAEA15) and the dashed blue lines shows the dispersion around the value.

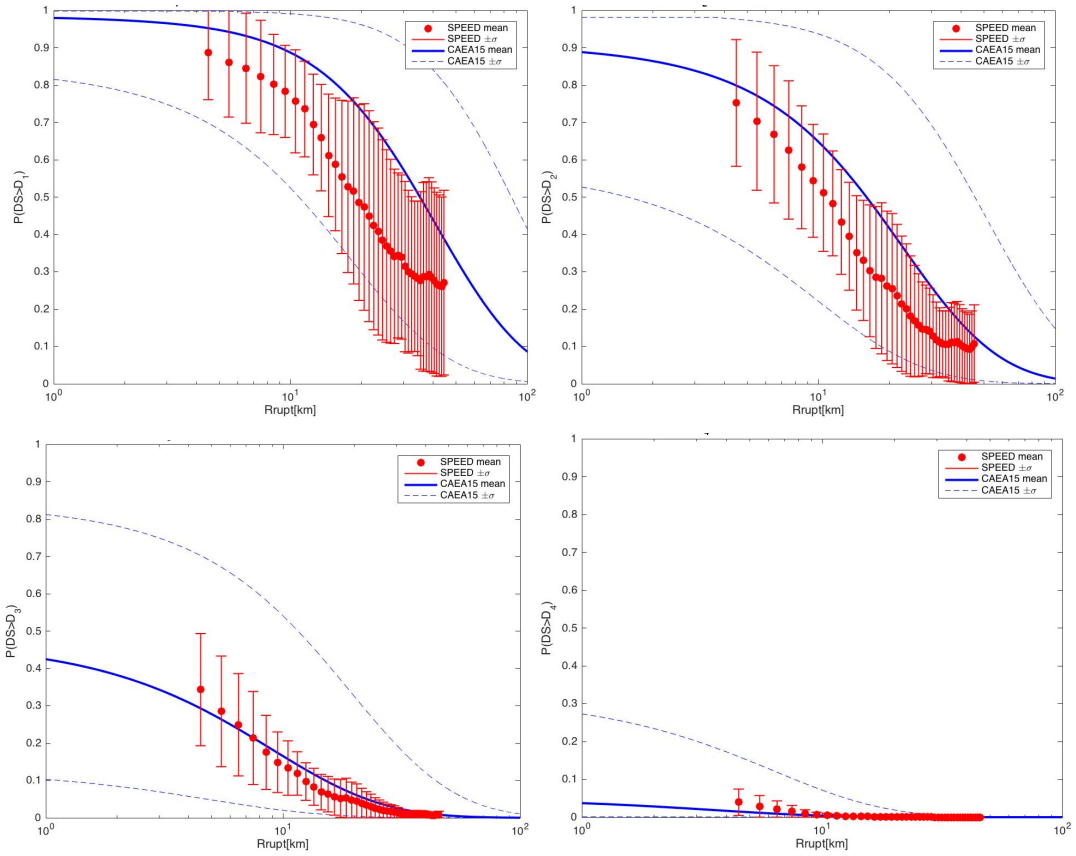

Figure 5.25 Comparison of exceeding probability at different damage states between the results obtained from 3DPBNS(SPEED) and GMPEs(CAEA15) Mw 7.3. Form left top to right bottom, exceeding probability of D1, D2, D3, D4. The red dot simply represents the mean obtained by SPEED and the bar by the dispersion around the value. The blue line shows the mean obtained by GMPEs (CAEA15) and the dashed blue lines shows the dispersion around the value.

Using the same procedure, probability of exceedance at a certain damage state for all the scenarios for Mw6.9 and Mw 7.3 can be obtained based on both 3DPBNS and GMPEs. Moreover, the same conclusion could be figured out as before. 3DPBNs provides higher values when Rrupt. is comparable small, which is smaller than the intersection value. It demonstrates that GMPEs have the limitation for PSHA in near source field, while 3DPBNS can be a good alternative tool for near source-to-site analysis.

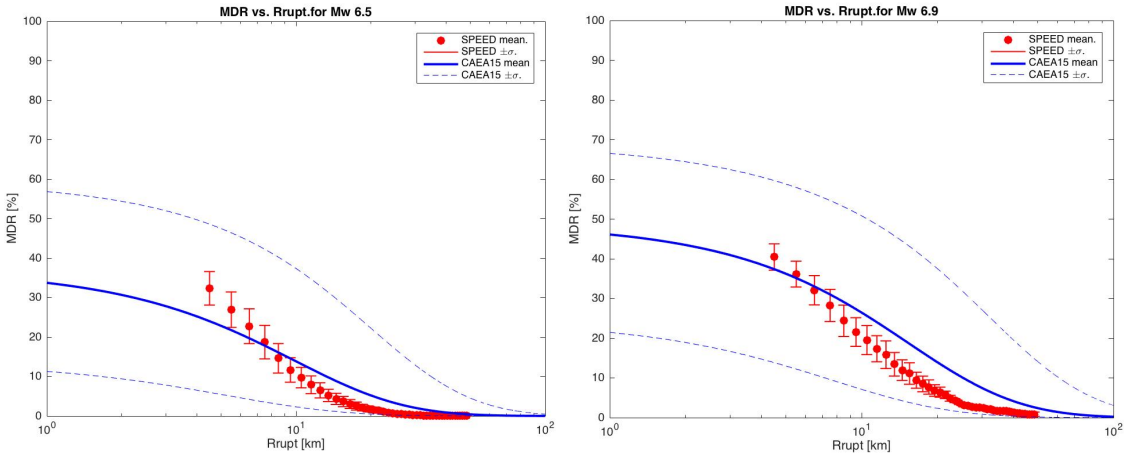

Figure 5.26 Comparison of MDR between the results obtained from 3DPBNS(SPEED) and GMPEs(CAEA15) Mw 6.9. Form left top to right bottom, Mw6.5, Mw6.93. The red dot simply represents the mean obtained by SPEED and the bar by the dispersion around the value. The blue line shows the mean obtained by GMPEs (CAEA15) and the dashed blue lines shows the dispersion around the value.

Mean damage ratio versus rupture distance has been carried out considering about the scenarios obtained by two methods. The red dot simply represents the mean obtained by SPEED and the bar by the dispersion around the value. The blue line shows the mean obtained by GMPEs (CAEA15) and the dashed blue lines shows the dispersion around the value.

From the results, it is possible to observe that the conclusion is similar as what we obtained for the exceeding probability at a certain damage state, which is the results obtained by SPEED are higher than those by GMPEs. And it proves that 3DPBNS can be an improved tool for near field analysis with large magnitude earthquake.

5.5 Sensitivity of results with respect to fragility curve

5.5.1 Sensitivity of MDR curves with respect to fragility curve.

Fragility model is of great significance for the seismic vulnerability analysis, and in the previous study WU13 has been used as a default fragility curve to carry out the analysis for high-rise buildings in China. Nevertheless, some further comparisons about the fragility curves used for vulnerability assessment are also essential to carry out.

Except WU13, Akkar17 is also a worthwhile fragility curve as we introduced in detail in Chapter 4. Therefore, Akkar17 has been chosen as a compared

fragility curve.

First of all, mean damage ratio versus spectral displacement at T=3s can be carried out. In order to obtain the MDR curve, it is necessary to assume the damage grade values related to corresponding damage states, see Table 5.6.

Damage Grade Values Li		
Damage State	**Wu et al.**	**Akkar and Odabasi**
D0	0.00	0.00
D1	0.10	0.10
D2	0.50	0.50
D3	0.70	0.70
D4	1.00	1.00

Table 5.6 Damage Grade Values for two fragility curves

Mean damage ratio can be considered as a vulnerability index with respect to intensity measure spectral displacement at certain vibration period, the MDR versus SD (T=3s) for two fragility curves is obtained, see Figure 5.27. It is worth to note that MDR and Sd has a nonlinear increasing trend, whose increasing speed is quite fast at beginning, then slowly as SD increases until SD is relatively large enough. When SD arrives in an extreme big value, the MDR trends to be equal around 1.

Moveover, it is not difficult to figure out that, when SD is small e, the MDR of WU13. is larger than that of Akkar17, which means when seismic hazard occurs, if the location has a comparative small SD value (smaller than 0.42 m), using fragility curve of WU13 will get more severe damage compared to the other two considering spectral displacement as intensity measure.

When Sd is around 0.42 m, for both two fragility curves, almost the same MDR values could be obtained. While when SD is larger than 0.42 m, MDR o WU13. always provides a value smaller than that of Akkar17, which represents WU13 has a comparable underestimate while seismic hazard assessment.

	MDR	
SD(T=3s)	WuEtAl	AkkarEtAl
0.00	0.000	0.000
0.01	0.000	0.000
0.02	0.001	0.000
0.03	0.004	0.000
0.04	0.011	0.000

0.34	0.429	0.388
0.35	0.437	0.400
0.36	0.445	0.413
0.37	0.453	0.425
0.38	0.460	0.436
0.39	0.467	0.448

1.23	0.741	0.964
1.24	0.743	0.965

1.98	0.843	0.999
1.99	0.844	0.999
2.00	0.845	0.999

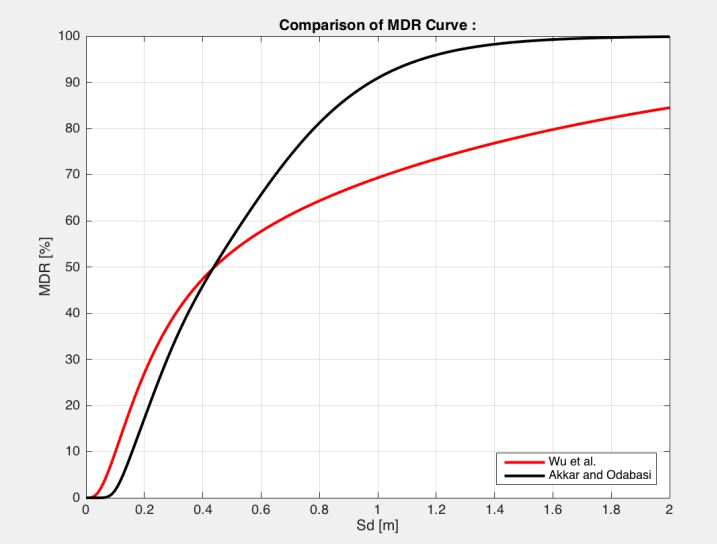

Figure 5.27 Comparison of MDR curve.

5.5.2 Sensitivity of fragility curves for selected locations Scenario 1 Mw6.5

Previously, Different MDR versus. spectral displacement at T=3s for two references has been compared. Now we study about the four locations, L2, L4, L11 and L12. Four selected locations are around the fault. L11 and L4 have pretty small rupture distances. According to the corresponding fragility curve, damage probability value can be obtained to plot the pie damage diagram. The Location map and SD value and damage table are expressed in Figure 5.28.

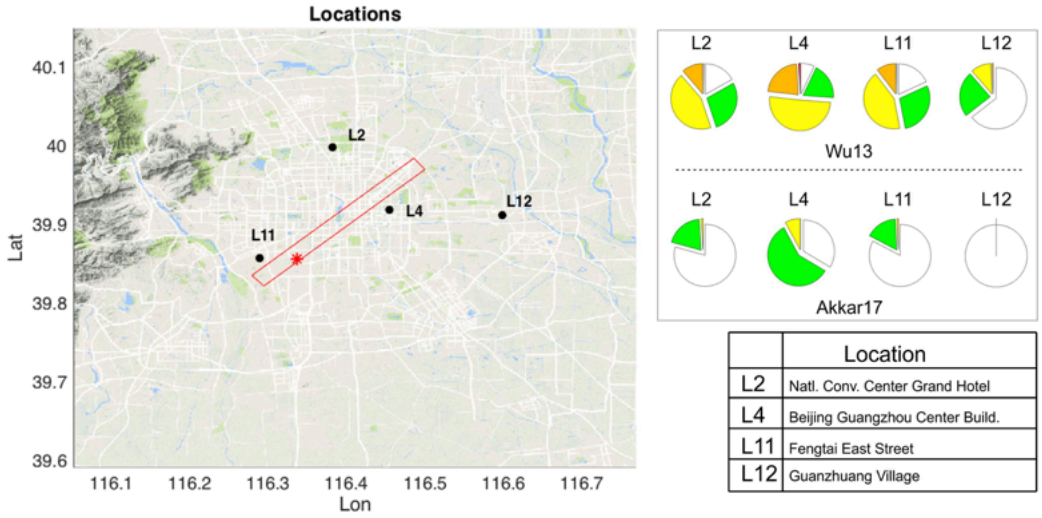

	Location
L2	Natl. Conv. Center Grand Hotel
L4	Beijing Guangzhou Center Build.
L11	Fengtai East Street
L12	Guanzhuang Village

			WU13					Akkar17				
	SD	Rrupt.[km]	D0	D1	D2	D3	D4	D0	D1	D2	D3	D4
L2	0.240	8	0.169	0.280	0.438	0.112	0.002	0.792	0.197	0.010	0.000	0.000
L4	0.350	5	0.871	0.104	0.024	0.001	0.000	1.000	0.000	0.000	0.000	0.000
L11	0.230	4	0.071	0.191	0.506	0.224	0.009	0.335	0.586	0.079	0.000	0.000
L12	0.090	13	0.718	0.203	0.076	0.004	0.000	1.000	0.000	0.000	0.000	0.000

Figure 5.28 Damage Pie Diagram for different locations using different fragility curves.

Location	Rrupt.[km]	SD[T=3s]	WU13	Akkar17
L2	8	0.240	32.476	23.939
L4	5	0.350	43.685	40.028
L11	4	0.230	31.187	22.272
L12	13	0.090	8.017	0.391

Table 5.7 MDR values for different locations

It is not difficult to obtain the MDR value versus Rrupt consequently, see Figure 5.29. Due to the locations we have chosen, the SD values are all smaller than 0.42m, where WU13 has a comparable larger MDR value than Akkar17.

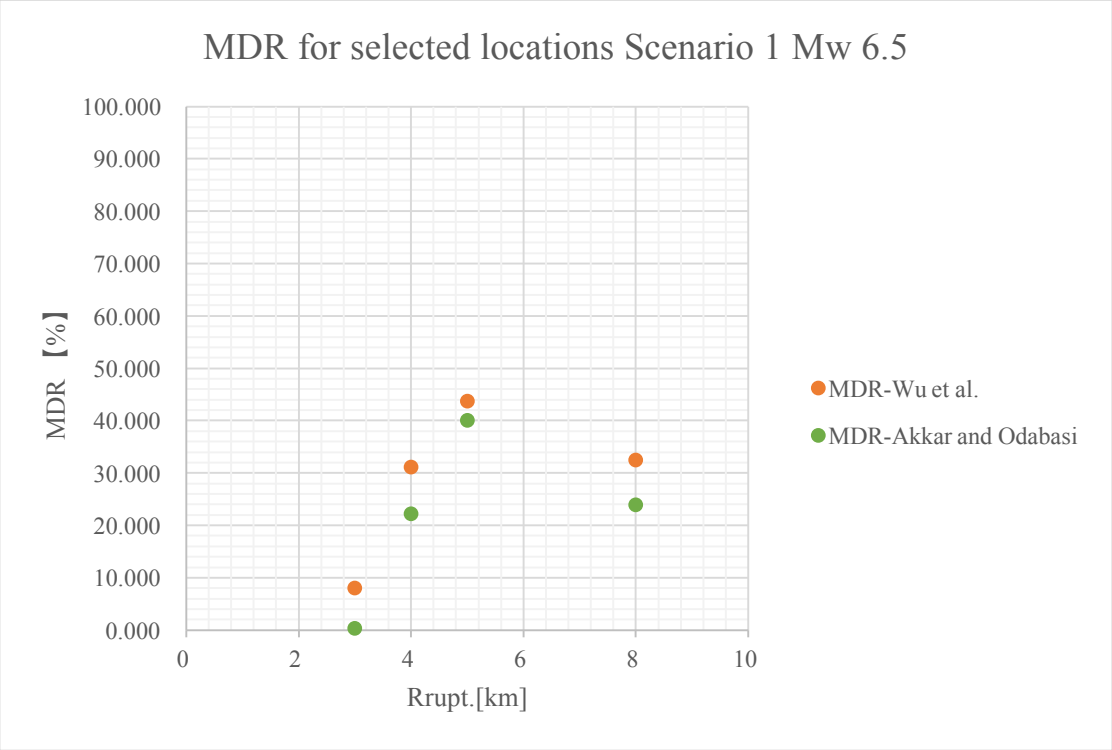

Figure 5.29 Comparison of MDR for different locations Scenario 1. Mw 6.5 The dots simply represent the mean of MDR for Scenario 1. Red filled dots represent the MDRs for WU13, while the green filled dots represent the MDRs for Akkar17.

5.5.3 Sensitivity of P(DS>Di) vs. Rrupt. with respect to fragility curve.

Previously, damage plots vs. Rrupt. were obtained by adopting the fragility curve WU13. In this section, another fragility curve has been selected as a comparison to check the sensitivity of fragility curve to the results. Using the same procedures, we introduced before, probability of exceedance, at a certain damage state for the average value of all scenarios for Mw6.5, has been obtained and plotted, see Figure 5.30.

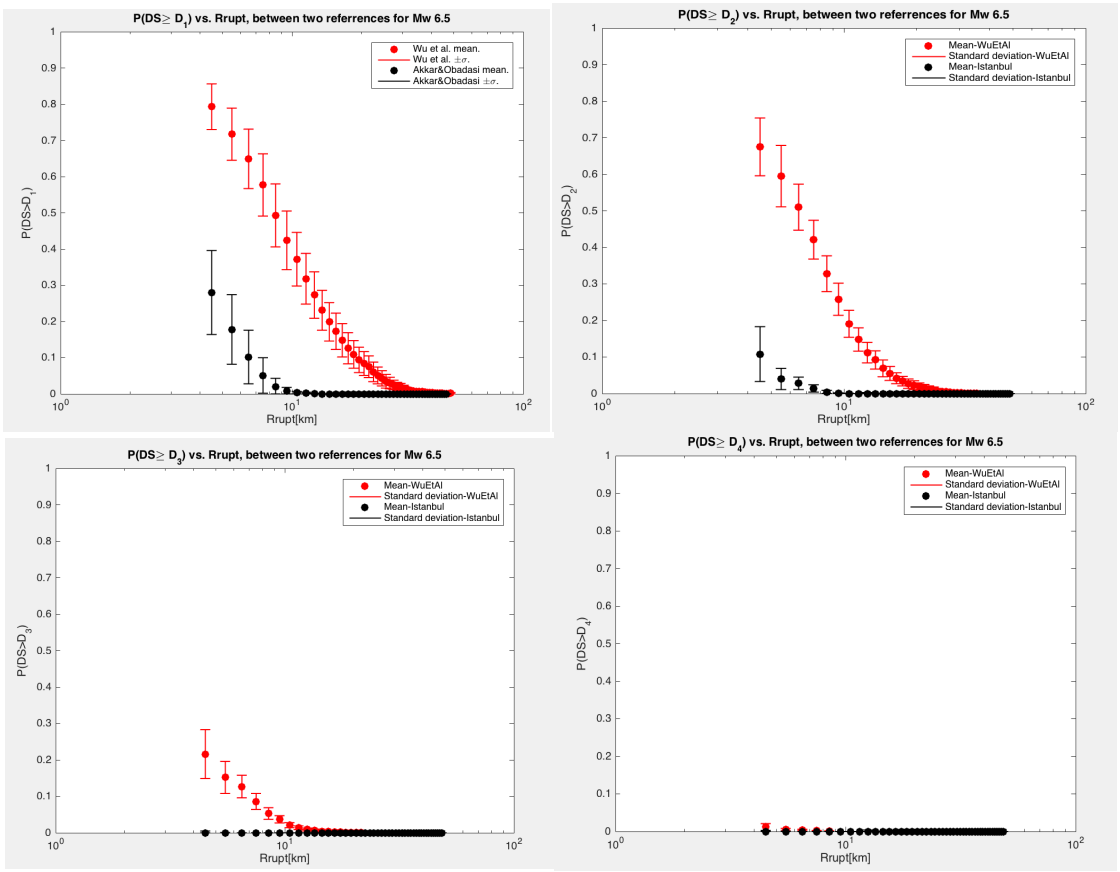

Figure 5.30 Comparison of exceeding probability at different damage states vs. Rupt. between the results obtained from WU13 and Akkar17 Mw 6.5. Form left top to right bottom, exceeding probability of D1, D2, D3, D4. The dots simply represent the mean of exceeding probability at certain damage state for scenarios and the bars represent the corresponding standard deviation.

It is possible to observe that the dots simply represent the mean of exceeding probability at certain damage state for scenarios and the bars represent the corresponding standard deviation. the exceeding probability vs Rrupt. has a non-linear trend. Moreover, as Rupture increases, the corresponding probability of exceedance decreases. Another observation is that for the same Rrupt, exceeding probability at a certain damage state, Wu13 provides a higher value than Akkar17.

5.5.4 Sensitivity of MDR vs. Rrupt. with respect to fragility curve

In this section, sensitivity of relationship between MDR and rupture distance with to fragility curve has been carried out. First of all, MDR values for two references in different locations are calculated, whose rupture distance starts from 4.5km to 48.5km. Furthermore, we calculate all the Mean values and

standard deviations for all the scenarios.

Furthermore, from the values it is possible to plot the distribution of the MDR compared to different rapture distances for WU13 Mw 6.5. It shows that as the rupture distance increases, the MDR ratio value decreases at beginning rapidly then slowly until zero, which means when the building is far away from the fault, the probability to get damage is very low representing as low vulnerability.

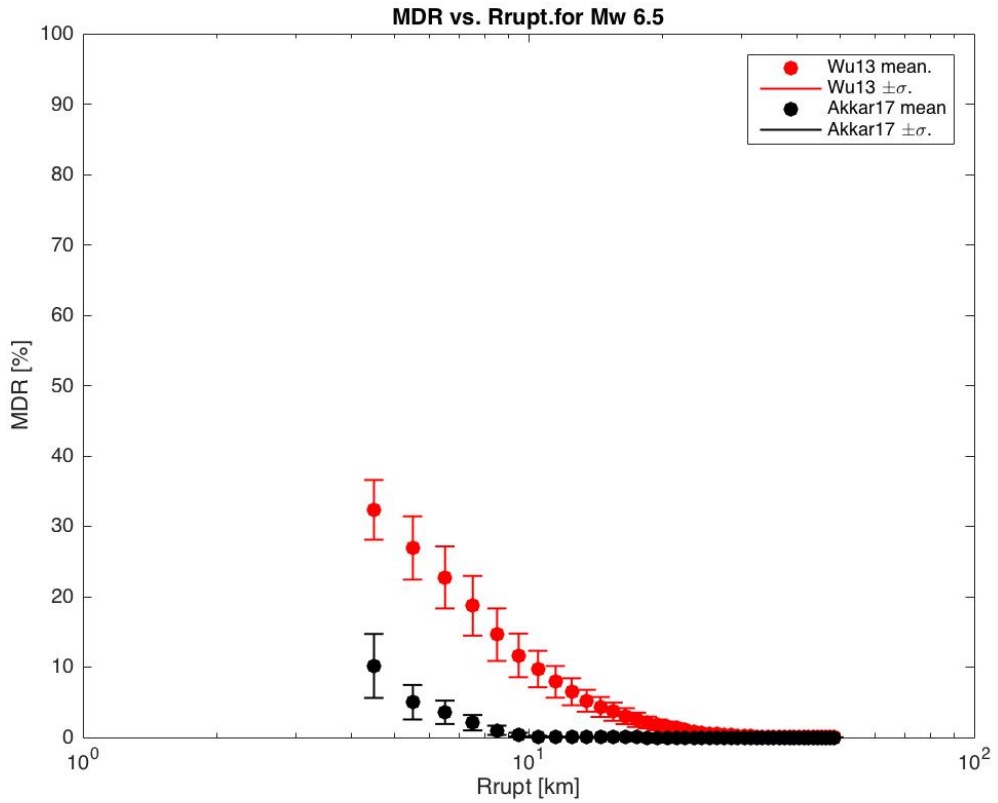

Figure 5.31 Comparison of MDR vs. Rrupt. for different fragility curves Mw 6.5. The dots simply represent the mean of MDR for scenarios and the bars represent the corresponding standard deviation.

Above all, we could plot MDR vs Rupture distance for two fragility curves Mw 6.5 in Figure 5.31. It is easy to notice that as the distance increases, the MDR decreases until almost zero and it seems that it is a non-linear relationship between MDR and Rupture distance. Furthermore, we could see that for the same rupture distance, WU13 has a higher MDR value, which

means more vulnerable. While Akkar17 has a comparative low MDR value, which means it has a more conservative fragility curve.

In this part by using the same previous method, we could easily obtain the plots MDR versus rupture distance for Mw 6.9 and Mw 7.3, see Figure 5.32. for the large magnitude earthquake from the plots, it could be noticed that for the same rupture distance, the MDR is becoming larger as the magnitude decreases since the ground motion increases.

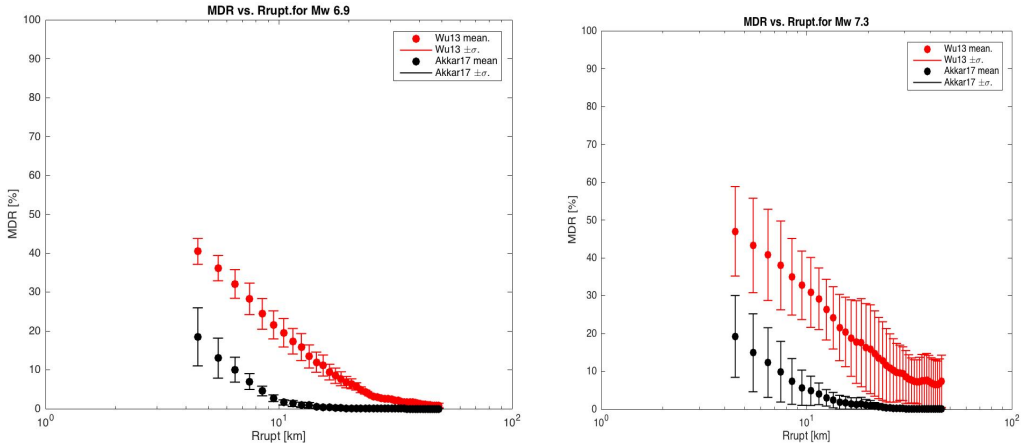

Figure 5.32 Comparison of MDR vs. Rrupt. for different fragility curves Mw 6.9，Mw7.3. The dots simply represent the mean of MDR for scenarios and the bars represent the corresponding standard deviation.

6. Conclusion

Probabilistic seismic hazard analysis (PSHA) (Cornell, 1968) has been considered as the most general used tools to describe attenuation of seismic ground motion in earthquake prone zone. Therefore, suitable approaches for earthquake ground motion prediction is of great significance for PSHA.

Generally, Ground Motion Prediction Equations (GMPEs) are the most adopted for this purpose. However, this method will have some limitations of the conditions such as the near source-to-site area, large earthquake magnitude, complex geological irregularities, soft soil site. Recently numerical simulation methods of strong earthquake ground motions have been becoming a better tool compared to GMPEs for seismic hazard analysis.

In this thesis, 3D numerical physics-based numerical simulation methods for seismic hazard assessment have been adopted to provide an improved estimation of strong ground motion including the factors such as near source, earthquake source process, seismic wave propagation, 3D geological and topographic configurations.

Beijing city has been selected as pilot case study to carry out the seismic risk assessment, since it is characterized by one of the many megacities with high-density population in the world and locating in high seismic hazard zone. Seismic risk assessment is needed to prioritize risk mitigation actions and could provide information for emergency planning. Totally 30 3D broadband physics-based ground shaking scenarios of possible earthquakes for Beijing area have been provided because of the achievement of the high-performance code SPEED developed by Politecnico di Milano.

Based on the scenarios and the selected fragility curve, distribution of probability of exceedance at a specified damage state for a certain scenario can be achieved to estimate the damage and losses. Moreover, the mean damage ratio diagrams of different scenarios are obtained considering the rupture distance to compare the damage.

Analysis of the seismic risk in terms of the ground motion using GMPEs were also done to make a comparison with 3D physics-based numerical simulation method. Finally, sensitivity of the fragility curve was analyzed to illustrate the effects of the fragility curve to the damage plots.

The analysis of the results provides some important conclusions as follows.

(1) Exceeding probability at one specific damage state for a certain scenario for one particular magnitude earthquake is closely associated with the characteristics of study scenarios, specifically the locations of hypocenter and fault.

(2) Exceeding probability at one specific damage state differs from the magnitude of the selected scenarios. In other words, as the magnitude increases, the exceeding probability at a given damage state increases.

(3) By comparison of the analyzed values between from GMPEs and 3D PBNS, in the near rupture distance, the values from GMPEs is lower than those from 3DPBNS, while it is higher than those from 3DPBNS in the far source-to-distance location. From here, we could get the conclusion, GMPEs could not account for near field seismic ground especially with larger magnitude.

(4) Sensitivity of the damage plots with respect to the fragility curve is also a crucial part, where from the results, it could be figured out that in the small spectral displacement (T=3s)， WU13 provides a higher estimation for MDR, while it gives a lower estimation in large spectral displacement. The intersection of SD is around 0.4 m. Moreover, for the selected representation locations, the MDR of WU13. is always higher than that of Akkar17, since the Sd is always smaller than 0.4 m. Mean damage ratio has a relationship with rupture distance, which normally is that as the rupture increases, the MDR decreases. Therefore, the sensitivity of fragility curve with respect to rupture distance is also a key point to carry out. As a matter a fact, similar conclusions were obtained for the comparison of exceeding probability at a given damage state for one scenario vs distance, and comparison of MDR vs. Rupture distance, which is that the WU13 provides a much higher estimation for exceeding probability at a given damage state for one specific scenario, also for the mean damage ratio according to the curves. Results demonstrated that the fragility curve WU13 provides an overestimation when seismic risk is assessed.

This thesis demonstrates that the procedures for the seismic risk assessment for high-rise buildings in urban area, Beijing, which mainly comprises seismic hazard assessment and seismic vulnerability assessment. The physics-based simulations scenarios could describe better the ground motion which can overcome the limitation of GMPEs and seem to be a promising approach for seismic hazard assessment. Vulnerability assessment could be achieved

through fragility curve, therefore proper choice of the fragility curve is a crucial work. Plots of damage with respect to rupture distance could contribute greatly to estimate the economic loss and further risk mitigation measure preparation of civil protection organization.

References

Antonietti, P.F., Ferroni, A., Mazzieri, I., Paolucci, R., Quarteroni, A., Smerzini, C., Stupazzini, M. (2017) 3D Physics-based numerical simulations: advantages and current limitations of a new frontier to earthquake ground motion prediction. The Istanbul case study.

Akkar S., Odabasi O. (2017) Probabilistic damage assessment and fragility functions of tall buildings in Istanbul. International Workshop on Performance-Based Seismic Design of Structures. Tongji University, Shanghai, China.

Alwaeli W., Mwafy A., Pilakoutas K., Guadagnini M. (2014) Framework for developing fragility relations of high-rise RC wall buildings based on verified modelling approach. Second European Conference on Earthquake Engineering and Seismology, Istanbul Aug. 25-29, 2014.

Baker J.W. (2015) Efficient analytical fragility function fitting using dynamic structural analysis, Earthquake Spectra, 31(1), 579-599, 2015.

Boore DM, Atkinson GM (2008) Ground-motion prediction equations for the average horizontal component of PGA, PGV, and 5 %-damped PSA at spectral periods between 0.01s and 10.0s. Earthq Spectra 24:99. doi:10.1193/1.2830434

Braga F., Dolce M., Liberatore D. (1982). "A Statistical Study on Damaged Buildings and an Ensuing Review of the MSK-76 Scale", Proceedings of the Seventh European Conference on Earthquake Engineering, Athens, Greece, pp. 431-450.

Calvi G.M., Pinho R., Magenes G., Bommer J. J., Restrepo -Velez L. F., Crowley H. Development of seismic vulnerability assessment methodologies over the past 30 years. ISET Journal of Earthquake Technology, Paper No. 472, Vol. 43, No. 3, September 2006, pp. 75-104

Cauzzi C., Faccioli E., Vanini M., Bianchini A. (2015) Updated predictive equations for broadband (0.01–10 s) horizontal response spectra and peak ground motions, based on a global dataset of digital acceleration records. Bull Earthquake Eng. (2015), 13, pp.1587–1612

Cherng. R. H (2001) Preliminary study on the fragility curves for steel structures in Taipei. Earthquake Engineering and Engineering Seismology,

Vol.3, No.1, pp. 35–42.

Comité Européen de Normalisation (CEN) (2004). Eurocode 8, Design of structures for earthquake resistance—part 1: general rules, seismic actions and rules for buildings. European Standard NF EN 1998-1, Brussels

Cornell A., Krawinkler H. (2000) Progress and challenges in seismic performance assessment. PEER Center New 3(2): 1-3.

Cornell C.A (1968). Engineering seismic risk analysis. Bull. Seismol. Soc. Am. 58, 1583–1606.

Crempien JGF, Archuleta RJ (2015) UCSB Method for Simulation of Broadband Ground Motion from Kinematic Earthquake Sources, Seismological Research Letters, 86 (1), 61-67.

Douglas J., Akkar S., Ameri G. et al (2014) Comparisons among the five ground-motion models developed using RESORCE for the prediction of response spectral accelerations due to earthquakes in Europe and the Middle East. Bull Earthq Eng 12:341–358. doi:10.1007/s10518-013-9522-8

Dumova-Jovanoska E. (2004). "Fragility Curves for RC Structures in Skopje Region", Proceedings of the 13th World Conference on Earthquake Engineering, Vancouver, Canada, Paper No. 3 (on CD).

Formisano A. (2012). Seismic behaviour and retrofitting of the Poggio Picenze Historical Centre damaged by the L'Aquila earthquake. In Proceedings of the eleventh international conference on computational structures technology, Civil Comp Press, Stirlingshire, UK, Paper (Vol. 199).

Gao M., Yu Y., Zhang X., Wu. (2004) Three-dimensional finite-difference modeling of ground motions in Beijing from a Mw 7 scenario earthquake. 13th World Conference on Earthquake Engineering Vancouver, B.C., Canada August 1-6, 2004 Paper No. 58

Giovinazzi S. and Lagomarsino S. (2001). "Una Metodologia per L'analisi Di Vulnerabilità Sismica Del Costruito", Proceedings of the X Congresso Nazionale on L'Ingegneria Sismica in Italia, Potenza-Matera, Italy, Paper No. 121 (on CD).

Giovinazzi S. and Lagomarsino S. (2004). "A Macroseismic Method for the Vulnerability Assessment of Buildings", Proceedings of the 13th World

Conference on Earthquake Engineering, Vancouver, Canada, Paper No. 896 (on CD).

Giardini, D., Grünthal, G., Shedlock, K. M. and Zhang, P. (1999) The GSHAP Global Seismic Hazard Map. Annali di Geofisica 42 (6), pp.1225-1228.

Graves R., Jordan T., Callaghan S., Deelman E., Field E., Juve G., Kesselman C., Maechling P., Mehta G., Milner K., Okaya D., Small P., Vahi, K. (2010) CyberShake: A Physics-Based Seismic Hazard Model for Southern California. Pure Appl. Geophys. doi:10.1007/s00024-010-0161-6.

Grossi P. Del Re D. Wang Z. (2006) The 1976 Great Tangshan Earthquake: 30-year. p.30

Grünthal G. (editor) (1998). "Cahiers du Centre Européen de Géodynamique et de Séismologie: Volume 15 – European Macroseismic Scale 1998", European Center for Geodynamics and Seismology, Luxembourg.

Gu G., Lin T., Shi Z. (1983) Catalogue of earthquakes in China (1831AD-1969BC). Science Press, Beijing (in Chinese).

Guagenti E. and Petrini V. (1989). "The Case of Old Buildings: Towards a Damage-Intensity Relationship", Proceedings of the Fourth Italian National Conference on Earthquake Engineering, Milan, Italy, pp. 145-153 (in Italian).

He Y., Li Y., Shen P. (2013) Performance-based seismic fragility analysis of tall hybrid structures engineering mechanics. Vol.30, No. 8, pp.142-147.

Infantino M. (2015) From 3D physics-based Scenarios to advanced methods for seismic hazard assessment: The case of Istanbul. Master thesis, Politecnico di Milano.

Jayaram N., Shome N., Rahnama M. Development of earthquake vulnerability functions for tall buildings. Earthquake Engineering & Structural Dynamics. 2012, 41:1495–1514

Ji L., Elnashai A.S., Kuchma.D.A. (2007) An analytical framework for seismic fragility analysis of RC high-rise buildings. Engineering Structures, 29, pp. 3197–3209.

Kappos A.J., Stylianidis K.C., Pitilakis K. (1998) "Development of Seismic Risk Scenarios Based on a Hybrid Method of Vulnerability Assessment", Natural Hazards, Vol. 17, No. 2, pp. 177-192

Kazantzi A., Vamvatsikos D., Porter, K., Cho, I.H. (2014) Analytical vulnerability assessment of modern highrise RC moment-resisting frame buildings in the western USA for the global earthquake model. Second European Conference on Earthquake Engineering and Seismology, Istanbul Aug. 25-29 2014.

Kramer, S.L. (1996). Geotechnical Earthquake Engineering, Prentice Hall, Inc., Upper Saddle River, New Jersey. pp.106-138

Krawinkler H. (2002). A general approach to seismic performance assessment. International Conference on Advances and New Challenges in Engineering Research, First Annual Meeting of ANCER, Hong Kong August 19-20, 2002, Hong Kong, China.

Lagomarsino S., Penna A., Galasco A., Cattari S. (2013). TREMURI program: an equivalent frame model for the nonlinear seismic analysis of masonry buildings. Engineering Structures, 56, pp.1787-1799.

Li J., Wang Y., Chen H., Lin L. (2013) Risk assessment study of fire following an earthquake: A case study of petrochemical enterprises in China. Natural Hazards and Earth System Sciences, 1(2), pp.1775-1798.

Maio R., Vicente R., Formisano A., Varum H. (2015). Seismic vulnerability of building aggregates through hybrid and indirect assessment techniques. Bulletin of Earthquake Engineering, 13(10), pp. 2995-3014.

McCormack, T.C. and Rad, F.N. (1997). "An Earthquake Loss Estimation Methodology for Buildings Based on ATC-13 and ATC-21", Earthquake Spectra, Vol. 13, No. 4, pp. 605-621.

McGuire, R.K. (2004). Seismic hazard and risk analysis. Earthquake Engineering Research Institute, MNO-10, p.221

Mustafa E. (2017) Earthquake risk assessment. Bull Earthquake Eng. (2017) 15, pp.5055–5092.

Mwafy A. (2010) Analytically derived fragility relationships for the modern high-rise buildings in the UAE the structural design of tall and special buildings. Struct. Design Tall Spec. Build. 21, 824–843 (2012).

Nasiri (2012) Structural Assessment and Retrofit Design for Golestan Historical Masonry Dam. 3rd National Conference on Earthquake & Structure

Novelli, V., I. (2017) Hybrid method for the seismic vulnerability assessment of historic masonry city centres. Phd thesis. University College London.

Paolucci R., Mazzieri I., Smerzini C., Stupazzini M. (2014): Physics-Based Earthquake Ground Shaking Scenarios in Large Urban Areas. Perspectives on European Earthquake Engineering and Seismology. Springer, pp. 331-359.

Paolucci R., Infantino M., Mazzieri I., Özcebe A.G., Smerzini C., Stupazzini M. (2017) 3D physics-based numerical simulations: advantages and current limitations of a new frontier to earthquake ground motion prediction. The Istanbul case study. Modeling and scientific computing report No. 68/2017.

Pejovic J., Jankovic S. (2016) Seismic fragility assessment for reinforced concrete high-rise buildings in Southern Euro-Mediterranean zone. Bull Earthquake Eng. (2016), 14, pp. 185-212.

Porter K. (2017) A Beginner's Guide to Fragility, Vulnerability, and Risk.

Quiroz L.G., Maruyama Y. (2014) Assessment of performance of Peruvian high-rise thin rc wall buildings using numerical fragility functions. The 2014 World Congress on Advances in Civil, Environmental, and Materials Research(ACEM14), Busan, Korea, August 24-28, 2014

REITER, L. (1990) Earthquake Hazard Analysis. Columbia University Press, New York, 1990. p. 254

Singhal A. & Kiremidjian A.S. (1996). "Method for Probabilistic Evaluation of Seismic Structural Damage", Journal of Structural Engineering, ASCE, Vol. 122, No. 12, pp. 1459-1467.

Smerzini C. (2010). The earthquake source in numerical modeling of seismic wave propagation in heterogeneous earth media. Ph.D. thesis, Rose School, IUSS Pavia.

Smerzini C., Pitilakis K. (2017) Seismic risk assessment at urban scale from 3D physics- based numerical modeling: the case of Thessaloniki Bull Earthquake Eng. Part of Springer Nature 2017.

Spence, R., Coburn, A.W. and Pomonis, A. (1992). "Correlation of Ground Motion with Building Damage: The Definition of a New Damage-Based Seismic Intensity Scale", Proceedings of the Tenth World Conference on Earthquake Engineering, Madrid, Spain, Vol. 1, pp. 551-556.

Vicente; C. Oliveira; T.M. Ferreira; H. Rodrigues; A.A. Costa (2014) Chap. 4: Seismic Structural Assessment of Existing Building at Urban Level. In: "Lisbon in Motion Workshop: Risk assessment, rehabilitation and urban plan". Alexandre A. Costa, Mónica Amaral Ferreira, Alexandra Carvalho, Cristina Oliveira, Isabel Lopes and Rui Carrilho Gomes (Eds.). SPES. Book ISBN: 978-989-20-5085-0. pp.39-48.

Whitman R.V., Reed J.W., Hong S.T. (1973). "Earthquake Damage Probability Matrices", Proceedings of the Fifth World Conference on Earthquake Engineering, Rome, Italy, Vol. 2, pp. 2531-2540.

Wu F., Wang M., Yang X. (2013) Building seismic vulnerability study for China high rises. Applied Mechanics and Materials Vol.353-356(2013), pp. 2301-2304.

Xu P., Fu X., Wang C., Xiao C. (2005) Design of complex high-rise structures. Chinese Architecture &Building Press, China (In Chinese).

Xu P., Xiao C., Li J. (2014) Relationship between natural vibration periods and structural heights for high-rise buildings in China. International Journal of High-rise Buildings, Vol.3, No.1, pp. 49-64.

Yasmin T., Chourasia A., Bhattacharyya S.K. and Parashar J. (2015) Fragility analysis for seismic vulnerability assessment of buildings: A review. International Research Journal of Engineering and Technology (IRJET), Vol 02, 06, pp.508-520.